PU/NE-03-06

U. S. Department of Energy
Nuclear Engineering Education Research

ANALYTICAL AND EXPERIMENTAL STUDY OF THE EFFECTS OF NON-CONDENSABLE IN A PASSIVE CONDENSER SYSTEM FOR THE ADVANCED BOILING WATER REACTOR

Yearly Progress Report
September, 2002 to July, 2003

Contact: Dr. Shripad T. Revankar
School of Nuclear Engineering
Purdue University
West Lafayette, In 47907-1290

765-496-1782
shripad@ecn.purdue.edu

Contributing Authors:

S. T. Revankar*, and S. Oh

Purdue University
School of Nuclear Engineering
West Lafayette, IN 47906-1290

July 2003

* *Project Director*

CONTENTS

LIST OF FIGURES

LIST OF TABLES

ACRONYMS

ABWR	Advanced Boiling Water Reactor
AP600	Advanced Passive 600 MWe Pressurized Reactor
DOE	Department Of Energy
DW	Dry Well
GDCS	Gravity Drain Cooling System
GE	General Electric
GE-SBWR	600 Mwe GE designed Simplified Boiling Water Reactor
ICS	Isolation Condensation System
LOCA	Loss Of Coolant Accident
LWR	Light Water Reactor
MIT	Massachusetts Institute of Technology
NRC	Nuclear Regulatory Commission
PCCS	Passive Containment Cooling System
RELAP5	A Reactor Safety Analysis Code
RPV	Reactor Pressure Vessel
SBWR	Simplified Boiling Water Reactor
SBWR-600	600 MWe GE Designed Simplified Boiling Water Reactor
SP	Suppression Pool
UCB	University of California Berkeley

NOMENCLATURE

A	Area [m^2]
C_p	Specific heat [j/kg·C]
d,D	Diameter [m] or diffusion constant [m^2/s]
f	Friction factor
g	Gravitational acceleration [m/s^2]
H	Height [m]
h	Heat transfer coefficient[$W/m^2·C$] or Enthalpy [J/kg]
h_{fg}	Latent heat of vaporization [J/kg]
j	Mass flux [kg/ m^2·s]
k	Conductivity [$W/m^2·C$]
m	Mass flow rate [kg/s]
M	Molecular weight [g/mol]
P, p	Pressure [Pa]
q″	Heat flux [W/m^2]
Q	Heat Transfer Rate [W]
r	Radial coordinate
R	Radius [m] or gas constant [kJ/kg·mol-K]
Re	Reynolds number
t	Time [s]
T	Temperature [K or C]
U	Overall heat transfer coefficient [$W/m^2·C$]
u	Axial velocity [m/s]
v	Radial velocity [m/s]
V	Volume [m^3]
x	Axial coordinate
y	Radial coordinate from wall
W	Mass fraction

Greek Symbols

α_s	Thermal Diffusion Coefficient
δ	Film thickness [m]
ε	Eddy diffusivity [m^2/s]
μ	Dynamic viscosity [kg/m·s]
ν	Kinematic viscosity [m^2/s]
ρ	Density [kg/m^3]
σ	Surface tension [N/m]
τ	Shear stress [Pa]

Subscripts

a	Ambient, air
avg	Average
b	Bulk
c	Condensation or coolant
g	Gas or steam-gas mixture
i	i-th component, i-th node, inside or interface
in	Inlet
l	Local
L	Liquid
m	momentum
mes	Measurement
o	Outside
out	Outlet
ref	Reference
s	Secondary side
sat	Saturation
sys	System
tot	Total
v	Vapor
W	Wall

EXECUTIVE SUMMARY

The main goal of the project is to study analytically and experimentally condensation heat transfer for the passive condenser system relevant to the safety of next generation nuclear reactor such as Simplified Boiling Water Reactor (SBWR). The objectives of this three-year research project are to: 1) obtain experimental data on the phenomenon of condensation of steam in a vertical tube in the presence of non-condensable for flow conditions of PCCS, 2) develop a analytical model for the condensation phenomena in the presence of non-condensable gas for the vertical tube, and 3) assess the RELAP5 computer code against the experimental data. The project involves experimentation, theoretical modeling and a thermalhydraulic code assessment. It involves graduate and undergraduate students' participation providing them with exposure and training in advanced reactor concepts and safety systems.

The present 3-year research program is structured around three phases.

Phase 1 – Phase 1 will have a duration of 12 months and will cover the following tasks: (1) Perform scaling analysis for PCCS condenser design; (2) Perform 5.08 cm tube condenser design, loop design, and construction and testing; (3) Experimental data on heat transfer for 5.08 cm condenser for three PCCS flow conditions: forced flow; continuous condensation (with zero flow velocity at bottom of the condenser); and cyclic condensation

Phase 2 – Phase 2 will have a duration of 12 months and will begin after Phase 1. Phase 2 will cover the following tasks: (1) Obtain experimental data are on 2.54 cm ID condenser for three PCCS flow conditions: forced flow; continuous condensation (with zero flow velocity at bottom of the condenser); and cyclic condensation; (2) Development of analytical model; (3) Comparison of analytical model and experimental data.

Phase 3 – Phase 3 will have duration of 12 months and will begin after Phase 2. Phase 3 will cover the following tasks: (1) Obtain additional experimental data with 5.08 cm and 2.54 cm condenser tube; (2) Perform RELAP5/MOD3 code model for the PCCS condensation; (3) Development of PCCS condensation heat transfer correlation.

Progress for the first year (May 2000- August 2001)

- A detailed scaling analysis for the PCCS condenser was performed. The scaling parameters were identified to scale down the prototype condenser design. The effect of the non-

condensable in the scaled condenser was discussed and its implication on the scaled test facility was presented.

- An experimental loop was designed with 5.08 cm inch diameter condenser. The design of the condenser tube was based on the scaling analysis. The test section and the loop were instrumented for required parameters.
- There was delay in completing the first year experimental task due to late start of the project. Permission was sought from DOE to extend the first year period 05/01/00 - 04/30/01 to 05/01/00 – 08/31/01, an extension of four months. DOE has granted an extension of four months to complete the first year task.
- A condensation model was developed for forced downflow of steam and non-condensable gas in vertical tube. First the model was tested for pure steam condensation and the predicted heat transfer results were compared with the experimental data. Then the model was tested for condensation in the presence of non-condensable gas, air, and results of the predictions were compared to the published experimental data The agreement was fairly good. Please note that this modeling task falls in second year period. Since the first year task on experiments has been extended to be performed by four months, this period of work is taken care by the modeling task.

Second year progress: (August 2001-August 2002)

- The test facility was completed and tested with 5.08 cm diameter condenser tube. Experimental data on heat transfer for 5.08 cm condenser for three PCCS flow conditions: forced flow; and continuous condensation (with zero flow velocity at bottom of the condenser) were obtained
- Development of analytical model was completed and the test data were compared with the analytical model. The interfacial friction factor was examined.
- The new test sections with 2.54 cm and 5.08 cm diameter condenser with secondary cooling by pool boiling were designed and constructed and are being tested.

Third year progress: (August 2002-July 2003)

- Condensation tests were carried out for 2.54 cm diameter condenser with pool boiling cooling on the secondary side. Condensation tests were conducted for three operational mode of PCCS, i.e., complete condensation, periodic venting, and through flow modes. Test results indicate the possibility of combining all three PCCS operation modes into one universal condensation heat transfer model.

- Kuhn's experiment data were compared with the condensation model developed in the second year.

- A new condensation model has been developed, which does not use the self-similar velocity profile assumption. The velocity profile predicted by new model was compared with the analysis of the FLUENT commercial code.

- Assessment of the condensation model in RELAP5 code was performed by comparison with experimental data. Default model and UCB model in RELAP5 show quite different results each other.

- Vent analysis was performed to check the degradation effect of the noncondensable gas for periodic venting condition.

1. INTRODUCTION

1.1 Significance of the Problem

The heat transfer analysis of film condensation is an important area in the design of heat exchangers. The condensation phenomenon plays an important role in the heat transfer process in the chemical and power industry, including nuclear power plants. This mode of heat transfer is often used in engineering because high heat transfer coefficients are achieved. Many industrial systems use vertical tube condensers and industrial practice has indicated that, often, much higher coefficients of heat transfer are obtained when vapors are condensed inside tubes rather than outside. However, in practical operations of the condensers, small amounts of non-condensable gas may exist in working vapors due to characteristics of the system or dissolution of working vapors. It is well known that the presence of non-condensable gases in a vapor can greatly reduce the performance of condensers. This is because of the fact that the presence of non-condensable gas lowers the partial pressure of the vapor, thus reducing the saturation temperature at which condensation occurs.

In the nuclear reactor industry, condensation heat transfer is very important in many situations. In the case of loss of coolant accident (LOCA), a large portion of the heat is removed by condensation of steam in the steam generators in reflux condensation mode. The presence of the noncondensable hampers the heat removal process. In the advanced light water reactors such as the Westinghouse designed Advanced Passive 600 MWe (AP600) [1.1] and General Electric Simplified Boiling Water Reactor (SBWR) [1.2], there is a greater emphasis on replacing the active systems with passive systems in order to improve the reliability of operation. For example, the SBWR is based on natural circulation cooling. SBWR uses the gravity driven cooling system (GDCS) as an emergency core cooling system following an accident. After the reactor is scrammed the pressure vessel is depressurized with system of valves and thus pressure in the vessel is reduced so that the GDCS is made functional. The containment steam is condensed by a condenser system called Passive Containment Cooling System (PCCS). In this reactor the containment pressurization thus depends on the condensing capability of the PCCS after the

blowdown process. Development programs on advanced light water reactor based on passive safety systems are underway in Europe and Japan. Design development of the European Simplified Boiling water Reactor (ESBWR) [1.3] and Japanese SBWR [1.4] are the longer-term goals in this effort.

In the SBWR the PCCS is a passive heat exchanger that allows the transfer of heat via steam condensation to the water pool. The PCCS condenser must be able to remove sufficient energy from the reactor containment to prevent containment from exceeding its design pressure following a design-basis accident. The efficient performance of the PCCS condenser is thus vital to the safety of the SBWR. The rate of heat transfer in the PCCS condenser is strongly coupled to the hydrodynamic characteristics of the PCCS. Hence a detailed knowledge of the variation of local heat transfer coefficient is necessary in order to predict the performance of the PCCS and for design optimization.

1.2 Research Focus

Uchida et al's [1.5] experiments on steam-gas condensation on outside wall of vertical tube provided first practical correlation for the degradation of condensation. Since then several theoretical works on the effects of the non-condensable on condensation in vertical pipe have been conducted [1.6-1.8]. The relevant separate effects experiments on PCCS condensation under the presence of noncondensable gas were conducted at Massachusetts Institute of Technology (MIT) [1.9,1.10] and at University of California Berkeley (UCB) [1.11,1.12]. Both MIT and UCB tests provided a new database and correlation for forced convection condensation of steam in a vertical tube in the presence of noncondensable gas. The flow of steam/gas mixture in the PCCS condenser tube as discussed in following section 1.2 is not always forced convection. Hence the UCB and MIT correlations do not apply for all flow conditions in the PCCS. This research addresses this particular problem by perform careful experiments for the flow conditions expected in the PCCS condenser and develop analytical model to predict the condensation heat transfer characteristics of PCCS in the presence of non-condensable gas. In addition to this task a RELAP5 code model will be developed for PCCS condensation in the presence of non-condensable and the RELAP5 code assessment is performed.

This report presents the experimental work and the analytical work carried out during third phase of this project. In Chapter 2, the overall project objectives are listed. In Chapter 3 the tasks accomplished during first and second phase of this project are given. In Chapter 4 the PCCS operation modes are described. In Chapter 5, the experimental work and results of the experiments are presented. In Chapter 6 the analytical work on film wise condensation in vertical tube is given. In Chapter 7, the assessment of RELAP5 code against the experimental data is presented. In Chapter 8, the third year accomplishments are summarized.

1.3 References

1.1. Bruschi H J., AP600-safety through simplicity. [Conference Paper] Proceedings of the International Topical Meeting on Advanced Reactors Safety. ANS. Part vol.1, pp.3-8 vol.1. La Grange Park, IL, USA, (1997).

1.2. GE Nuclear Energy, SBWR Standard Safety Analysis Report, Report No. 25A5113 Rev. A, August, (1992).

1.3. Bandurski T. Dreier J. Huggenberger M. Aubert C. Fischer O. Healzer J. Lomperski S. Strassberger H-J. Varadi G. Yadigaroglu G. PANDA passive decay heat removal transient test results. Eighth International Topical Meeting on Nuclear Reactor Thermal-Hydraulics. NURETH-8. New Horizons in Nuclear Reactor Thermal-Hydraulics. Atomic Energy Soc. Japan. Part vol.1, pp.474-84 vol.1. Tokyo, Japan, (1997).

1.4. Yoshioka Y. Arai K. The analysis of PCCS heat removal performance for the 1300 MWe simplified BWR Eighth International Topical Meeting on Nuclear Reactor Thermal-Hydraulics. NURETH-8. New Horizons in Nuclear Reactor Thermal-Hydraulics. Atomic Energy Soc. Japan. Part vol.1, pp.468-73 vol.1. Tokyo, Japan (1997).

1.5. Uchida, H., Oyama, A., and Togo, Y., Evaluation of Post-Incident Cooling Systems of Light Water Reactors, Proc. 3rd Int. Conf. Peaceful Uses of Atomic Energy, Vienna, Austria, Vol. 13, p. 93, International Atomic Energy Agency (1964).

1.6. Wang, D. Y. and Tu, C. J., Effects of Noncondensable Gas on Laminar Film Condensation in a Vertical Tube, Int. J. Heat Mass Transfer, Vol. 31, 2339 (1988).

1.7. Denny, V. E., Mills, A. F. and Jusionis, V. J., Laminar Film Condensation from a Steam-Air Mixture Undergoing Forced Flow Down a Vertical Surface, J. Heat Transfer, Vol. 93, 297 (1971)

1.8. Al-Diwani, H. K. and Rose, J. W., Free Convection Film Condensation of Steam in the Presence of Noncondensing Gases, Int. J. Heat Mass Transfer, Vol. 16, 1359 (1973).

1.9. Siddique, M., The Effects of Noncondensable Gases on Steam Condensation under Forced Convection Conditions, Ph.D. Dissertation, Massachusetts Institute of Technology (1992).

1.10. Siddique, M., Golay, M. W., and Kazimi, M. S., Local Heat Transfer Coefficients for Forced Convection Condensation of Steam in a Vertical Tube in the Presence of a Noncondensable Gas, Nucl. Technol., Vol. 102, 386 (1993).

1.11. Vierow, K. M., Behavior of Steam-Air Systems Condensing in Concurrent Vertical Downflow, MS Thesis, Department of Nuclear Engineering, University of California at Berkeley (1990).

1.12. Ogg D. G., Vertical Downflow Condensation Heat Transfer in Gas-Steam Mixture, MS Thesis, Department of Nuclear Engineering, University of California at Berkeley (1991)

2. GOALS AND OBJECTIVES

The goals of this research are to: 1) obtain experimental data on the phenomenon of condensation of steam in a vertical tube in the presence of non-condensable for flow conditions of PCCS, 2) develop a analytical model for the condensation phenomena in the presence of non-condensable gas for the vertical tube, and 3) assess the RELAP5 computer code against the experimental data.

The objectives of the research are:

1. Design a well-scaled condensation test facility and identify PCCS condenser flow conditions based on scaling.
2. Obtain database on local and overall condensation heat transfer coefficient as a function of flow condition and inlet non-condensable gas concentration.
3. Develop an analytical model for condensation in the vertical tube in the presence of non-condensable gas for PCCS flow conditions.
4. Compare analytical predictions and experimental data on heat transfer coefficient.
5. Develop a correlation for heat transfer coefficient for condensation in the presence of non-condensable for use in codes.
6. Assess RELAP5 code against the experimental data.

3. FIRST AND SECOND YEAR ACCOMPLISHMENTS

First Year Accomplishment

Here the accomplishments of the first year are summarized.

- A detailed scaling analysis for the PCCS condenser was performed. The scaling parameters were identified to scale down the prototype condenser design. The effect of the non-condensable in the scaled condenser was discussed and its implication on the scaled test facility was presented.

- An experimental loop was designed with 5.04 cm inch diameter condenser. The design of the condenser tube was based on the scaling analysis. The test section and the loop were instrumented for required parameters.

- There was delay in completing the first year experimental task due to late start of the project. Permission was sought from DOE to extend the first year period 05/01/00 - 04/30/01 to 05/01/00 – 08/31/01, an extension of four months. DOE has granted an extension of four months to complete the first year task. Currently the test loop is being constructed and tested. The first year experimental task will be completed by August 31, 2001.

- A condensation model was developed for forced downflow of steam and non-condensable gas in vertical tube. First the model was tested for pure steam condensation and the predicted heat transfer results were compared with the experimental data. Then the model was tested for condensation in the presence of non-condensable gas, air, and results of the predictions were compared to the published experimental data. The agreement was fairly good. Please note that this modeling task falls in second year period. Since the first year task on experiments has been extended to be performed by four months, this period of work is taken care by the modeling task, which ultimately will be refined and studied in detail in second year.

Second Year Accomplishment

Here the accomplishments of the second year are summarized.

- Condensation tests were carried out for forced flow and no through flow conditions for 5.08 cm inch diameter condenser for pure steam with forced flow cooling on the secondary side. These tests were carried out to compare the results with existing data and verify the analytical condensation model.

- Condensation tests were carried out for forced flow condition and for no through flow conditions with non-condensable gas (air) and steam mixture. Data have been obtained for various non-condensable gas concentrations (0.1% -10%) and operating pressures (101 – 450 kPa). The data showed that the condensation rate decreased substantially for no through flow conditions.

- A condensation model was developed for forced downflow of steam and non-condensable gas in vertical tube. The model predictions on condensation heat transfer coefficient fairly agree with pure steam data (present and other) and with steam-noncondensable mixture data of MIT and UCB.

- The condensation model was tested with various interfacial friction factor correlations. The iteration based analytical interfacial friction factor results on heat transfer were compared with the heat transfer results from the existing correlations for the interfacial friction factor.

- Two new condenser test sections were designed and built. The diameters for these condenser tubes are 2.54 cm and 5.08 cm. These sections have the secondary side boiling water that provides constant wall temperature condition. Thus these test sections simulate the PCCS condenser wall heat transfer condition.

4. PCCS CONDENSER

Here the operation of the PCCS condenser is described to justify the experiments for different mode of condenser operation. A flow diagram of the PCCS is shown in Figure 4.1. The PCCS condensers condense steam from the drywell (DW) [4.1, 4.2]. They are immersed in a large interconnected Isolation Condenser System (ICS) pool of water. The ICS pool is located outside and above the containment. Condensed water produced in the PCCS condensers returns to the GDCS pool and then to the Reactor Pressure Vessel (RPV). Non-condensable gases from the PCCS are vented to the Suppression Pool (SP). The driving head of the PCCS is provided by the pressure difference between the DW and the SP. There are no valves or pumps in the PCCS and any operational actions or signals are not needed which makes the PCCS a truly passive system.

4.1 PCCS Operation

Three different operational modes are possible in the PCCS depending on the non-condensable gas concentration and the pressure difference between the DW and the SP. These are Bypass Mode, Continuous Condensation Mode and Cyclic Condensation and Venting Mode. The PCCS will be in Bypass Mode when the pressure difference between the DW and the SP is relatively high compared with the head due to the submergence of the vent line in the SP. This condition is realized during the blowdown process. In this mode, steam and non-condensable gas pass through the PCCS condensers with condensation. This mode of operation corresponds to forced convection. When the pressure difference between the DW and the SP is comparable with the head due to the submergence of the vent line in the SP, the PCCS will be in either Continuous Condensation mode or Cyclic Condensation and Venting Mode depending on the non-condensable gas concentration. The PCCS will be in Continuous Condensation Mode when the non-condensable gas concentration is very low. This condition will be obtained in the later stage of an accidental transient after most of non-condensable gas is vented to the SP.

The PCCS will be in Cyclic Condensation and Venting Mode when the non-condensable gas concentration is relatively high. This condition sets in immediately after the blow down process. In this mode, steam has enough time to be condensed in

the PCCS condensers. In the condensation process, non-condensable gas is accumulated in the PCCS condensers. Hence the DW pressure begins to rise as the condensation decreases. The DW pressure continues to increase after the condensation process totally stops. When the pressure difference is high enough to overcome the head due to submergence of the vent line in the SP, non-condensable gas is vented to the SP. The condensation process begins again after clearing of non-condensable gas from the PCCS. This cycle repeats. Thus the forced convection flow condensation is one of three PCCS flow conditions.

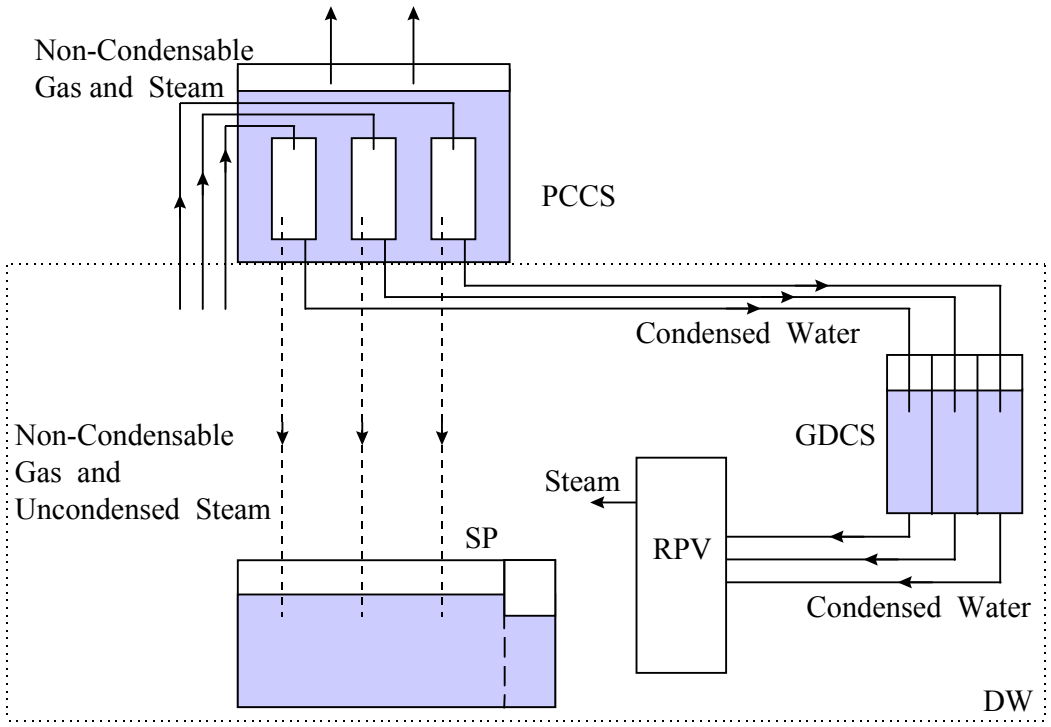

Figure 4.1. Flow diagram in SBWR during a loss of coolant accident

4.2 References

4.1 GE Nuclear Energy, "SBWR Standard Safety Analysis Report," Report No. 25A5113 Rev. A, August, (1992).

4.2 Ishii, M., Revankar S. T., Dowlati, R., Bertodano, M. L., Babelli, I., Wang, W., Pokharna, H., Ransom, V. H., Viskanta, R., Wilmarth, T., Han, J. T.," Scientific Design of Purdue University Multi-Dimensional Integral Test Assembly (PUMA) for GE SBWR," Purdue University Report PU-NE-94/1, U.S. Nuclear Regulatory Commission Report NUREG/CR-6309, (1996).

5. EXPRIMENTAL PROGRAM

The experimental program consists of design of the experimental loop, setting up experimental procedures, performing condensation tests with and without non-condensable gas and data analysis.

5.1 Experimental Loop

The schematic of the experimental set-up is shown in Figure 5.1. The test loop is comprised of boiler vessel, instrumented condenser test section with secondary pool boiling section, condensate tank, suppression pool, blowdown & secondary steam dump tank, air supply line, secondary steam dump line and associated piping.

Steam Generator

The steam generator (SG) is made of schedule 10, 4.06 m (16 inch) diameter stainless steel pipe. Its total length is 2.26 m. An immersion type sheathed electrical heater of 10kW capacity is mounted at the lower flange of this vessel. The vessel is instrumented with thermocouples, pressure gauge and DP cells to measure and monitor temperature, pressure and water level. Sight glass is also mounted on mid level of the steam generator. The power to the heater is measured with A.C. Voltmeter and Ammeter. A relief valve is mounted at the 25.4 mm piping connected to the upper shell of steam generator. The set pressure of the relief valve is 200 psig. Downstream of the relief valve is routed to blowdown & secondary steam dump tank. The detail design drawings of the steam generator design are presented in Ref. 5.1.

Test Section

The specific design of the PCCS condenser tube test section (T/S) was based on the scaling analysis. Tube diameter is 47.5 mm ID, 50.8 mm OD. A height scaling of 1/2 was taken in the present design. The assembly and the detailed dimensioned design drawings for the 25.4 mm condenser tube design with secondary pool boiling are shown in Figs. 5.2 to 5.5. In Fig. 5.6, the

photograph of the 25.4 mm and 50.8 mm condenser tubes and the secondary pool tank are shown. Pool boiling test section is comprised of two subassemblies. One is the condenser outside tube where the boiling takes place and the other is inside condenser tube where the condensation takes place.

The condenser outside tube is common for 25.4 mm and 50.8 mm test section. The outside tube is made of 152.4 mm (6 inch) schedule 10 Type 304 stainless steel pipe with a top flange and a bottom plate welded to the pipe. The top flange is a 279.4 mm (11 inch) diameter and 25.4 mm thickness with a 168 mm (6.625 inch) inside hole and 8 bolt holes. The bottom plate is a 168 mm (6.625 inch) diameter and 6.35 mm (¼ inch) thickness with a 60.3 mm (2.375 inch) inside hole and 4 bolt holes. Along the outside surface of the 152.4 mm (6 inch) pipe, various nozzles for thermocouple, sight glass, feed, drain, and steam exit are installed. The three 38.1 mm (1.5 inch) diameter steam exit nozzles are located at the almost top level of pipe with 120 degree each other.

The inside condenser tube for 25.4 mm test section is made of 25.4 mm schedule 40 Type 304 stainless steel pipe and 101.6 mm (4 inch) schedule 10 Type 304 stainless steel pipe with a top flange welded to 25.4 mm pipe, another top flange welded to 101.6 mm (4 inch) pipe, a middle plate welded to both 25.4 mm and 4 inch pipe and a bottom flange welded to 25.4 mm pipe. The top flange welded to 25.4 mm pipe is for the connection with upstream piping. The top flange welded to 101.6 mm (4 inch) pipe is connected to the top flange of the condenser outside tube. It has 8 bolt holes and 3 holes for thermocouple line outlet. The middle plate welded to both 25.4 mm and 101.6 mm (4 inch) pipe act as a border of condenser. 25.4 mm (1 inch) pipe below this plate is an actual condenser. The gap between 101.6 mm (4 inch) and 25.4 mm pipe above this plate will be filled with insulation material. The bottom flange welded to 25.4 mm pipe is connected the bottom plate of the condenser outside tube. For this connection, 4 bolts are welded to the top surface of the bottom flange. At the top and bottom of the inside tube assembly pressure measurement taps are installed.

Active tube length of condensing is 0.978 m (38.5 inch). Along the active tube, 5 nozzles for inside bulk temperature measurement are welded at different axial and circumferential location. At the opposite side of the nozzle, a thermocouple junction is made to measure the tube outside wall temperature at 5 axial locations.

For 50.8 mm test section, the outside tube assembly is common with 25.4 mm test section. The inside tube assembly has basically the same design with 25.4 mm test section. The differences are 50.8 mm schedule 40 pipe instead of 25.4 mm pipe and two 50.8x25.4 mm reducers are welded between 50.8 mm condenser pipe and 25.4 mm connecting pipe.

Steam and Air Supply Line

The steam supply line to the condenser is made of 25.4 mm (1 inch) stainless steel pipe except the upstream and downstream piping of vortex flow meter. Since the diameter of the vortex flow meter is 19 mm (¾ inch), the upstream and downstream piping of vortex flow meter is also 19 mm (¾ inch) piping. To minimize the flow disturbance effect on the flow meter, the length of 19 mm (¾ inch) upstream piping was selected as greater than the required L/D specified in flow meter installation manual. To determine the flow condition at vortex flow meter, pressure transducer and thermocouple are installed at the downstream of the vortex flow meter. The sensing line to this pressure transducer is routed upward to drain the condensate in the sensing line.

Air supply line is connected to the steam line and suppression pool. Before the connection to steam line, three rotameters with different flow ranges are installed to measure the wide range of air flow rate. A pressure gauge and a thermocouple are also installed to measure pressure and temperature of air.

Pressure tabs are made at upstream and downstream piping of the test section to measure the test section differential pressure. A pressure gauge is also installed at the downstream piping of the tube. To collect the condensate in the DP sensing line, the sensing lines to DP transducer are routed upward and condensate drain lines are connected to the high and low pressure side of sensing lines. If condensate fills the sensing line, normally closed drain valves are opened to drain the condensate.

Condensate Tank

The condensate tank (CT) collects the condensate. It is made of Schedule 10, 3.05 m (4 inch) pipe and is mounted vertical. The water level in the suppression pool can be maintained at desired level by continuous bleeding water from the tank.

Suppression Pool

The suppression pool (SP) serves as a collector of the noncondensable gas and the uncondensed steam. During the complete condensation mode, the suppression pool is isolated from the condensing loop. It is made of Schedule 10, 3.05 m (12 inch) pipe and is mounted vertical. The water level in the suppression pool can be maintained at desired level by continuous bleeding water from the tank. The condenser operating pressure is set by the pressure level in the suppression pool. An airline is connected to the suppression pool to set the pressure higher than the atmosphere pressure. A blowdown line is connected to blowdown & secondary steam dump tank. The suppression pool is instrumented with thermocouple, pressure gauge and DP cells to measure and monitor temperature, pressure and water level. The detail design drawings of the suppression pool are presented in Ref. 5.1.

Blowdown & Secondary Steam Dump Tank

The blowdown & secondary steam dump tank (BDT) is made of 5mm thick stainless steel plate with 0.61 m (24 inch) width, 0.61 m (24 inch) depth and 0.91 m (36 inch) height. It serves as heat & mass sink and de-ionized water storage. By use of pump, de-ionized water in this tank is supplied to steam generator, suppression pool, secondary pool, condensate tank and instrument sensing line. Water in SG, SP, CT, and secondary pool can be drained to this tank by gravity. The discharges from relief valve at steam generator and from steam/gas space of suppression pool are routed to this tank for the blowdown purpose. The discharge line is submerged into the water space of blowdown & secondary steam dump tank. The secondary steam generated in the test section is also discharged to this tank through 3 independent 1.25 inch copper tubings. To cool the water in BDT, ½ inch copper tubing is submerged in the BDT and the city water flow through the tube.

Table 5.1 List of Instruments

Variable	Process	Instrument	Tag. No.
Flow Rate	Steam	Vortex Flow Meter	FT1
	Air	Rotameter	FA1, FA2, FA3
Pressure	SG	Pressure Gauge	PG1
	Vortex Flow Meter	Pressure Transducer	PT1
	SP	Pressure Gauge	PG2
	CT	Pressure Gauge	PG3
	Air Supply line	Pressure Gauge	PG4
Water Level	SG	DP Transducer	LT1
	SP	DP Transducer	LT2
	CT	DP Transducer	LT3
	Secondary Pool	DP Transducer	LT4
Temperature	SG	Thermocouples	TS1, TS2
	Vortex Flow Meter	Thermocouple	TS3
	Test section	Thermocouples	TS4-TS8, TW1-TW5, TP1-TP6
	Air line	Thermocouples	TA1
	CT	Thermocouples	TS9-TS11
	SP	Thermocouples	TS12
DP	Test section DP	Pressure Transducer	DP1
Power	Heater	Voltmeter and Ammeter	-

Description of Instrument

Temperature :

TS1 : SG water temperature

TS2 : SG steam temperature

TS3 : Vortex flow meter downstream temperature

TS4 ~ TS8 : Test section steam bulk temperature (TS4-top, TS9-bottom)

TS9 ~ TS11 : Condensate tank temperature (TS9-center, TS11-bottom)

TS12 : SP water temperature

TW1 ~ TW5 : Condenser tube outside wall temperature (TW1-top, TW5-bottom)

TP1 ~ TP3 : secondary side pool temperature (above test section, TP1-top)

TP4 ~ TP6 : secondary side pool temperature (test section, TP6-bottom)

TA : Air supply line temperature

Pressure & Differential Pressure

PT1 : Vortex flow meter downstream pressure (pressure transducer)

PG1 : SG pressure (pressure gauge)

PG2 : Condensate Tank pressure (pressure gauge)

PG3 : SP pressure (pressure gauge)

PG4 : Air supply line pressure (pressure gauge)

DP1 : Test Section DP

Level

LT1 : SG water level
LT2 : SP water level
LT3 : Condensate Tank water level
LT4 : Secondary side pool water level

Flow

FT1 : Vortex flow meter for steam flow measurement
FA1 : Rotameter for air flow rate measurement (high flow)
FA2 : Rotameter for air flow rate measurement (medium flow)
FA3 : Rotameter for air flow rate measurement (low flow)

Description of Valves

Valve type and normal position (NO-normal open, NC-normal closed) are shown in parenthesis.

Steam Line

VS1 : Steam flow control valve (ball, NO)
VS2 : Steam flow control valve (needle, NO)
VS3 : Steam/noncondensable vent valve to SP (ball, NO)

Air Supply Line

VA1 : Air supply line valve (ball, NO)
VA2 : Air supply line valve downsteam flowmeter (needle, NC)
VA3 : Air supply line valve just before main steam supply line (ball, NC)
VA4 : Air supply line valve to the SP (ball, NC)

Water Feed and Drain Line

VD1 : Water feed line valve from BDT (needle, NO)
VD2 : Water feed line valve to SG (ball, NC)
VD3 : Water feed line valve to SP (ball, NC)
VD4 : Water feed line valve to secondary pool (ball, NO)
VD5 : Water feed line valve to instrument sensing line (ball, NC)
VD6 : Water drain line valve from SG (ball, NC)
VD7 : Water drain line valve from SP (ball, NC)
VD8 : Water drain line valve from CT (ball, NC)
VD9 : Water drain line valve from secondary pool (ball, NC)
VD10 : Water feed line valve to secondary pool (ball, NC)

Steam/Air Blowdown Line

VB1 : SG relief valve (relief, NC)
VB2 : SP blowdown valve to BDT (ball, NC)
VB3 : SP blowdown valve to atmosphere (needle, NC)
VB4 : SP blowdown valve to atmosphere (ball, NC)

5.2 Test Procedures

The test procedures are prepared fot the preparatory work, testing and shut down.

5.2.1 Preparatory Work:

The preparatory work is comprised of the following steps: (1) filling steam generator, (2) filling suppression pool, (3) filling secondary pool and (4) purging of the instrument line. The following lists the tasks in each of the preparatory steps.

1. Steam Generator Filling

- Check and verify the normal valve position
- Open VB3 and VB4 for the initial feed operation (These valve should be opened to bleed the air in the loop for the water filling)
- Open VD2 to fill steam generator
- Fill steam generator monitoring the level using sight glass and LT1 signal
- Close VD2

2. Suppression pool Filling

- Open VD3
- Fill suppression pool monitoring the level using LT2
- Close VD3

3. Secondary Pool Filling

- Open VD9
- Fill secondary pool monitoring the level using sight glass and LT4 signal
  Note : Do not fill the full height. Just fill the ¾ of the full height. Due to the thermal stratification during heating, it is more efficient to heat this level of water first and then fill again the remaining height.
- Close VD9

4. Instrument Line Purging

- Open VD5

- Turn on pump
- Fill and vent the air in the instrument sensing lines for each level transducer (LT1~LT4).
  1) Fill the water using the instrument sensing line valves for high pressure side
  2) Vent air in sensing line using transmitter venting screw for high pressure side
  3) Fill the water using the instrument sensing line valves for low pressure side
  4) Vent air in sensing line using transmitter venting screw for low pressure side

  Note : When filling the condensate tank level instrument, establish the initial CT level by monitoring LT3 signal.
- Close VD5
- Close VB3 and VB4 which were opened for the initial feed operation

5.2.2 Testing

The procedures for the test operations are given below.

1) SG Heating
- Check the normal valve position
- Close VS1
- Turn on heater
- Set the heater controller setpoint about 240C.

2) SG Venting
- When SG water temperature, TS1, reach about 100C, open VS1 for several seconds to vent the air in the SG.
- Verify the SG water temperature, TS1, and SG steam temperature, TS2, are almost same.

3) Loop Heating
- When SG pressure (PG1) reaches about 150 psig, slightly open VS1 to heat up the loop and secondary water pool
- If necessary, close vent valve to SP, VS3, to increase the loop system pressure.

Note : At low pressure, the heat transfer rate to secondary side is small. So, it needs to increase the system pressure (recommended pressure – 30 psig from PG2 reading).

- When the secondary water temperatures (TP4 and TP5) reach about 90C, regulate the VS1 to establish the required steam flow rate.
- When the secondary water temperatures (TP4 and TP5) reach about 100C, fill the secondary pool to the full height by turning on the pump and opening VD10.
- Close VD10
- Turn off the pump
- Open the city water supply valve to cool the BDT

  Note :

  1) During the loop heating, vent the air in the loop several times by opening the VS3 to establish the pure steam condition in the loop
  2) During the loop heating, periodically drain the CT water by opening BD8 if the condensate fill enough the CT

4) Steady State Condition

- Check the steam flow rate to verify the steady state
- Check the steam temperature at flowmeter (TS3) to verify the steady state and the superheat condition
- Check the secondary water pool temperature to verify the steady state (TS4~TS6 should be almost same temperature)
- Check the test section pressure (PG2) to verify the steady state

5) Initial Condition and Test Method for each Operation Mode

A. Complete Condensation Mode

- Verify that the VS3 is closed
- Verify that the air in the loop has been vented during the heating period
- Verify the steady state condition described in 4)
- Do the data log described in 6)

B. Periodic Venting Mode

- Initially establish the Complete Condensation Mode described above
- Open VA3
- Regulate FA1 ~ FA3 to obtain required small amount of air flow
- Select the base pressure, vent DP (Usually 0.5 psi) and measurement duration
- Start to log the data
- Open VS3 to reduce the test section pressure below the base pressure
- Use stop-watch to log the periodic vent time interval. When the test section pressure reach the base pressure, reset the stop-watch. (start time)
- When the test section pressure reach the base pressure + vent DP, quick open the VS3
- When the test section pressure decrease below to the base pressure, quick close the VS3

Note : To maintain the vent DP properly, it needs some undershooting in the pressure before close the VS3.

- Count the vent number in mind
- Repeat the periodic venting until the predetermined measurement duration
- Log the number of vent and the measurement duration.

C. Through Flow Mode

- Verify that the VS3 is opened
- Open VA3 for noncondensable gas test and regulate FA1 ~ FA3 to obtain required amount of air flow
- Maintain the test section pressure at a desired level by use of the blowdown valves (VB2 ~ VB4) or air supply line valve (VA4)
- Verify the steady state condition described in 4)
- Do the data log described in 6)

6) Data Log

- When the initial condition is obtained for each operating mode, start to record the DAS.
- Fill the log sheet

Note :

1) During the test, check the test section DP signal. If the condensate fills the DP sensing line, DP output will not show correct signal. For this condition, open the condensate drain valve to drain condensate in the sensing line.
2) During the test, periodically fill the secondary pool with water by use of VD10
3) During the test, periodically drain the condensate tank water by use of VD8

5.2.3 Shutdown Operation

The following are the tasks in shutdown of the facility after the test.

1) Loop Cooling

- Turn off the heater
- Close VA3 if necessary
- Wide open VS1
- Open VB2 if necessary
- Periodically fill the secondary pool with water by use of VD10
- Periodically drain the condensate tank water by use of VD8
- When system pressure reach to almost 1 atm, open VB3 & VB4.
- When no steam is generated from the system, close the city water supply line valve

2) Drain

- Drain the secondary pool water when its temperature decreases below 60C
- Drain SG, SP, and CT water into the BDT if necessary.

5.3 Data Reduction

The overall heat transfer coefficient in condenser is defined as follows:

$$U = \frac{Q_{con}}{A_i\left(T_{SAT} - T_P\right)} \quad , \tag{5.1}$$

where Q_{con} is the condensation heat transferred by condenser tube, A_i is the heat transfer area of tube inside, T_{SAT} is the saturation temperature at the steam partial pressure (P_{SAT}) and T_P is the secondary pool water temperature.

The condensation heat transferred by condenser tube, Q_{con} can be calculated as follow:

$$Q_{con} = m_{con} h_{fg}(P_{SAT}), \tag{5.2}$$

where m_{eva} is the condensation mass flow rate calculated from the condensate tank water level difference during the test and $h_{fg}(P_{SAT})$ is the latent heat of condensation based on the steam partial pressure P_{SAT}. The condensation mass flow rate can be checked by the comparison with the supplied steam flow rate during the complete condensation mode.

This condensation heat transfer rate should be equal to the secondary side heat removal rate, Q_{tot}, which is sum of the evaporative heat transfer rate and the heat loss from the secondary tube surface.

$$Q_{con} = Q_{tot} \tag{5.3}$$

$$Q_{tot} = m_{eva} h_{fg}(T_P) + Q_{hl}, \tag{5.4}$$

where m_{eva} is the evaporative mass flow rate calculated from the secondary pool water level difference during test, $h_{fg}(T_P)$ is the latent heat of evaporation based on the secondary pool water temperature, and Q_{hl} is the heat loss rate loss from the secondary tube surface obtained from the heat loss measurement test.

The heat transfer area of tube inside, A_i, can be calculated as follows:

$$A_i = \pi D_i H_{tube} \ . \tag{5.5}$$

The measured steam bulk temperature was slightly higher than the saturation temperature at the system pressure. It means that the state of the steam-air mixture is superheat. However, the

amount of sensible heat transfer is much less than that of condensation heat transfer. So, the sensible heat transfer is ignored.

The overall heat transfer coefficient is given by the following equation derived by the heat balance among the condenser tube inside, tube wall and tube outside.

$$U=\left[\frac{1}{h_c}+\frac{1n\left(D_o/D_i\right)D_i}{2k_w}+\frac{D_i}{h_{\sec}D_o}\right]^{-1} . \tag{5.6}$$

The first term of the right hand side of above equation corresponds to the tube side condensation heat transfer, the second term corresponds to the tube wall conduction heat transfer, and the third term corresponds to the secondary side pool boiling heat transfer.

Neglecting the heat transfer along condenser tube length, the condensation heat transfer coefficient, h_c, is defined as follows:

$$h_c=\frac{Q_{con}}{A_i\left(T_{SAT}-T_{Wi}\right)} , \tag{5.7}$$

where T_{Wi} is the tube inside wall temperature.

The secondary side pool boiling heat transfer coefficient, $h_{\sec}$, is defined as follows:

$$h_{\sec}=\frac{Q_{con}}{A_o\left(T_{Wo}-T_P\right)} , \tag{5.8}$$

where T_{Wo} is the tube outside wall temperature and A_o is the heat transfer area of tube outside.

A_o is expressed as follows:

$$A_o=\pi D_o H_{tube}=\frac{D_i}{D_o}A_i \quad . \tag{5.9}$$

From equation (5.6), the condensation heat transfer coefficient can be expressed as follows:

$$\frac{1}{h_c}=\frac{1}{U} \quad - \quad \frac{1n\left(D_o/D_i\right)D_i}{2k_w} \quad - \quad \frac{D_i}{h_{\sec}D_o} \tag{5.10}$$

Substituting eqs. (5.1), (5.2), (5.3), (5.8) and (5.9) to eq. (5.10), the condensation heat transfer coefficient can be simplified as follows:

$$\frac{1}{h_c} = \frac{A_i(T_{SAT} - T_P)}{m_{con} h_{fg}(P_{SAT})} - \frac{1n(D_o/D_i)D_i}{2k_w} - \frac{D_i A_o(T_{Wo} - T_P)}{D_o m_{con} h_{fg}(P_{SAT})}$$

$$= \frac{A_i(T_{SAT} - T_P)}{m_{con} h_{fg}(P_{SAT})} - \frac{1n(D_o/D_i)D_i}{2k_w} - \frac{A_i(T_{Wo} - T_P)}{m_{con} h_{fg}(P_{SAT})}$$

$$= \frac{A_i(T_{SAT} - T_{Wo})}{m_{con} h_{fg}(P_{SAT})} - \frac{1n(D_o/D_i)D_i}{2k_w}$$

$$= \frac{2k_w A_i(T_{SAT} - T_{Wo}) - m_{con} h_{fg}(P_{SAT}) 1n(D_o/D_i)D_i}{2k_w m_{con} h_{fg}(P_{SAT})}$$

Finally, the condensation heat transfer coefficient can be expressed with the known or experimentally obtainable values as follows:

$$h_c = \frac{2k_w m_{con} h_{fg}}{2k_w \pi D_i H_{tube}(T_{SAT} - T_{Wo}) - m_{con} h_{fg} 1n(D_o/D_i)D_i} \quad . \tag{5.11}$$

The condensation mass flow rate can be calculated with the following equation.

$$m_{con} = \frac{\Delta H_{ref}}{\Delta t} \rho_{ref} A_{CT} \tag{5.12}$$

where ΔH_{ref} is the condensate tank level difference converted to the reference temperature (4C) condition, Δt is the measurement time, ρ_{ref} is the density at the reference temperature, and A_{CT} is the cross-sectional area of the condensate tank.

Air mass flow can be calculated and then the non-condensable gas mass fraction can be determined.

$$m_{air} = \rho_{air} V_{air} \ , \tag{5.13}$$

$$V_{air} = F_{air} \sqrt{\frac{T_{ref}}{T_{mes}} \frac{P_{mes}}{P_{ref}}} \ , \tag{5.14}$$

$$W_{air} = \frac{m_{air}}{m_{air} + m_{steam}} \ , \tag{5.15}$$

where F_{air} is the air flow reading from rotameter, T_{ref} is the absolute temperature at standard condition (294K or 530R), T_{mes} is the absolute temperature of air, P_{ref} is pressure at standard condition (1 atm or 14.7 psia), P_{mes} is the measured pressure of air and m_{steam} is the steam inlet mass flow rate measured by vortex flow meter.

Vapor partial pressure can be calculated from Gibbs-Dalton ideal gas mixture equation as follow:

$$\frac{P_{SAT}}{P_{TOT}} = \frac{1 - W_{air}}{1 - W_{air}\left(1 - \frac{M_v}{M_a}\right)} \tag{5.16}$$

where, P_{TOT} is the total pressure which is the sum of the vapor partial pressure and air partial pressure, M_v and M_a are the molecular weight of the vapor and air, respectively.

Inlet steam Reynolds number and average condensation Nusselt number can be calculated with the following equation.

$$\mathrm{Re}_{steam} = \frac{\rho_{steam} V_{steam} D_i}{\mu_{steam}} = \frac{4 m_{steam}}{\pi D_i \mu_{steam}} \tag{5.17}$$

$$Nu_c = \frac{h_c D_i}{k_{condensate}}, \tag{5.18}$$

where μ_{steam} is the viscosity of steam and $k_{condensate}$ is the thermal conductivity of the condensate film.

The experimental error associated with the average condensation heat transfer coefficient was conservatively estimated to be ±20%. Detail analysis is shown in Appendix A.

5.4 Test Results

Condensation experiments were performed for three PCCS operation modes, i.e., 1) Through flow mode, 2) Periodic venting mode, and 3) Complete condensation mode. The complete condensation mode was performed for the pure steam condition varying the inlet steam flow rate. For a given steam flow rate in this mode, the system pressure is uniquely determined by the heat removal capacity of the condenser. The periodic venting mode was initiated from the complete condensation mode by putting small amount of air. Through flow mode was performed varying the inlet steam flow rate, inlet air flow rate, and system pressure.

1) Complete Condensation Mode

To obtain the complete condensation condition, the vent line valve (VS3) to the SP is closed during the experiment. For a given inlet steam flow rate, the system pressure is uniquely determined by the heat removal capacity of the condenser. If the inlet steam flow rate is large, the system pressure increases to condense all the steam.

Fig. 5.9 ~ 5.11 show the representative raw temperature data. Fig. 5.9 shows the steam bulk temperature at the vortex flow meter (TS3) and condenser tube (TS4 ~ TS8). At this specific case, the system saturation temperature is 130C. As shown in this figure, the test section steam bulk temperature is slightly superheated (3~6C) and decreases with the condenser length. Temperature at the vortex flow meter (TS3) is highly superheated. This high superheat condition can be obtained by maintaining the SG at high pressure (150 ~ 160 psig) and by choking the steam from the SG. Also, this high superheat condition makes it possible to eliminate the pre-heater of the air supply line. Without the pre-heater, high superheat steam has enough heating capacity to heat up the air from ambient temperature to slightly superheat condition. Fig. 5.10 shows the condenser tube outside wall temperature. The overall trend of the outside wall temperature is the increase of temperature with the condenser length except the TW4. Fig. 5.11 shows the secondary pool temperature. Temperatures above the active condenser (TP1 ~ TP3) are about 101 ~ 101.5C. It means the secondary pool is almost saturated at 1 atmospheric pressure or slightly pressurized but the degree of pressurization is very small. Temperatures at

the active condenser (TP4 ~ TP6) are about 102 ~ 103C. These temperatures correspond to the saturation temperature considered the water head of the secondary pool.

Fig. 5.12 shows the mass balance between the steam flow rate measure from vortex flow meter and the condensation rate calculated from the condensation tank level measurement. For the complete condensation mode, the steam flow rate must be equal to the condensation rate since the vent valve (VS3) is closed during the measurement. At low flow condition, steam flow rate is significantly smaller than the condensation rate. This is the general phenomenon for the vortex flow meter. Except this small flow region, the steam flow rate is generally greater than the condensate flow rate about 5%.

Fig. 5.13 and 5.14 show the energy balance between the condensation heat transfer rate calculated by the condensation rate and the evaporation heat transfer rate calculated by the secondary pool evaporation rate (+ heat loss measurement). These data include the through flow mode data as well as complete condensation mode data.

Fig. 5.15 shows the condensation rate and steam flow rate with system pressure and Fig. 5.16 shows the system pressure with the condensation rate. From these two figures, it is evident that system pressure is a function of the inlet steam flow rate, i.e., the condensation rate for a complete condensation mode. As steam flow rate increases at complete condensation mode, system pressure also increases. This results in the increase of heat removal rate. Fig. 5.17 shows the condensation heat transfer rate with the system pressure.

Fig. 5.18 shows the various heat transfer coefficient for the complete condensation mode with system pressure and Fig. 5.19 shows the measured secondary pool temperature (Tpool), the condenser outside wall temperature (Two), steam saturation temperature (Tsat) and the calculated tube inside wall temperature (Twi) with system pressure. The overall HTC remains almost constant since the temperature difference (Tsat-Tpool) increases with the same rate of heat removal. The tube outside wall temperature increases slightly with system pressure. So the secondary HTC increases with the same rate of heat removal. The calculated inside wall temperature also increase and the temperature difference (Tsat-TWi) increases more rapidly than the increase of heat removal rate. So, condensation HTC decreases with increase of system pressure.

2) Periodic Venting Mode

Periodic venting mode is initiated from the Complete Condensation Mode by putting small amount of air. As the noncondensable air is accumulating in the system, the condensation performance is degraded and this lead to the increase of the system pressure. Besides this effect, adding the air itself also increases the system pressure. For the prototype SBWR, the PCCS vent line is submerged in the SP with 800mm depth from the SP water surface. It corresponds to approximately 1 psi hydrostatic head. If the drywell pressure is greater than the SP pressure by this amount of the hydrostatic head, the noncondensable gas and uncondensed steam in the PCCS will be vented to the SP. During the venting, the noncondensable gas in the PCCS is cleared and the DW pressure decreases. After the venting, the pressurization in the DW resumes and this cycle repeats. Our test facility is designed for ½ height scaling, the head due to submergence of the vent line (DPvent) in the SP is 0.5 psi. So, when the pressure increases about 0.5 psi from the base pressure, the vent line valve (VS3) is quickly opened by manually to discharge the air and decrease the pressure. After the venting, the vent valve is quickly closed by manually. This process is repeated for the pre-determined test time.

Periodic Venting Data

Figs. 5.20 ~ 5.24 show the results of the periodic venting mode with different amount of noncondensable gas input at the system pressure is 0.305 MPa. These tests are conducted for DPvent = 0.5 psi and 1.0 psi. Fig. 5.20 shows the vent frequency. As the noncondensable mass fraction increases, the vent frequency also increases. The vent frequency for DPvent = 0.5 psi is greater than that for DPvent = 1.0 psi. Fig. 5.21 shows the venting period which is the inverse of the vent frequency. As the noncondensable mass fraction increases, the vent period decreases. For a limiting case, if the noncondensable gas fraction is large enough, the venting period will go to zero. It means the continuous venting, i.e., through flow mode. For a opposite limiting case, if the noncondensable gas fraction go to zero, the venting period will go to the infinite. It means no venting, i.e., continuous condensation mode. Therefore, through flow mode and continuous condensation mode can be considered as one of the limiting condition of the periodic venting mode. It suggests the possibility of combining all three PCCS operation modes into one universal condensation heat transfer model.

Figs. 5.22 and 5.23 shows the condensation rate and condensation heat transfer rate, respectively. Fig. 5.24 shows the condensation heat transfer coefficient. It is clear that the condensation performance is degraded with the noncondensable gas fraction. For a given air fraction, the condensation performance of large DPvent is slightly better. This is mainly due to the fact that the average system pressure for large DPvent is higher than that of small DPvent. The periodic venting mode test was performed between the base pressure (0.305 MPa for this case) and the base pressure + DPvent. However, for the condensation HTC, it is very hard to find the effect of the different DPvent.

Complete Condensation + Periodic Venting + Through Flow Data

Figs. 5.25 ~ 5.44 show the results of the 3 PCCS operation modes, i.e., the complete condensation, periodic venting, and through flow mode at a given system pressure and steam flow rate. In these figures, 5 sets of data for different system pressure (0.194, 0.24, 0.32, 0.35, 0.39 MPa) are presented. For each pressure condition, 4 figures show the vent frequency and period, the condensation rate, the condensation heat transfer rate, and the condensation HTC.

Vent frequency increases and vent period decreases with the noncondensable mass fraction. For a given noncondensable mass fraction, vent frequency increases with system pressure. For P=0.194 MPa, we can obtain the periodic vent data up to Wair = 3%. For P=0.39 MPa, the maximum obtainable Wair is obout 0.5% for the periodic vent mode. It means that for high system pressure, through flow condition can be easily obtained for small noncondensable gas fraction and continuous condensation mode is hardly obtained. For low system pressure, the noncondensable gas fraction range for the periodic vent mode is relatively wide and the continuous condensation mode can be easily obtained.

From the figures the condensation rate, the condensation heat transfer rate, and the condensation HTC, the condensation performance for the through flow mode show slightly better results than the periodic vent mode at a same noncondensable gas mass fraction. However, the degree of the improvement is very small and within the measurement error. It should be also noted that the periodic vent mode data and through flow data can be joined smoothly at the maximum noncondensable gas fraction for the vent mode. This phenomenon is shown very well in the Figs. 5.42 ~ 5.44. For this data set, the through flow mode data are obtained for very low

noncondensable gas fraction to compare directly with periodic venting mode. As shown in these figures, there is almost no difference between the through flow and periodic vent mode. As noted previously, this result suggests the possibility of combining all three PCCS operation modes into one universal condensation heat transfer model.

3) Through Flow Mode

For the through flow mode, the vent line valve (VS3) is always opened to vent the air and the uncondensed steam to the SP. Some data for the through flow mode are already presented in the previous section to compare with the periodic venting mode data. In this section, additional data are shown to see the effects of the noncondensable gas mass fraction, system pressure, inlet steam flow rate.

Pure Steam Data as a Function of Pressure

Figs. 5.45 ~ 5.48 show the effect of system pressure for pure steam condition (inlet steam flow rate = 4.96 g/s) for through flow mode. As shown in Figs. 5.45 and 5.46, the condensation rate and condensation heat transfer rate are almost linearly increasing with system pressure. Fig. 5.47 shows the various heat transfer coefficients with system pressure. Overall HTC is almost constant with system pressure. Secondary HTC increases with system pressure and condensation HTC decreases with system pressure. This trend is very similar to the results of complete condensation mode as shown in Figs. 5.17 ~ 5.19. Fig. 5.48 shows the measured secondary pool temperature (Tpool), the condenser outside wall temperature (Two), steam saturation temperature (Tsat) and the calculated tube inside wall temperature (Twi) with system pressure. The overall HTC remains almost constant since the temperature difference (Tsat-Tpool) increases with the same rate of heat removal. The tube outside wall temperature increases slightly with system pressure. So the secondary HTC increases with the same rate of heat removal. The calculated inside wall temperature also increase and the temperature difference (Tsat-TWi) increases more rapidly than the increase of heat removal rate. So, condensation HTC decreases with increase of system pressure.

Effect of Noncondensable Gas

Figs. 5.49 ~ 5.51 show the Effects of noncondensable gas mass fraction for P=0.28 MPa, Msteam=3.6 g/s. As shown in these figures, the noncondensable gas degrades the performance of the condensation.

Effect of Steam Flow Rate

Figs. 5.52 ~ 5.54 and Figs. 5.55 ~ 5.58 show the Effects of noncondensable gas mass fraction and steam flow rate for P=0.34 MPa and P=0.26 MPa, respectively. From these figures, the condensation performance and condensation HTC increase with inlet steam flow rate.

Effect of System Pressure

Figs. 5.59 and 5.60 show the condensation heat transfer rate and the condensation HTC, respectively, with noncondensable mass fraction for difference system pressure at Msteam=3.8 g/s. As shown in Fig. 5.59, the condensation heat transfer rate increases with system pressure. However, the condensation HTC decreases with system pressure from Fig. 5.60.

Figs. 5.61 ~ 5.63 show the effects of system pressure at Msteam=2.5 g/s, Wair=0.2% condition. These figures also show that the condensation heat transfer rate increases with system pressure, but the condensation HTC decreases with system pressure.

5.5 Vent Analysis

If small amount of noncondensable gas is added at a steady state complete condensation mode, the pressure is increase. This increase in pressure comes from two sources. One is due to the addition of the noncondensable gas itself. Since it is not condensable, the gas is accumulated in the system and it makes one part of the pressure increase. The other is due to the addition of steam in the system caused by the degradation of the condensation. At a complete condensation condition, all steam is condensed. So there is no actual steam accumulation in the system. As small amount of the noncondensable gas is added in the system, the condensation performance is degraded, i.e., some amount of steam is not condensed. The uncondensed steam acts as a second source of system pressure increase.

In Appendix B, the pressurization caused by the addition of the noncondensable gas is analyzed based on the ideal gas law.

5.6 Reference

5.1 S. T. Revankar, and S. Oh, Analytical and Experimental Study of the Effects of Non-Condensable in a Passive Condenser System for the Advanced Boiling Water Reactor, PU/NE-02-10, Sep. 2002.

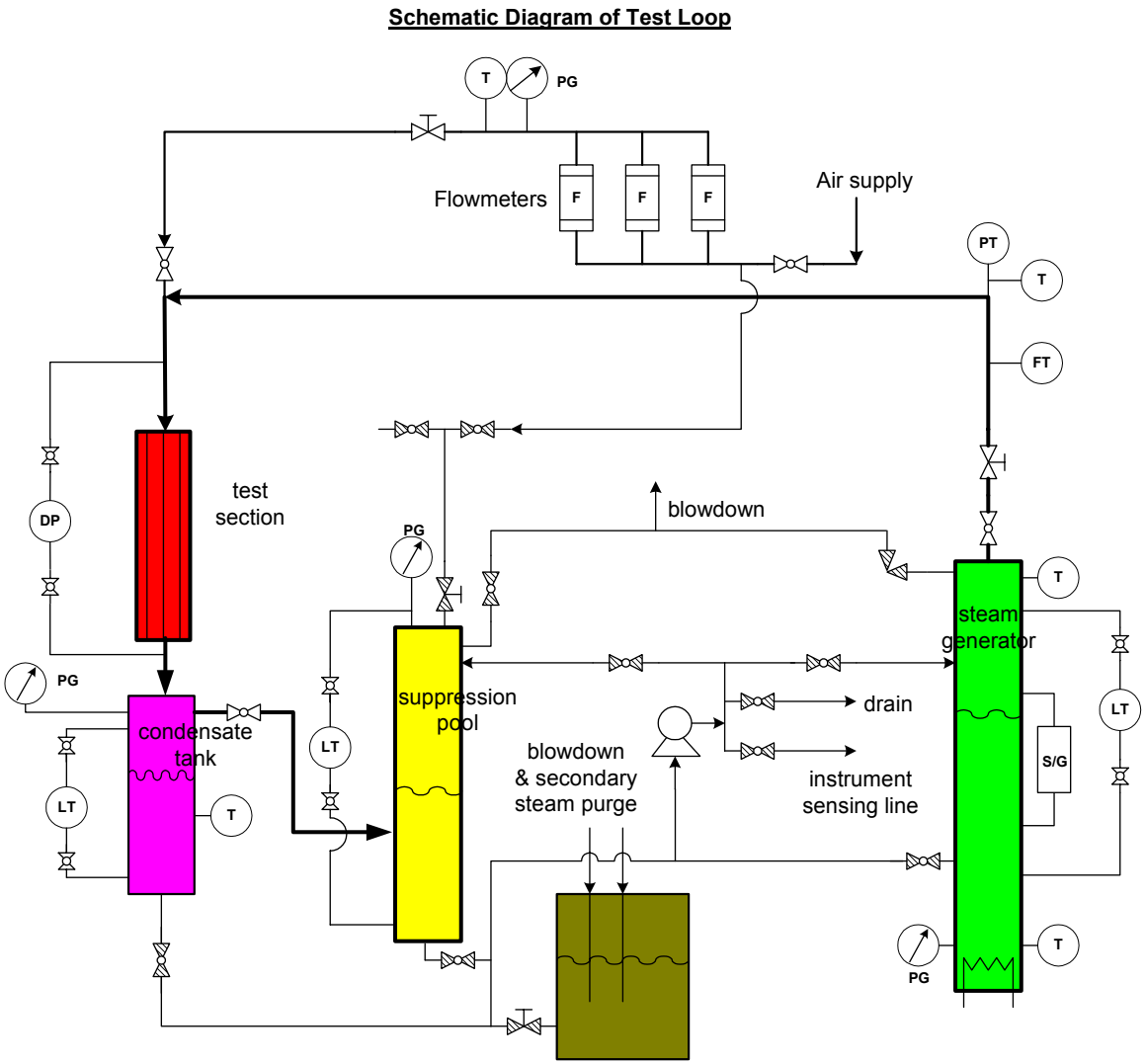

Figure 5.1 Schematic Diagram of Test Loop

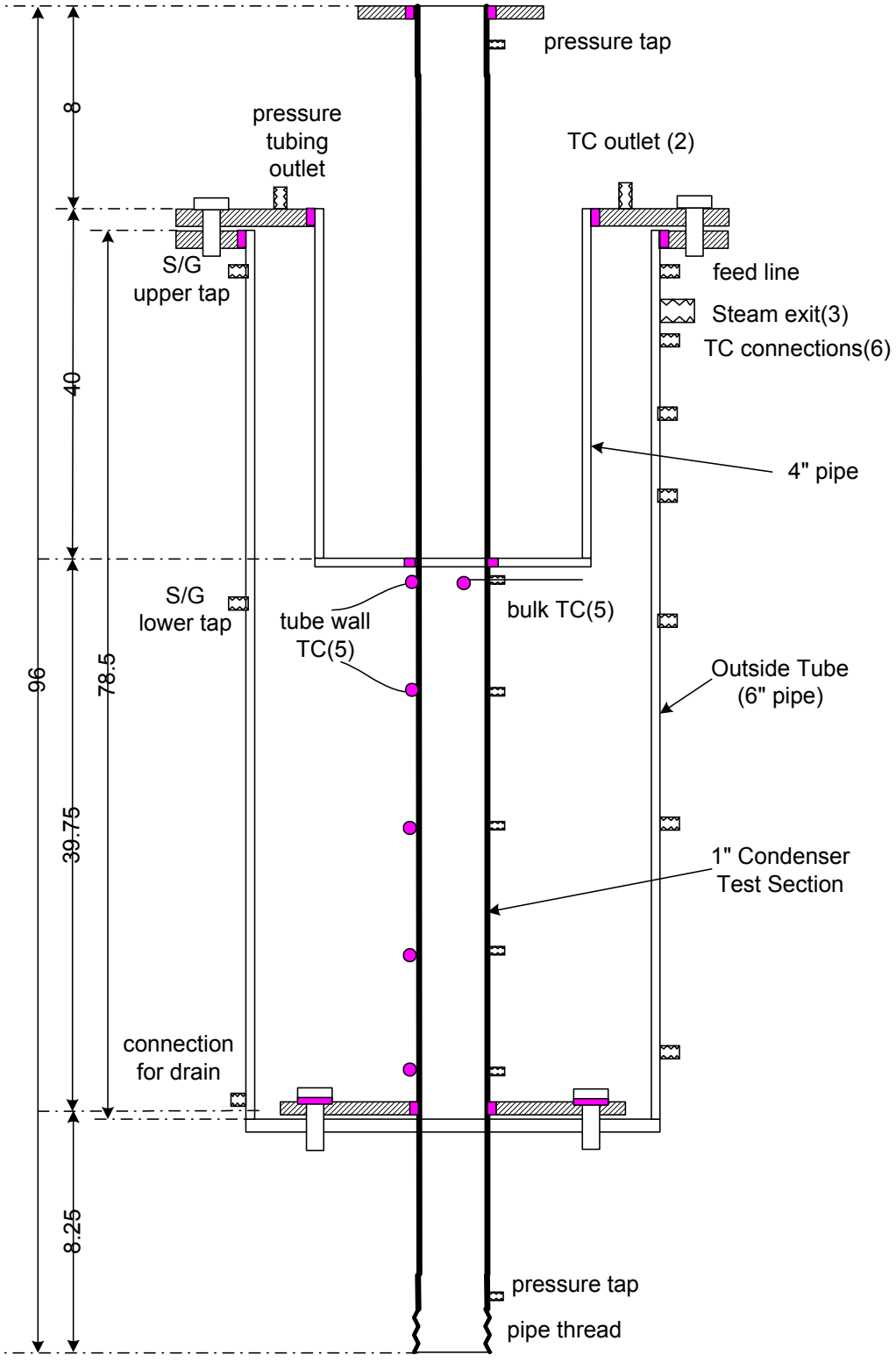

Figure 5.2 Schematic Diagram of Pool Boiling Test Section –Complete Assembly

1) 6" Type 304 Sch 10 SS pipe
2) 11" OD Type 304 Slip-on flange
3) 6.625" OD - 2.375" ID 3/4" thick SS circular plate
4) 1.5" Type 304 SS half coupling (3ea)
5) 1/2" Type 304 SS half coupling (4ea)
6) 1/4" Type 304 SS half coupling for TC (6ea)

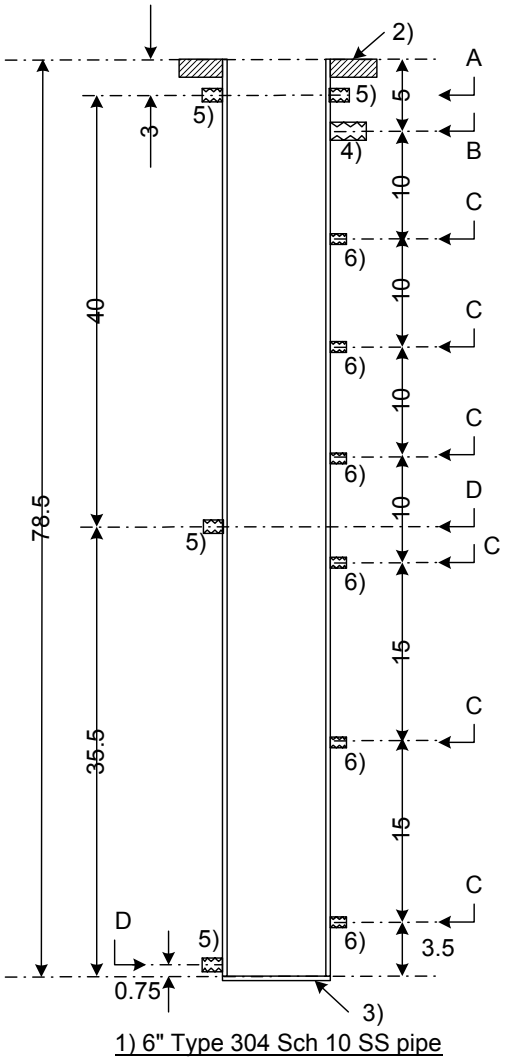

1) 6" Type 304 Sch 10 SS pipe

Note : 6" outside tube is common
for 2" and 1" test section

Unit is inch

11" slip-on flange
welded to 6" pipe

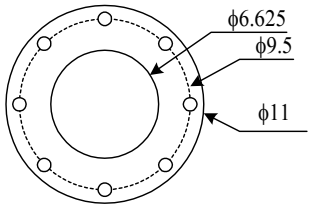

2) 11" OD Type 304 Slip-on flange

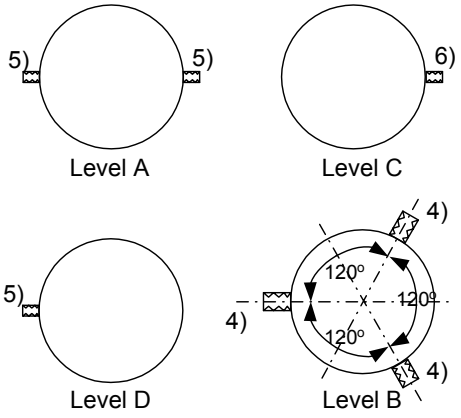

Angular Distribution for Taps

circular plate welded to
6" pipe

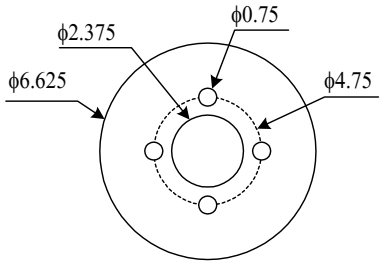

3) 6.625" OD - 2.375" ID SS circular plate

Condenser Outside Tube (6" Pipe)

Figure 5.3 Schematic Diagram of Pool Boiling Test Section – Pool Side Tank

1) 1" Type 304 Sch 40 SS pipe
2) 4" Type 304 Sch 10 SS pipe
3) 11" OD Type 304 blind flange
4) 6" OD Type 304 blind flange
5) 4.5" OD - 1.315" ID circular plate
6) 1/2" Type 304 SS half coupling (2ea)
7) 1/8" Type 304 SS half coupling for TC (5ea)
8) 1/4" Type 304 SS half coupling (4ea)
9) 4.25" OD Type 304 slip-on flange (1 ea)
10) 5/8" OD Type 316 SS bolt (4 ea)

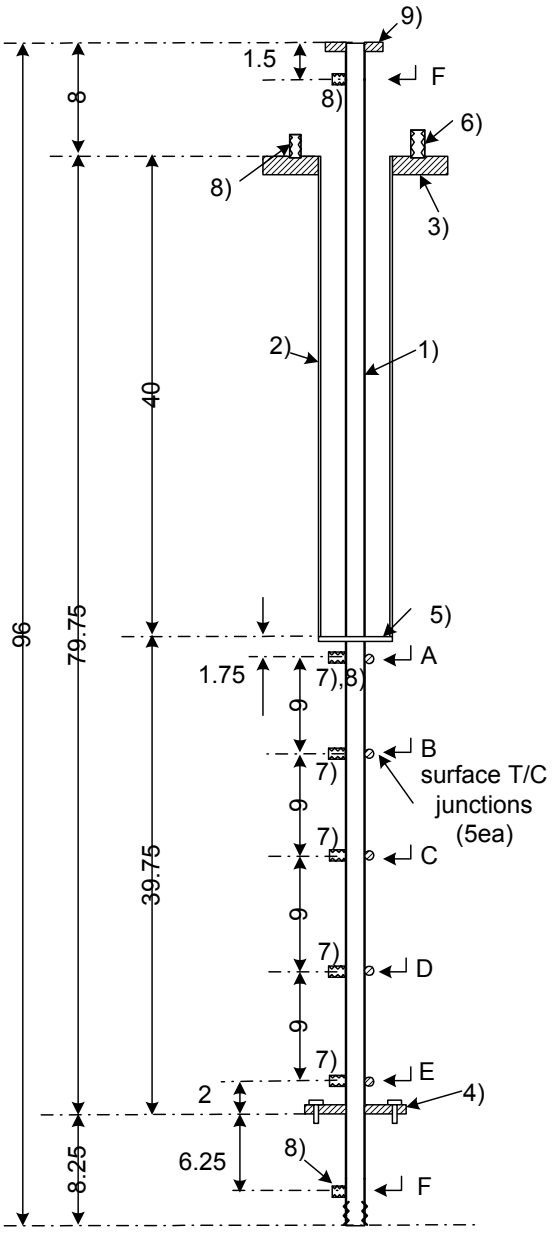

Note:
1. Top side 1" pipe(Item 1) will be welded to 4.25" OD flange(Item9). Bottom side 1" pipe will be threaded for standard pipe fitting.
2. Hole Diameter
Item 6) 1/2" coupling : same bore size
Item 7) 1/8" coupling : 1/16"
Item 8) 1/4" coupling at 1" pipe : 1/32"
1/4" coupling at flange : same bore size

circular plate welded to 4" & 1" pipe

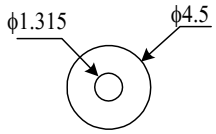

5) 4.5" OD - 1.315" ID SS circular plate

flange welded to 1" pipe

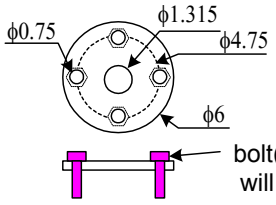

bolt(Item10) head will be welded to flange

4) 6" OD Type 304 blind flange

Unit is inch

1" Condenser & 4" Pipe(1/2)

Figure 5.4 Schematic Diagram of Pool Boiling Test Section –Condenser Tube

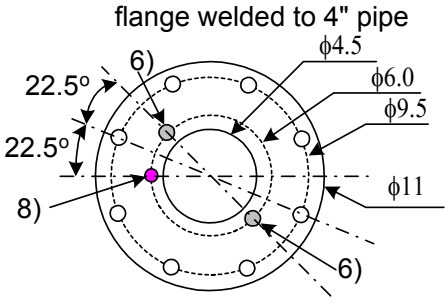

3) 11" OD Type 304 blind flange

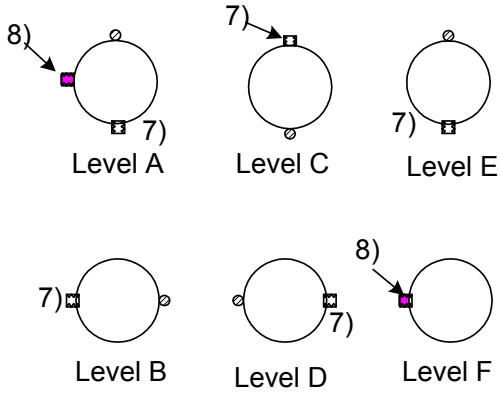

Angular Distribution for Taps & T/C Junction

Note :
Four 1/4" half couplings (Item8) welded on 11" OD flange(Item3),
at Level A, and Level F must be aligned with same angle.

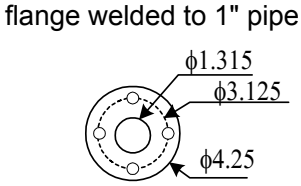

9) 4.25" OD Type 304 slip-on flange

Unit is inch

1" Condenser & 4" Pipe(2/2)

Figure 5.5 Schematic Diagram of Pool Boiling Test Section- Flange Design

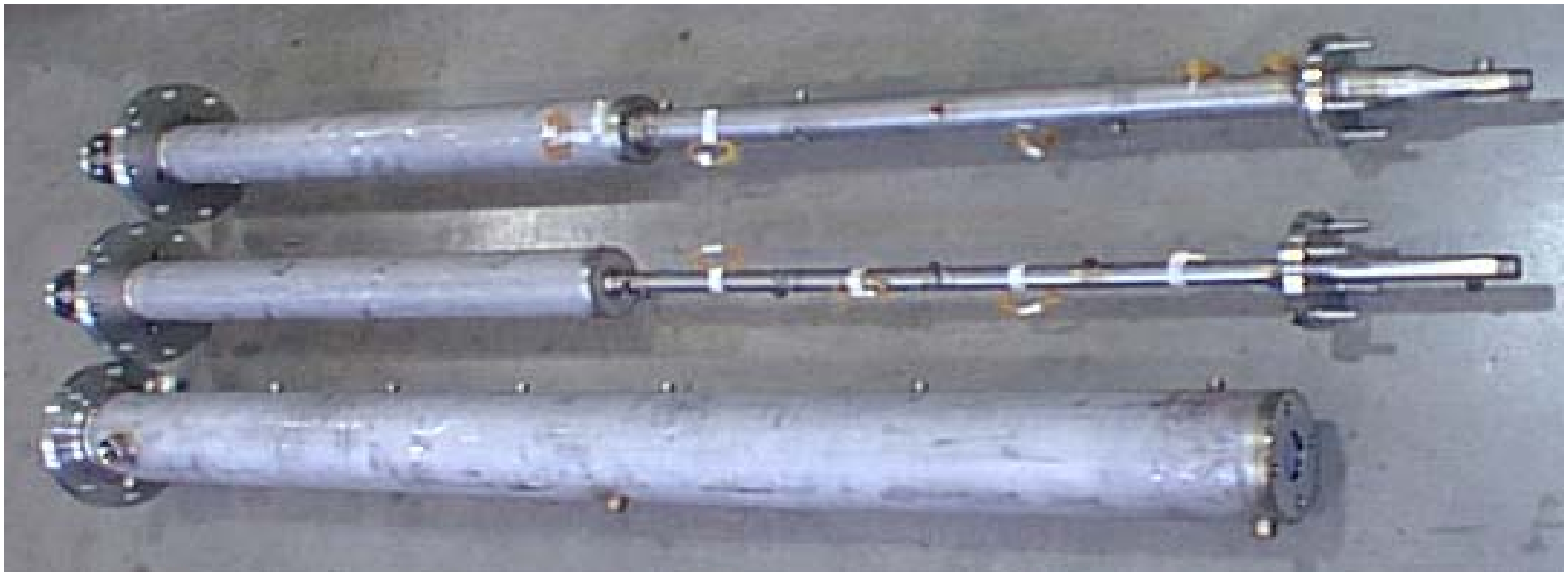

Figure 5.6 Picture of the Pool Boiling Test Section

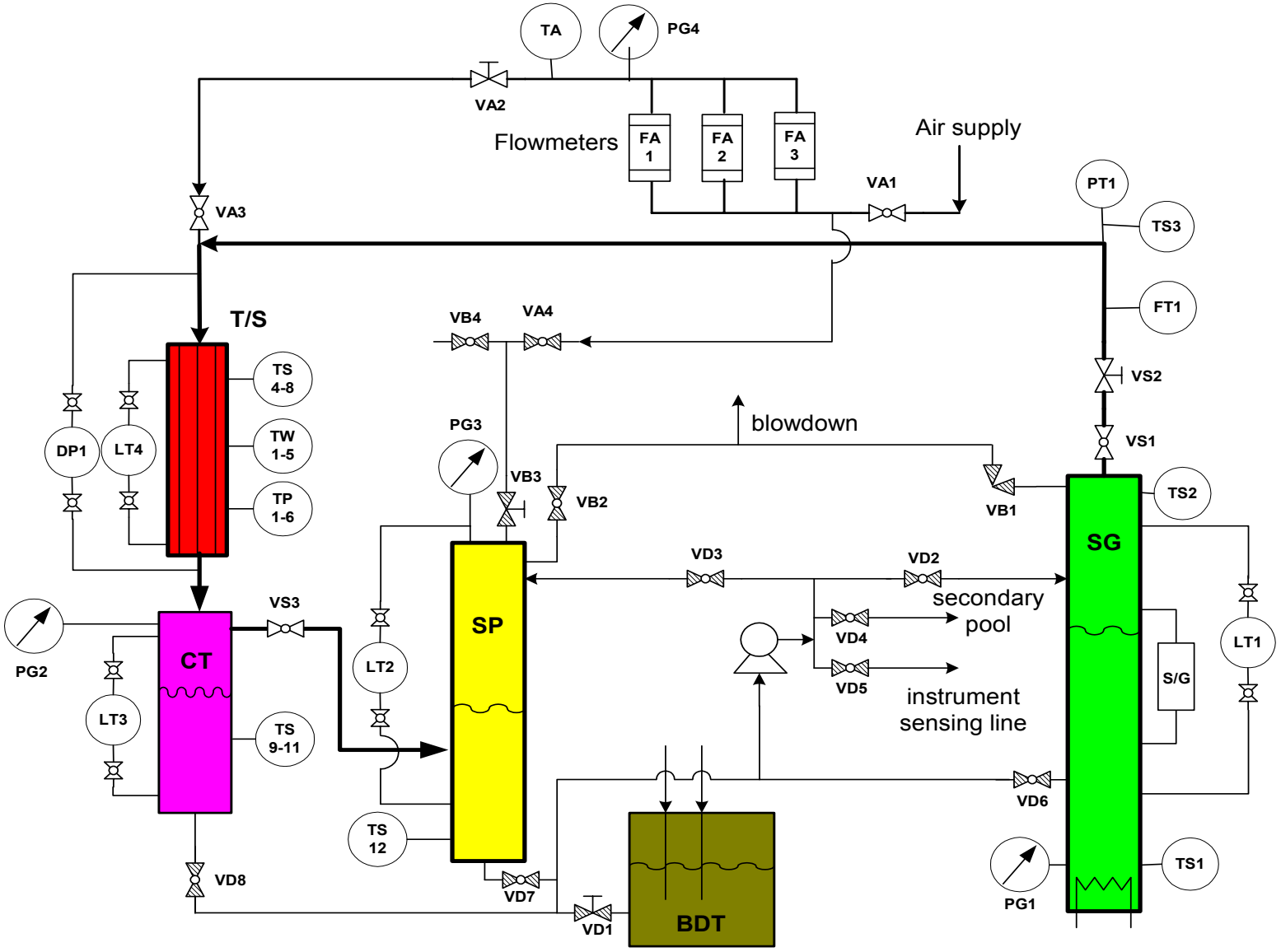

Figure 5.7 Instrumentation of the Test Loop

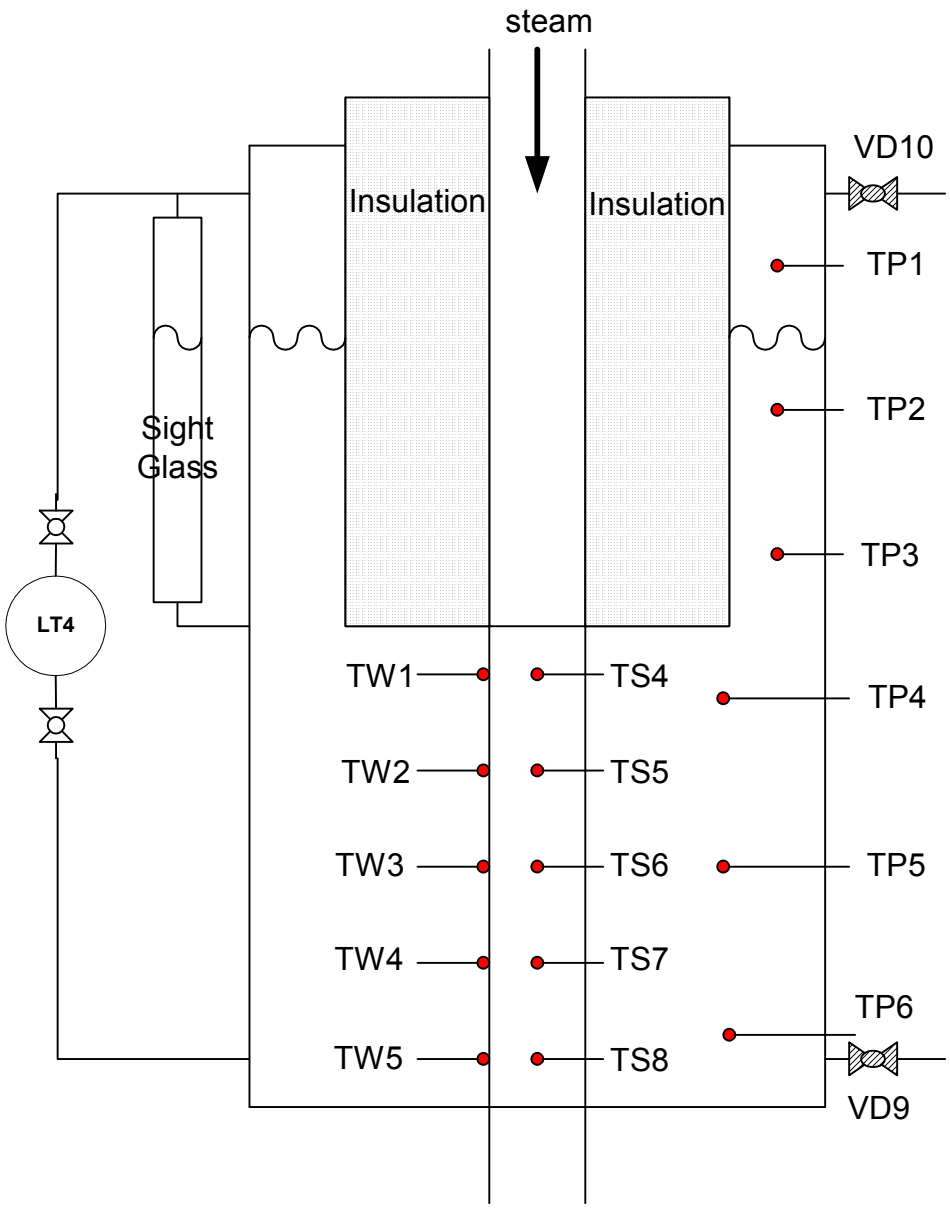

Figure 5.8 Test Section Instrumentation

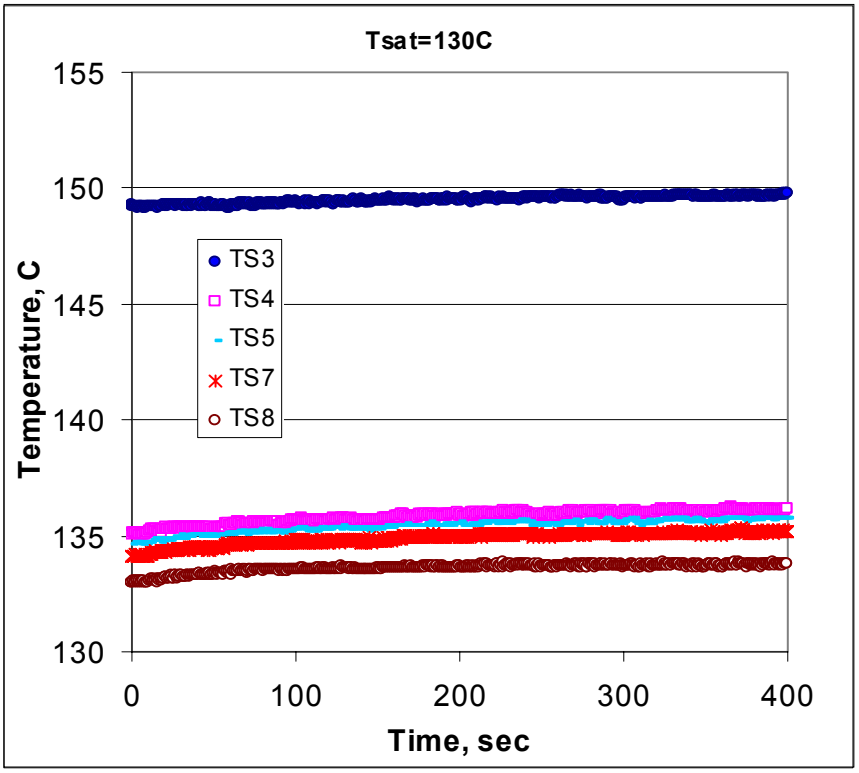

Figure 5.9 Raw Data – Steam Temperatures

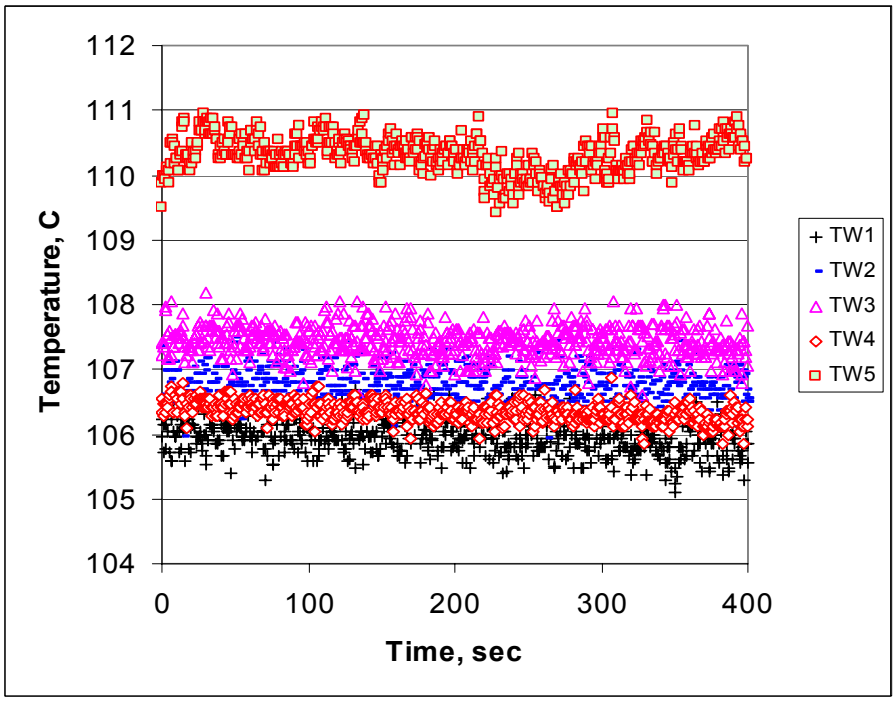

Figure 5.10 Raw Data – Condenser Outside Wall Temperatures

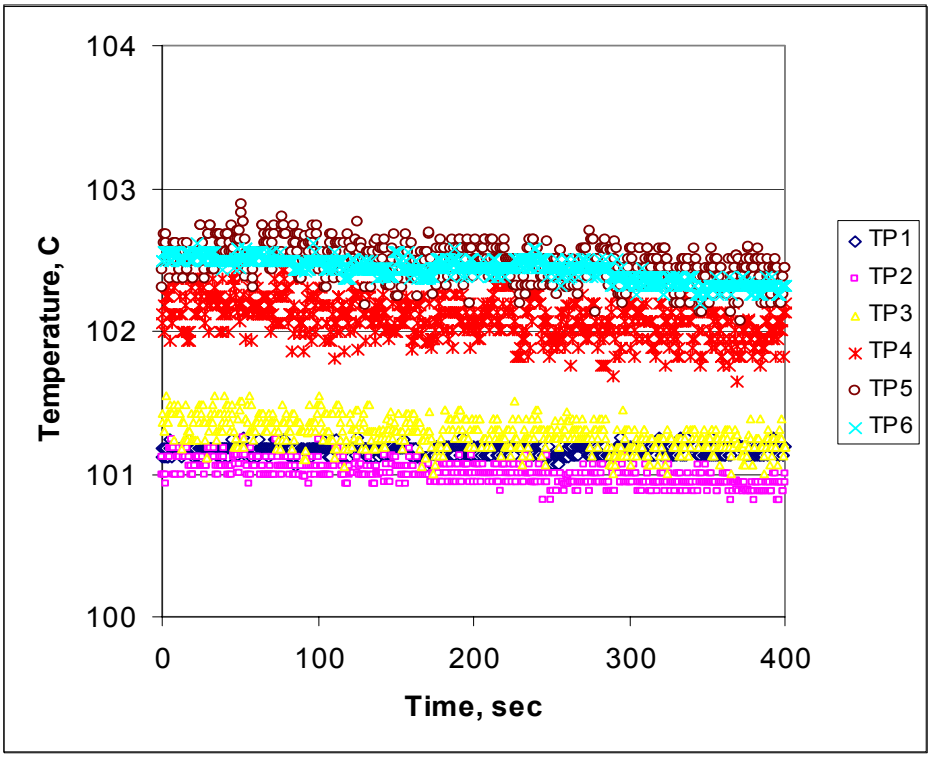

Figure 5.11 Raw Data – Secondary Pool Temperatures

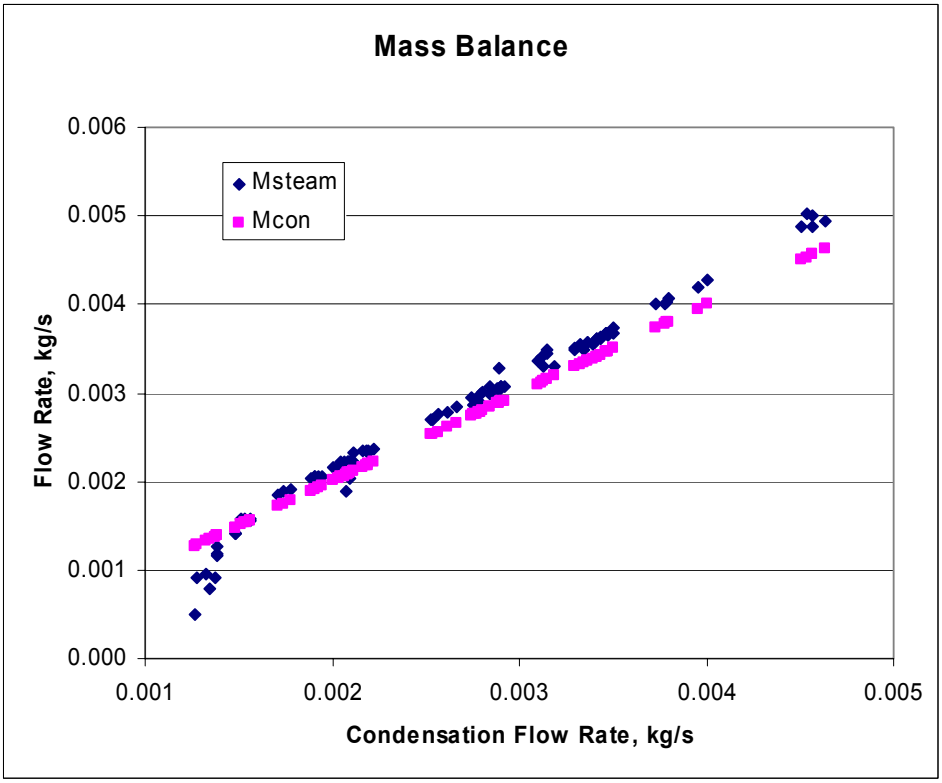

Figure 5.12 Mass Balance for the Complete Condensation

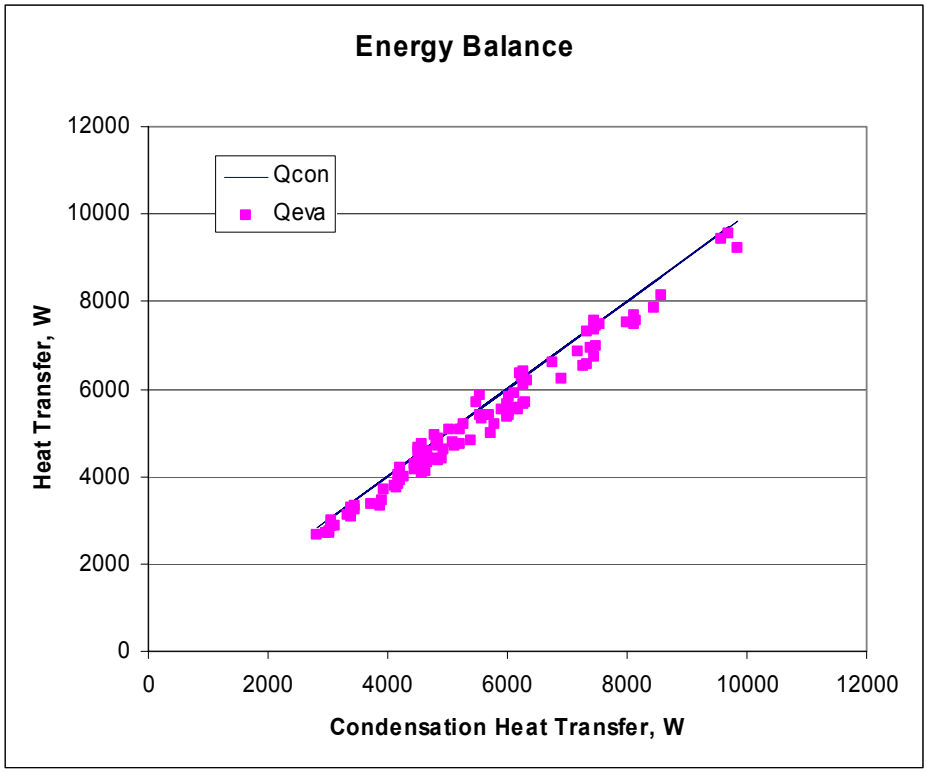

Figure 5.13 Energy Balance: Condensation vs. Evaporation

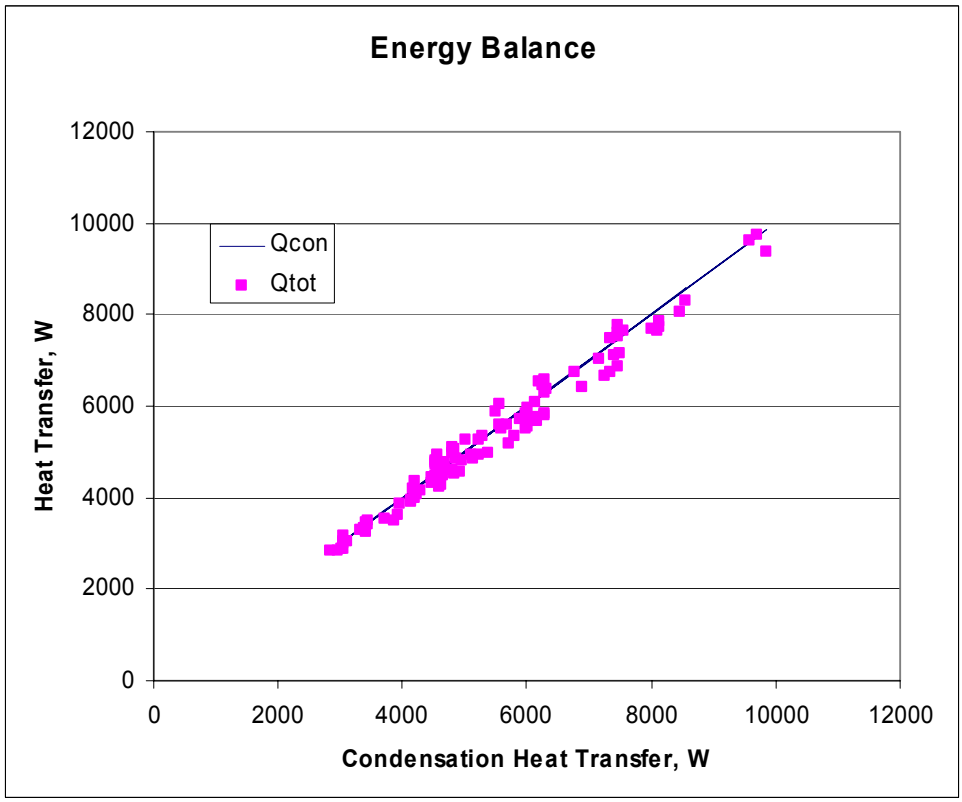

Figure 5.14 Mass Balance: Condensation vs. Evaporation + Heat Loss

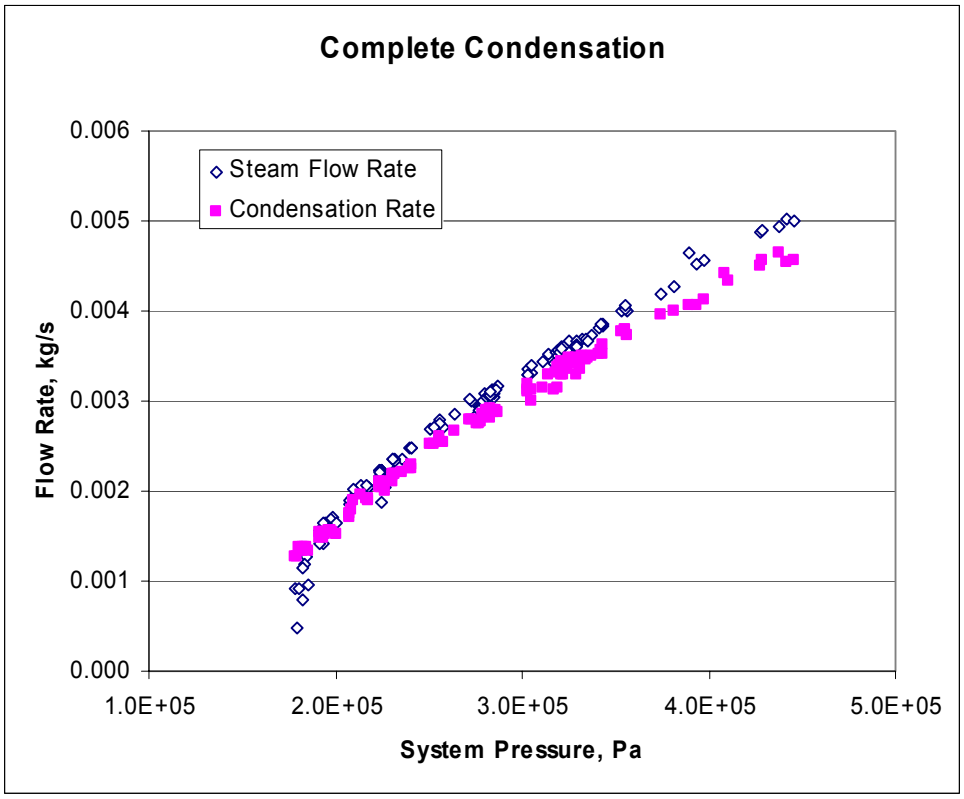

Figure 5.15 Complete Condensation: Mass Flow Rate with System Pressure

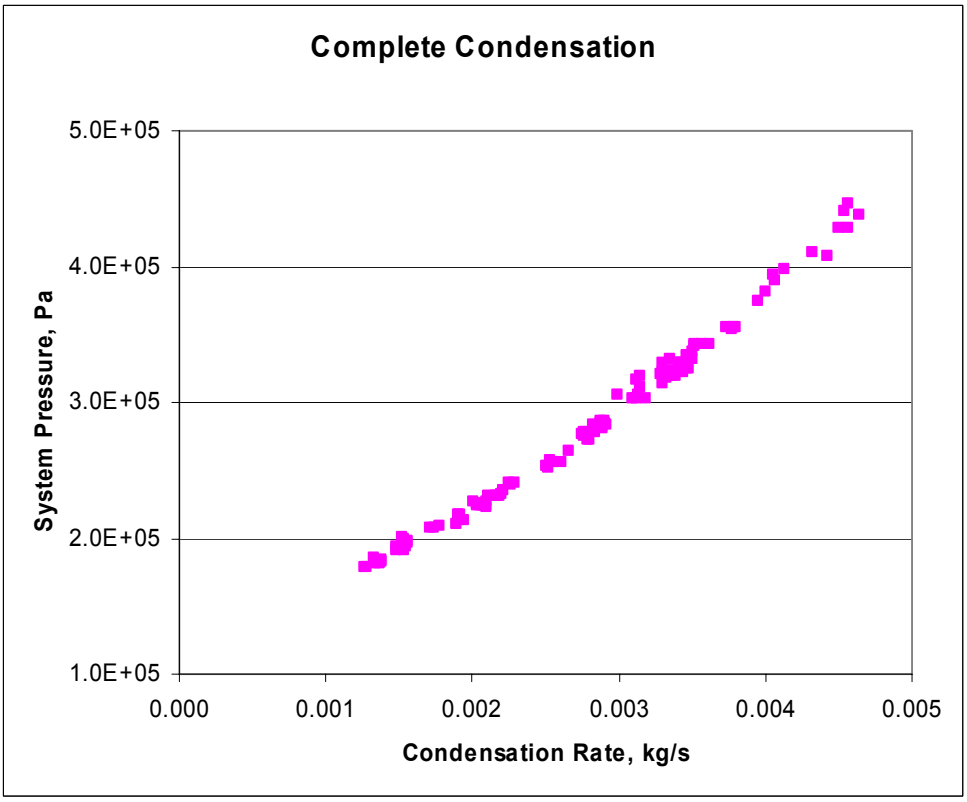

Figure 5.16 Complete Condensation: System Pressure with Mass Flow Rate

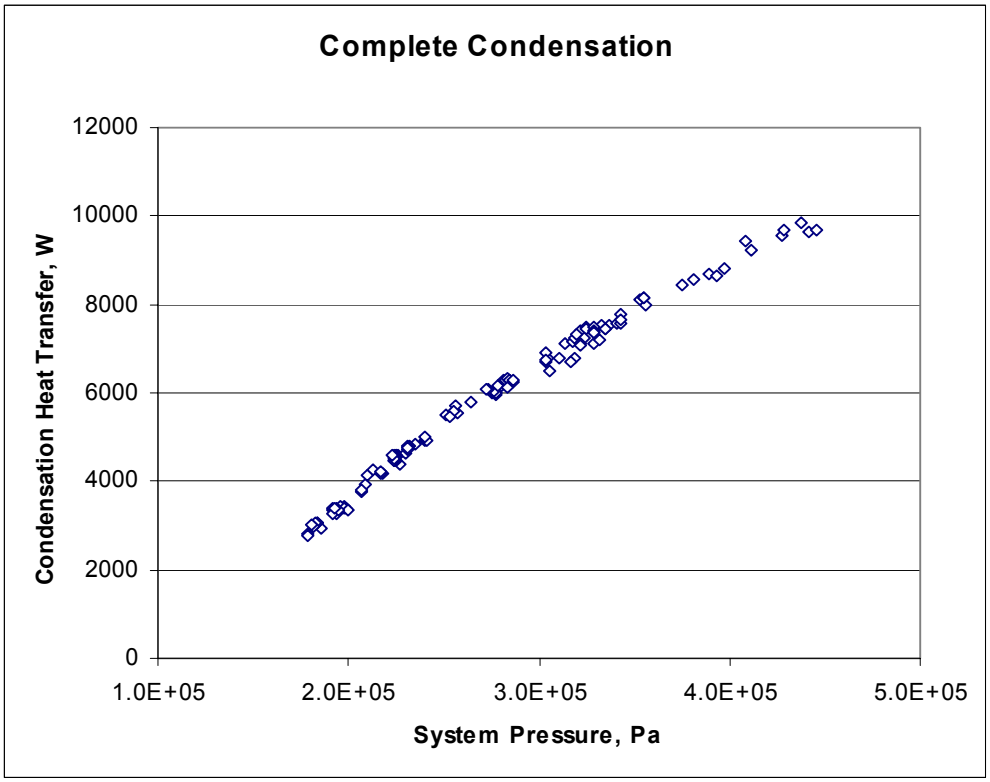

Figure 5.17 Complete Condensation: Condensation Heat Transfer Rate

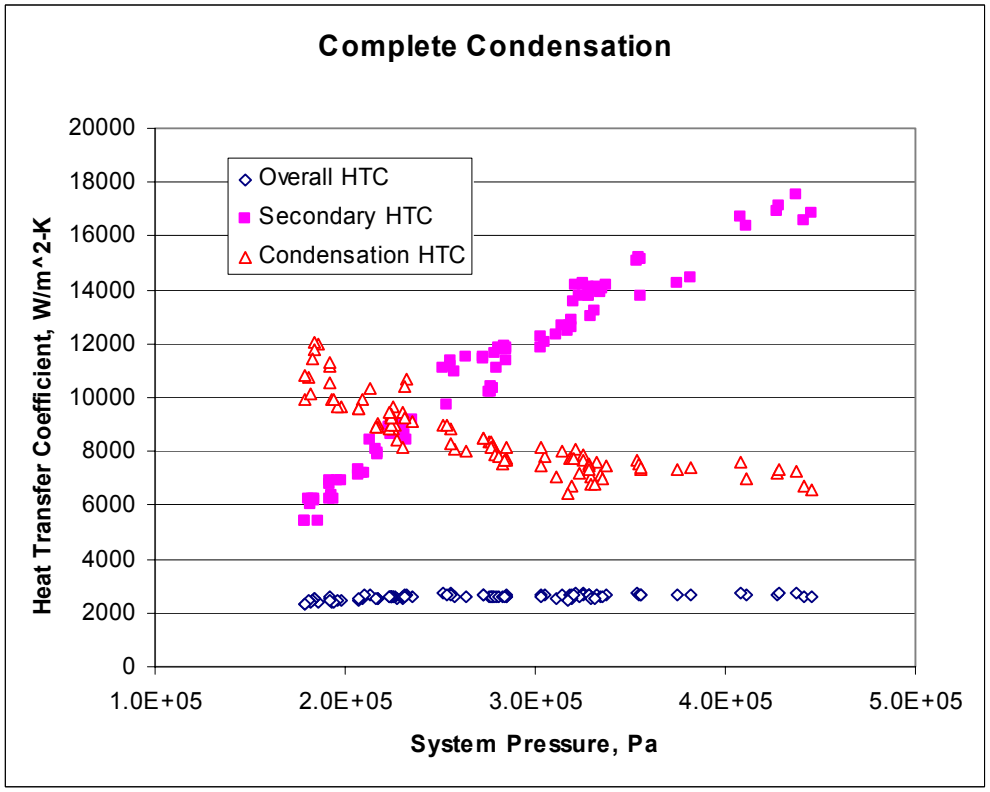

Figure 5.18 Complete Condensation: Heat Transfer Coefficients

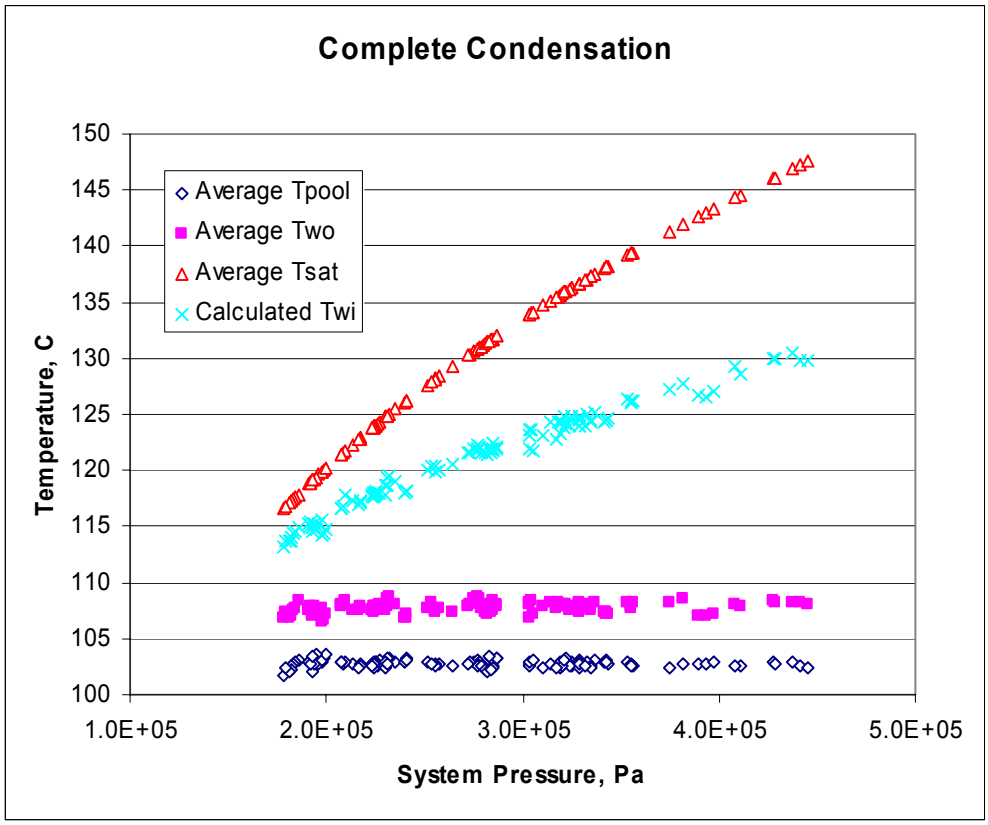

Figure 5.19 Complete Condensation: Temperatures

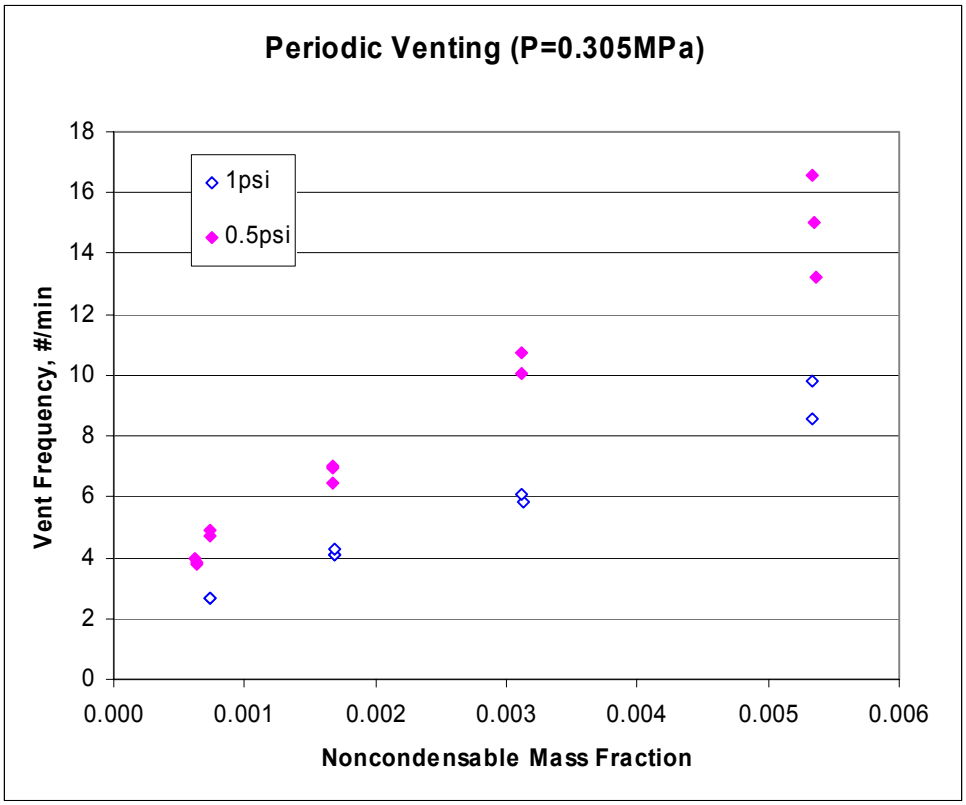

Figure 5.20 Periodic Venting: Vent Frequency for DPvent = 0.5 psid and 1.0 psid

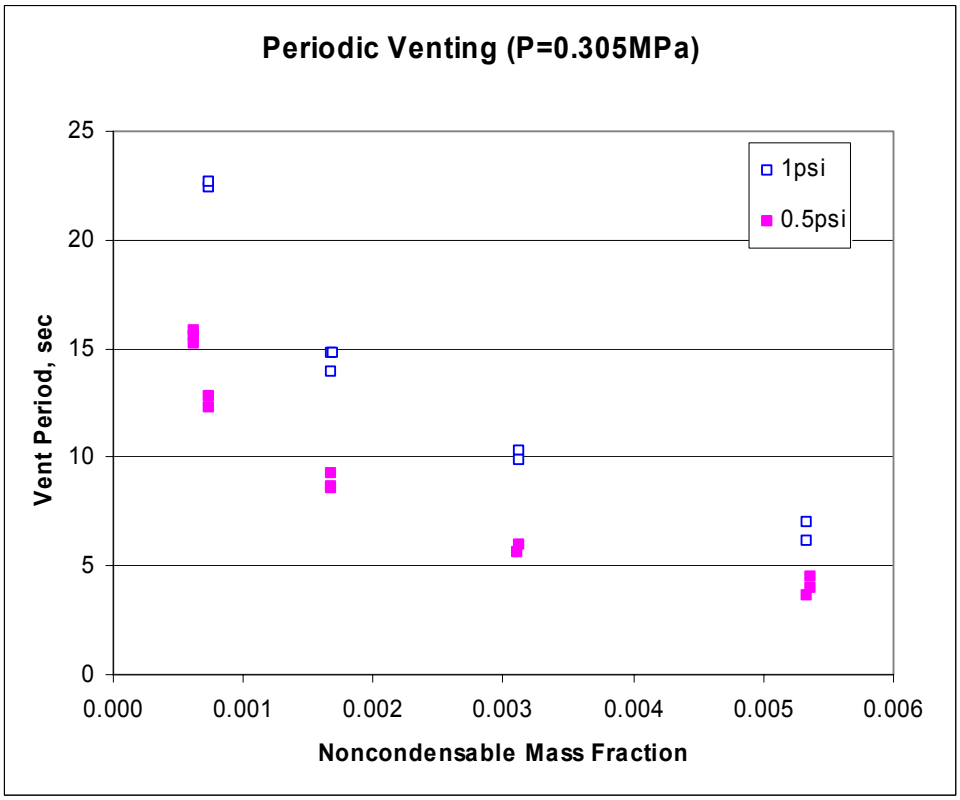

Figure 5.21 Periodic Venting: Vent Period for DPvent = 0.5 psid and 1.0 psid

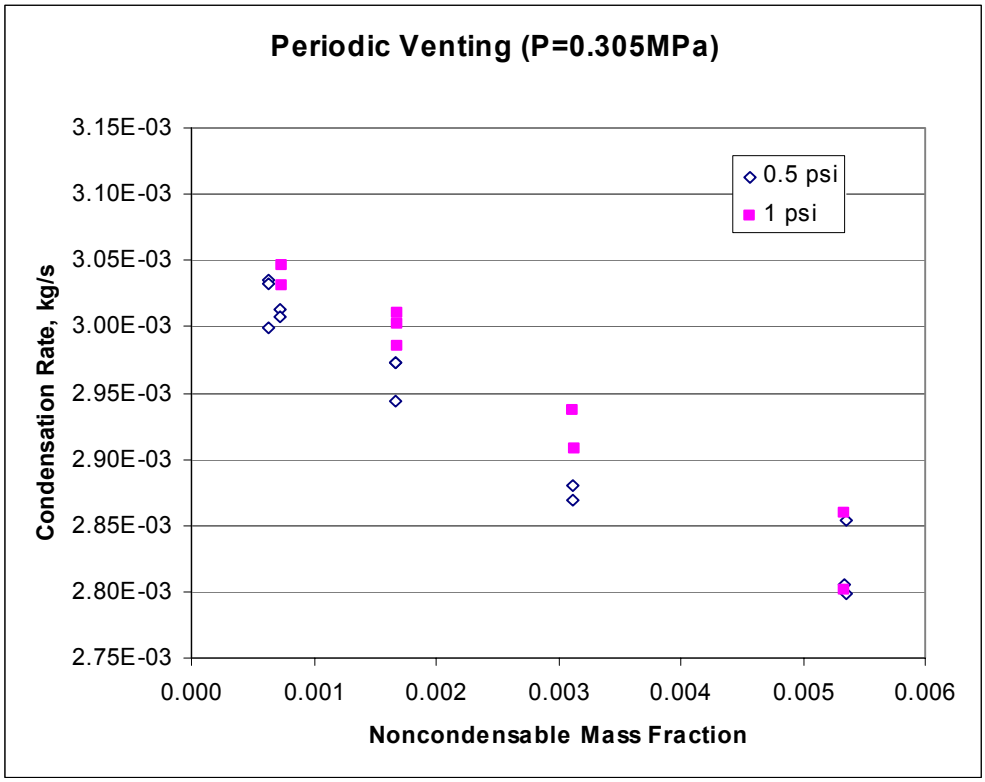

Figure 5.22 Periodic Venting: Condensation Rate

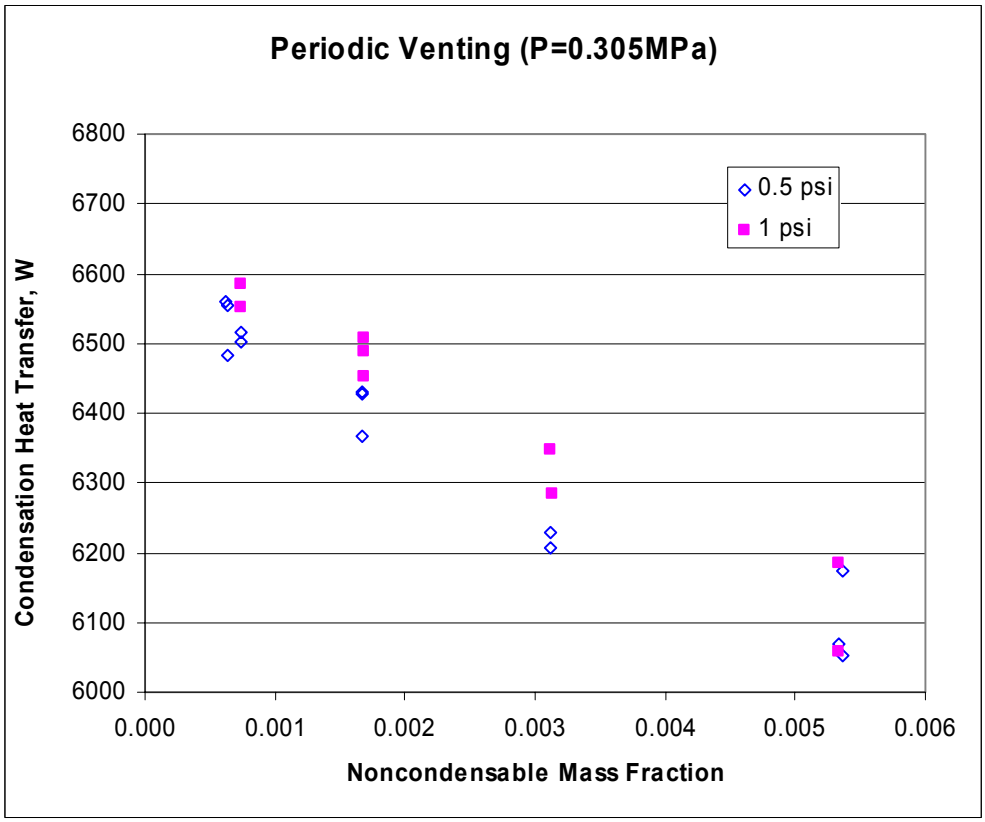

Figure 5.23 Periodic Venting: Condensation Heat Transfer Rate

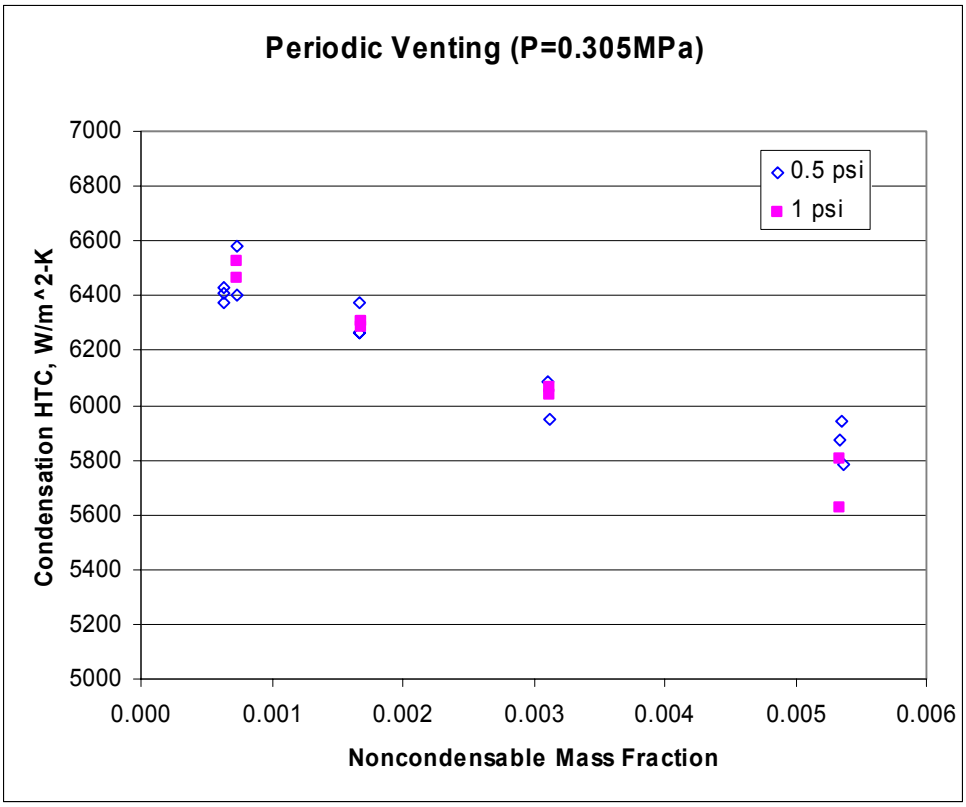

Figure 5.24 Periodic Venting: Condensation Heat Transfer Coefficients

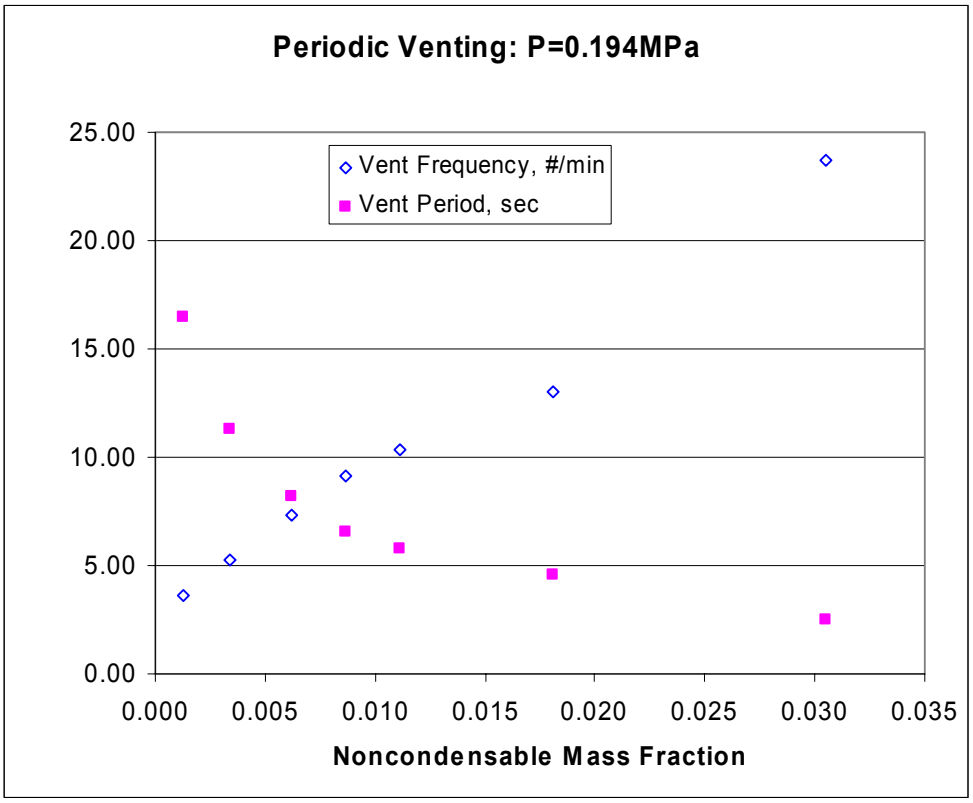

Figure 5.25 Vent Frequency and Vent Period for P=0.194MPa

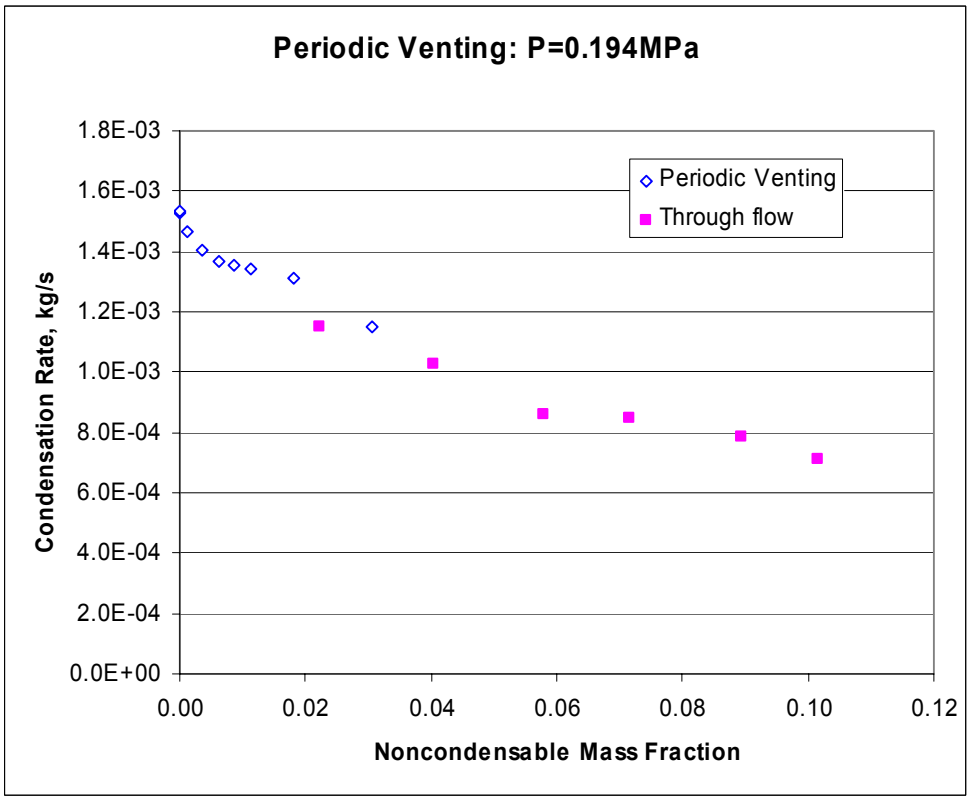

Figure 5.26 Condensation Rate for P=0.194MPa

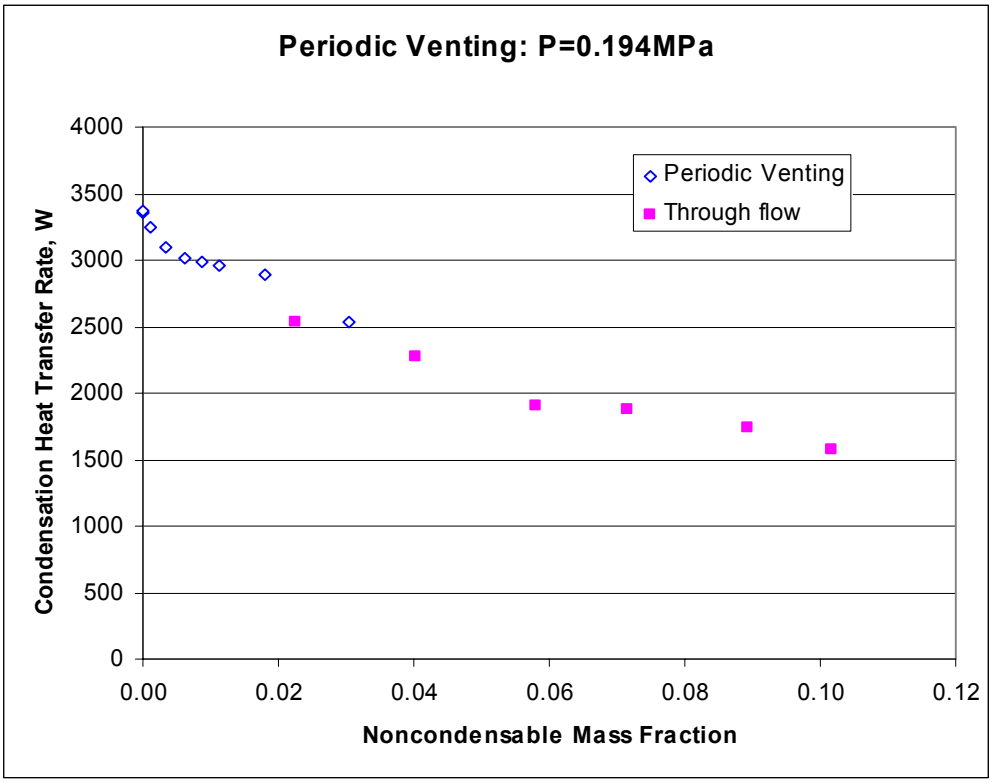

Figure 5.27 Condensation Heat Transfer Rate for P=0.194MPa

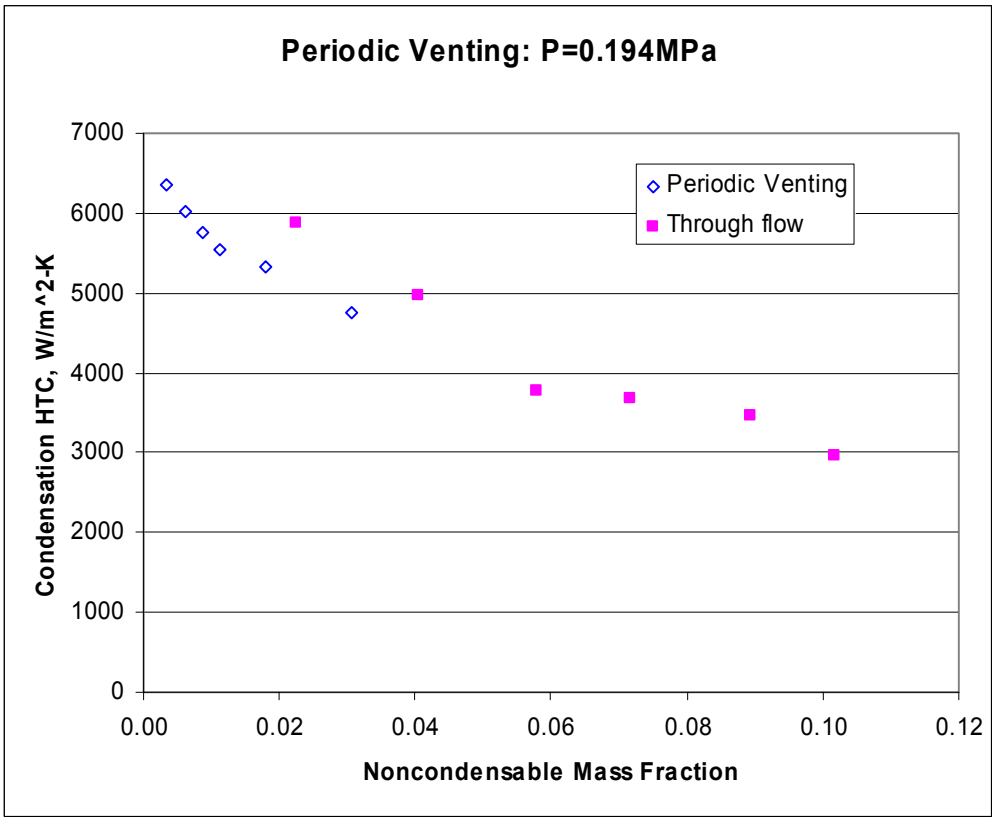

Figure 5.28 Condensation Heat Transfer Coefficients for P=0.194MPa

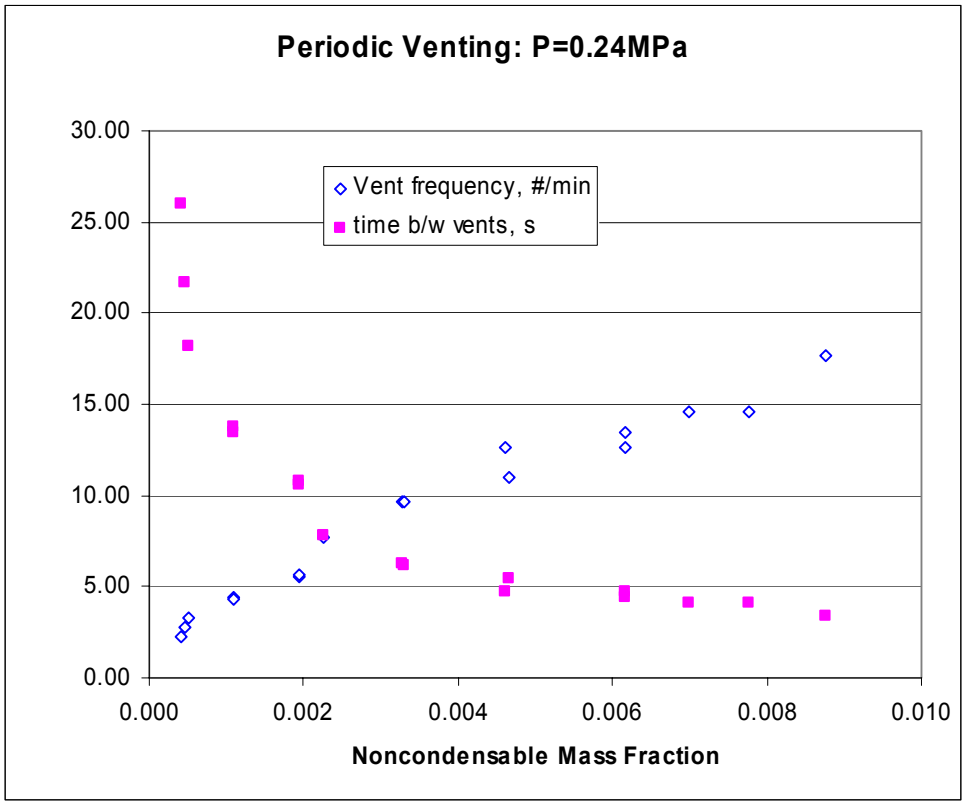

Figure 5.29 Vent Frequency and Vent Period for P=0.24MPa

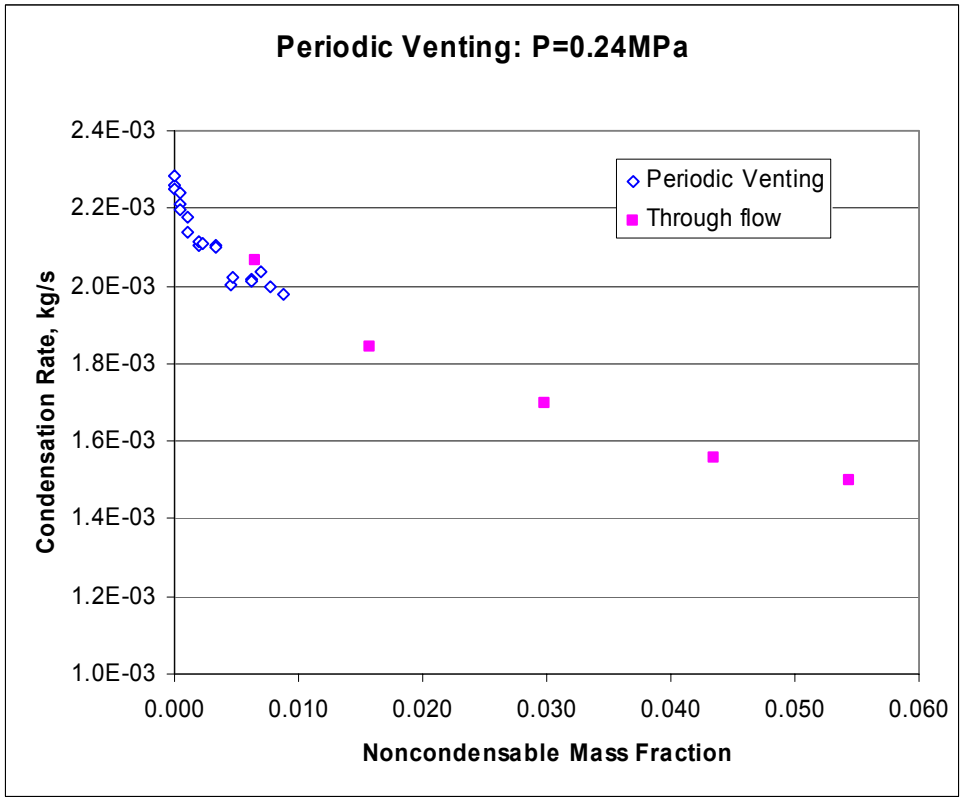

Figure 5.30 Condensation Rate for P=0.24MPa

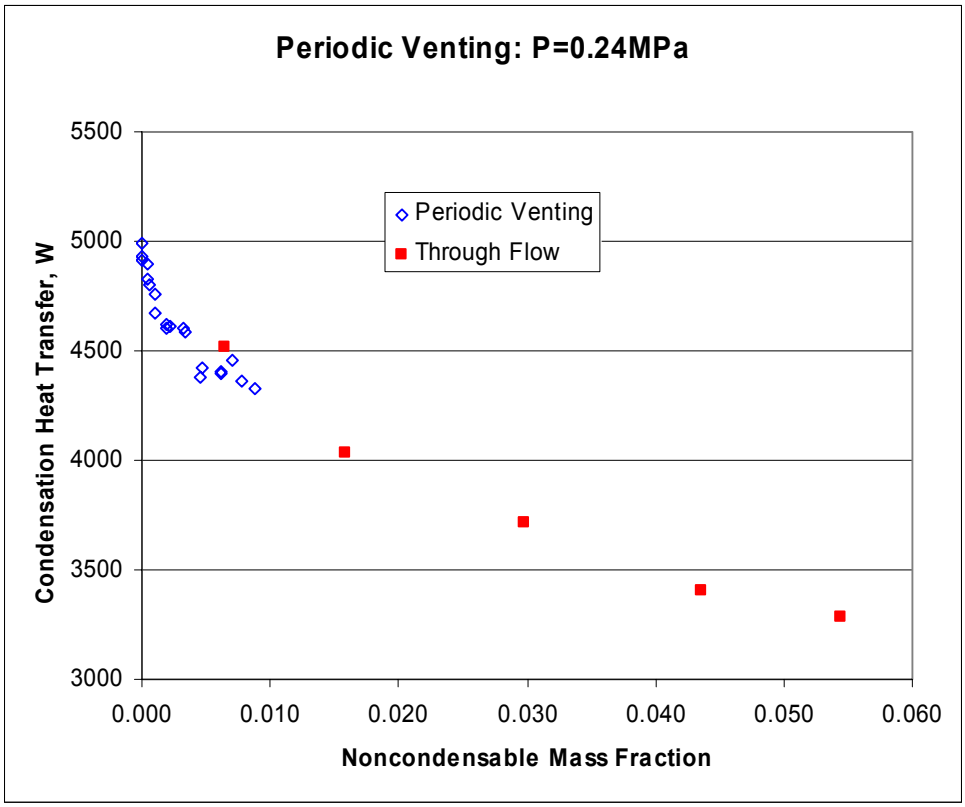

Figure 5.31 Condensation Heat Transfer Rate for P=0.24MPa

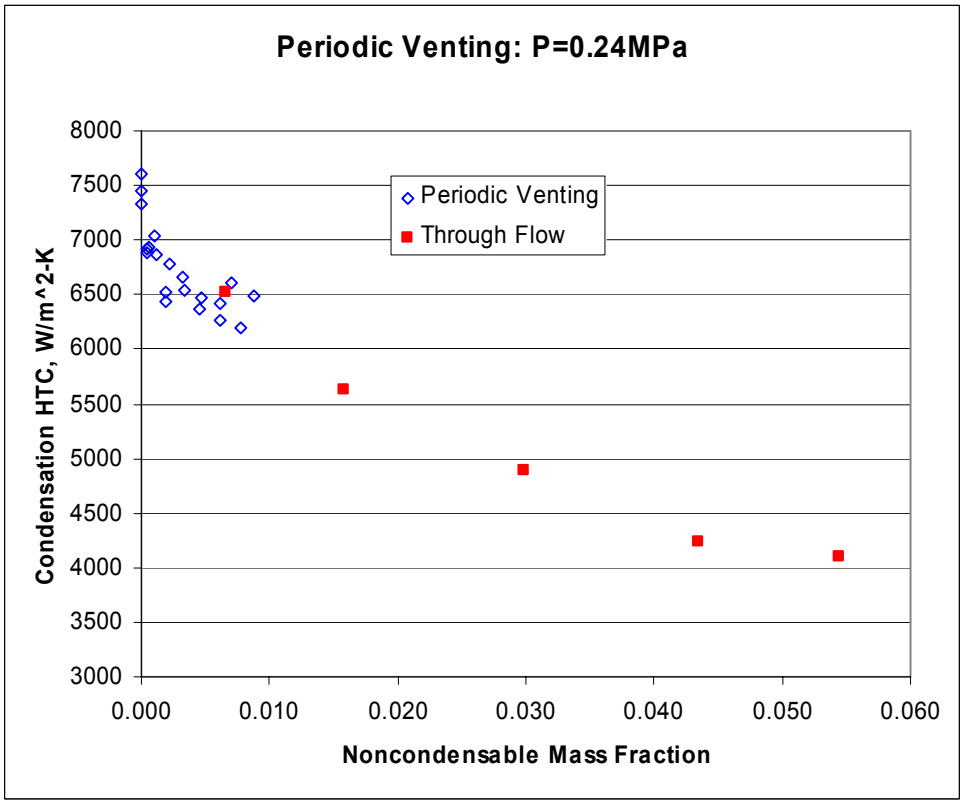

Figure 5.32 Condensation Heat Transfer Coefficients for P=0.24MPa

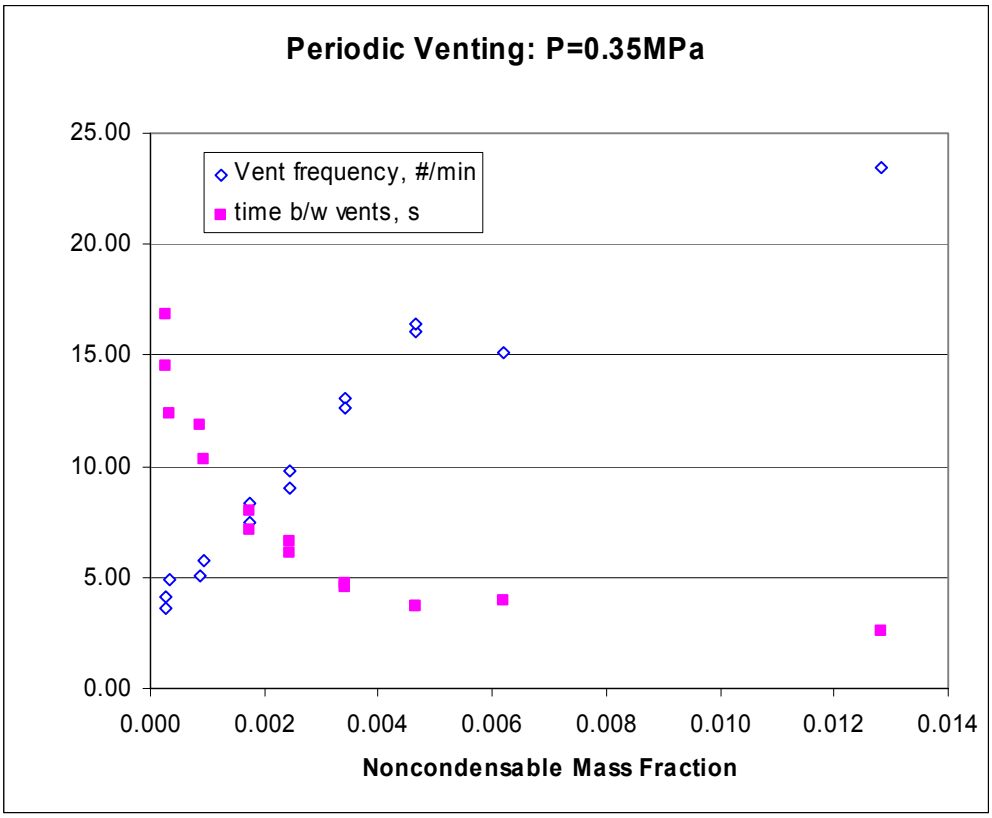

Figure 5.33 Vent Frequency and Vent Period for P=0.35MPa

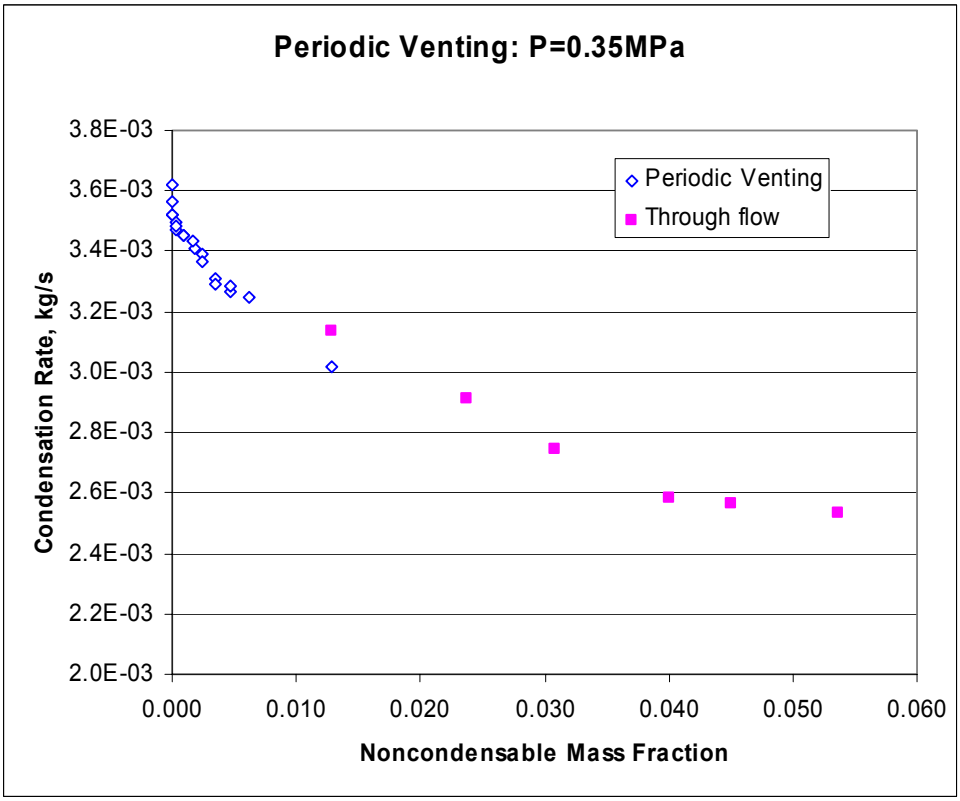

Figure 5.34 Condensation Rate for P=0.35MPa

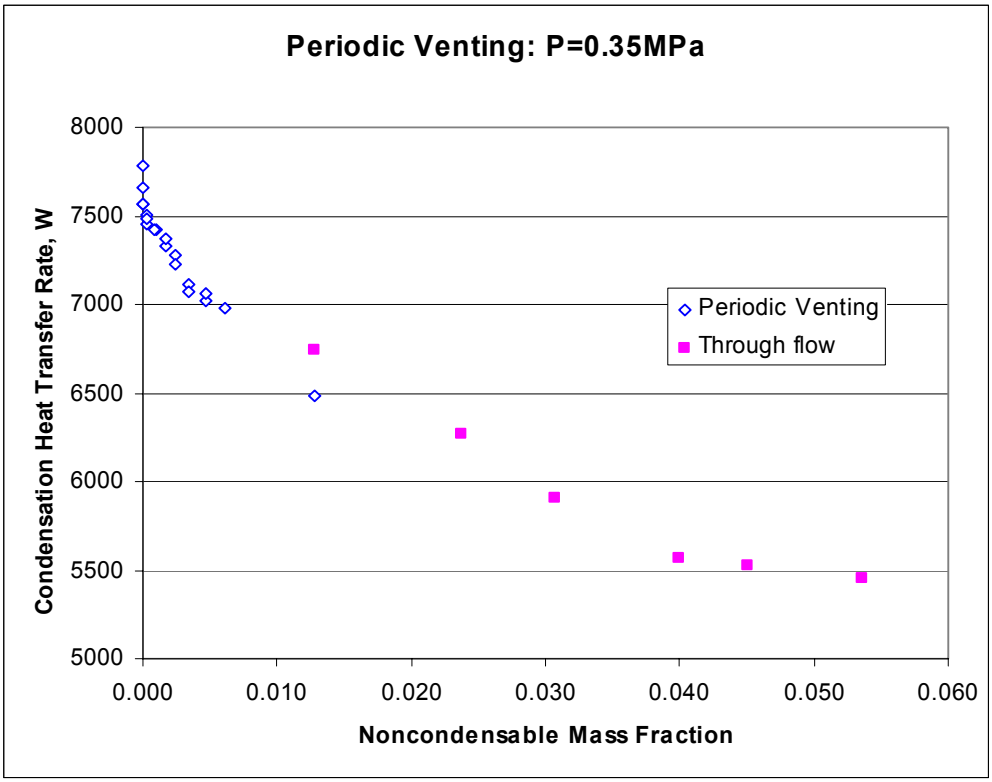

Figure 5.35 Condensation Heat Transfer Rate for P=0.35MPa

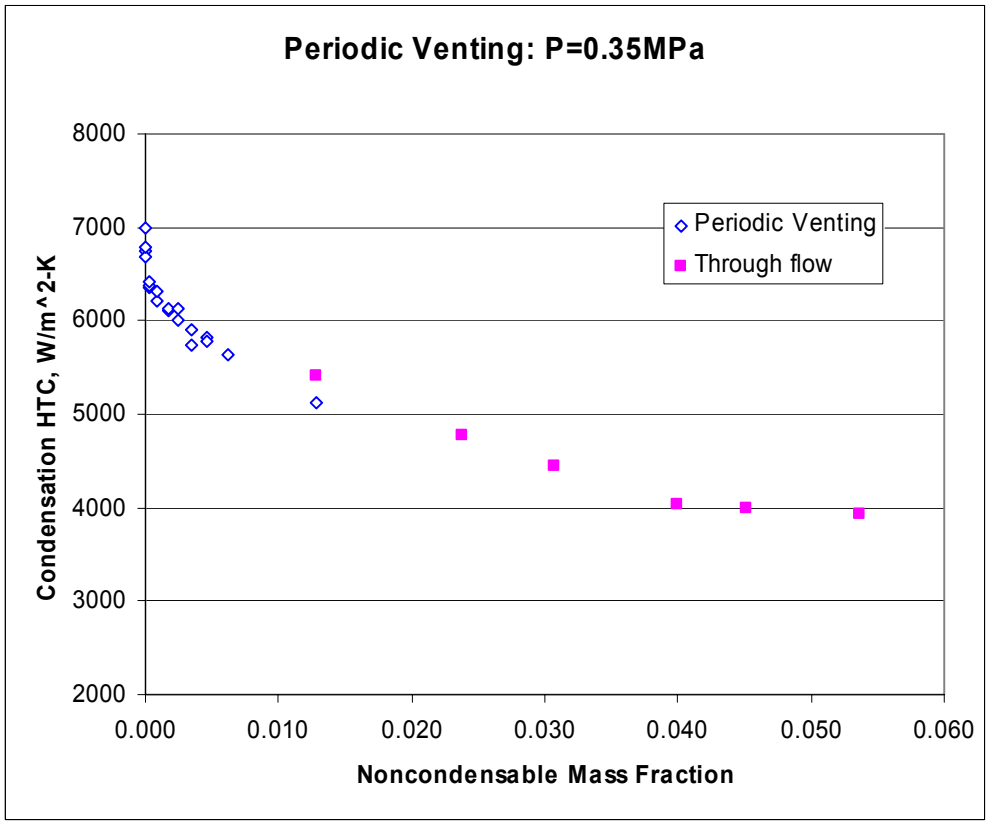

Figure 5.36 Condensation Heat Transfer Coefficients for P=0.35MPa

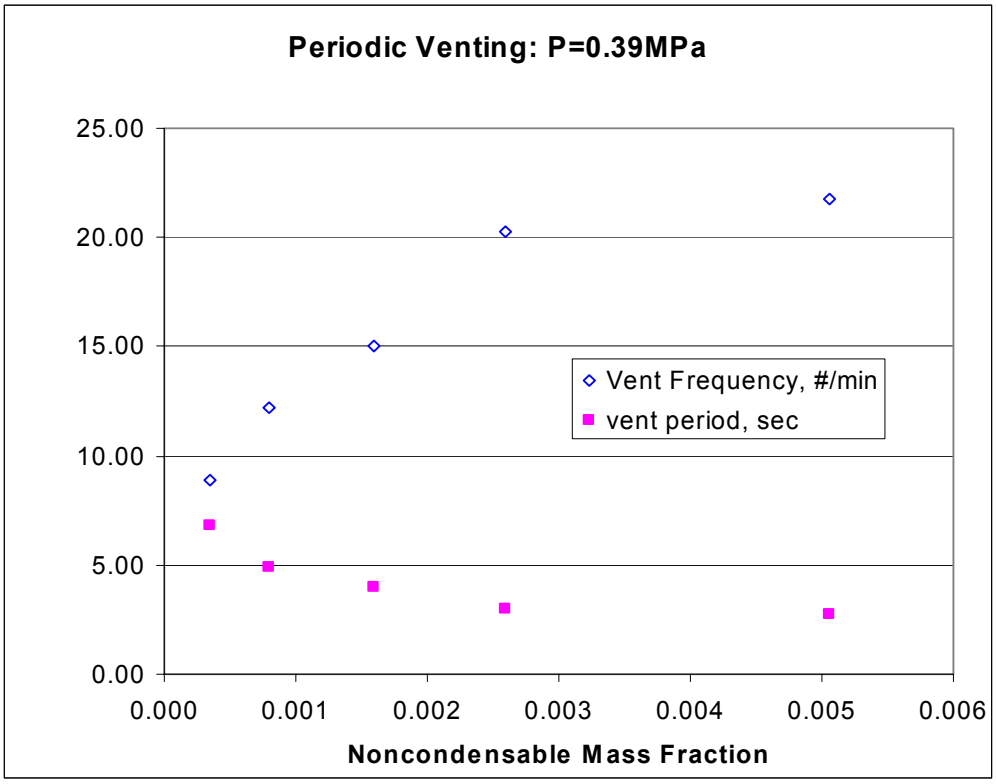

Figure 5.37 Vent Frequency and Vent Period for P=0.39MPa

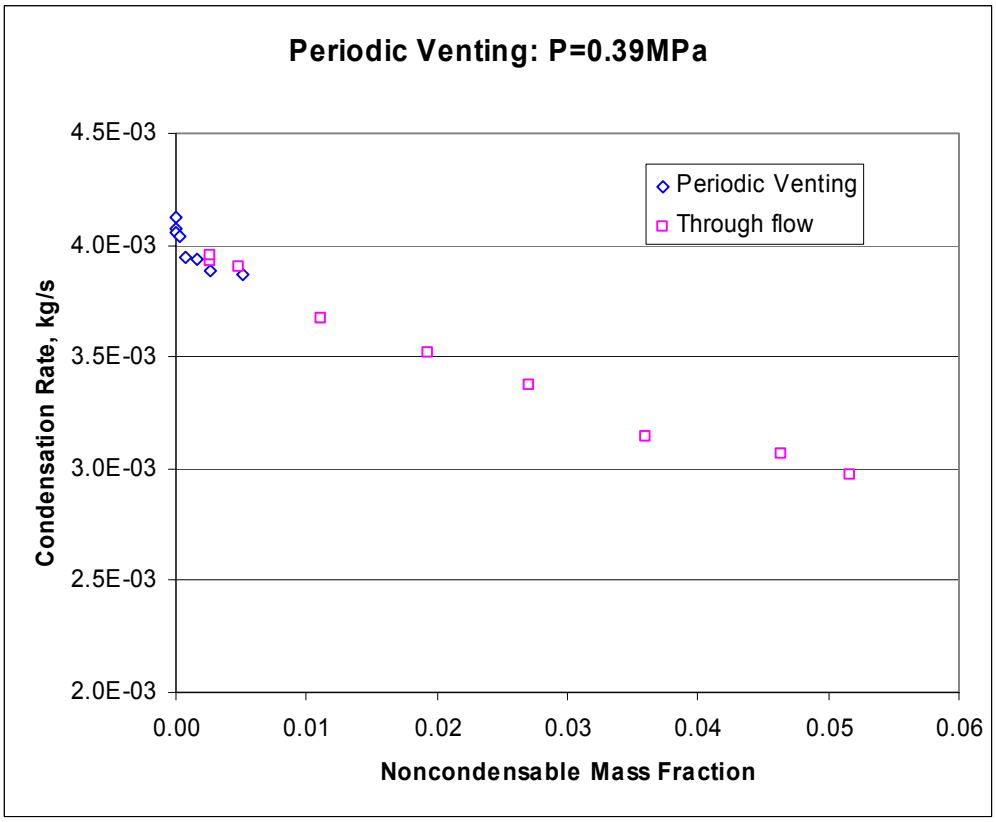

Figure 5.38 Condensation Rate for P=0.39MPa

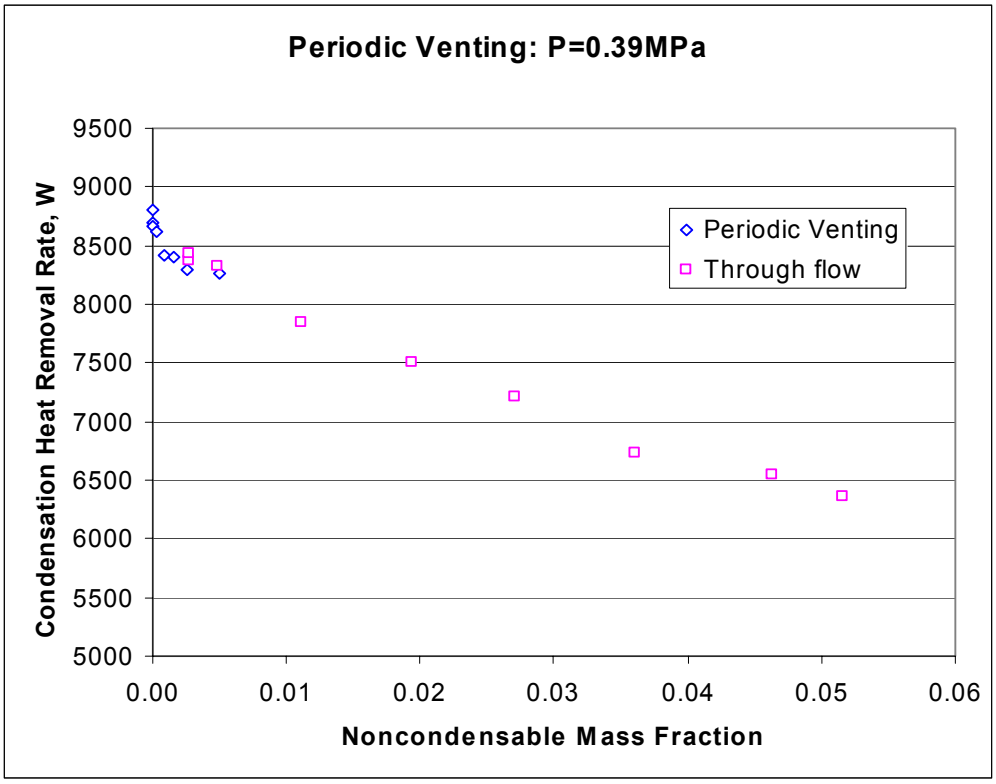

Figure 5.39 Condensation Heat Transfer Rate for P=0.39MPa

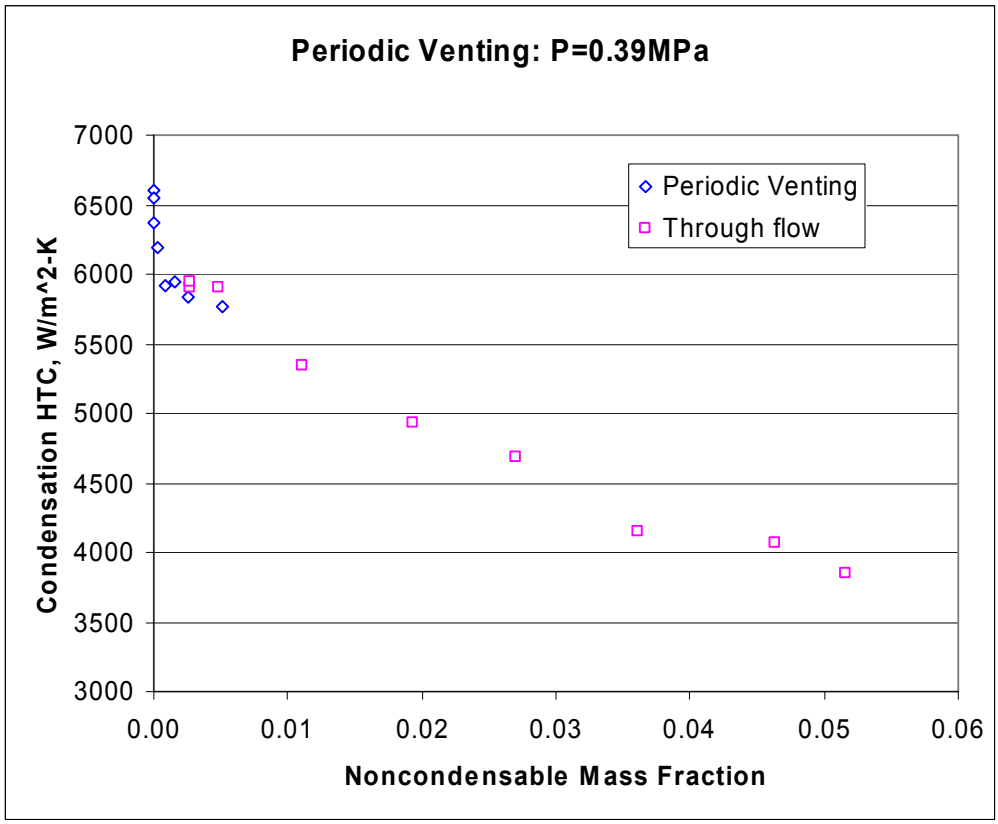

Figure 5.40 Condensation Heat Transfer Coefficients for P=0.39MPa

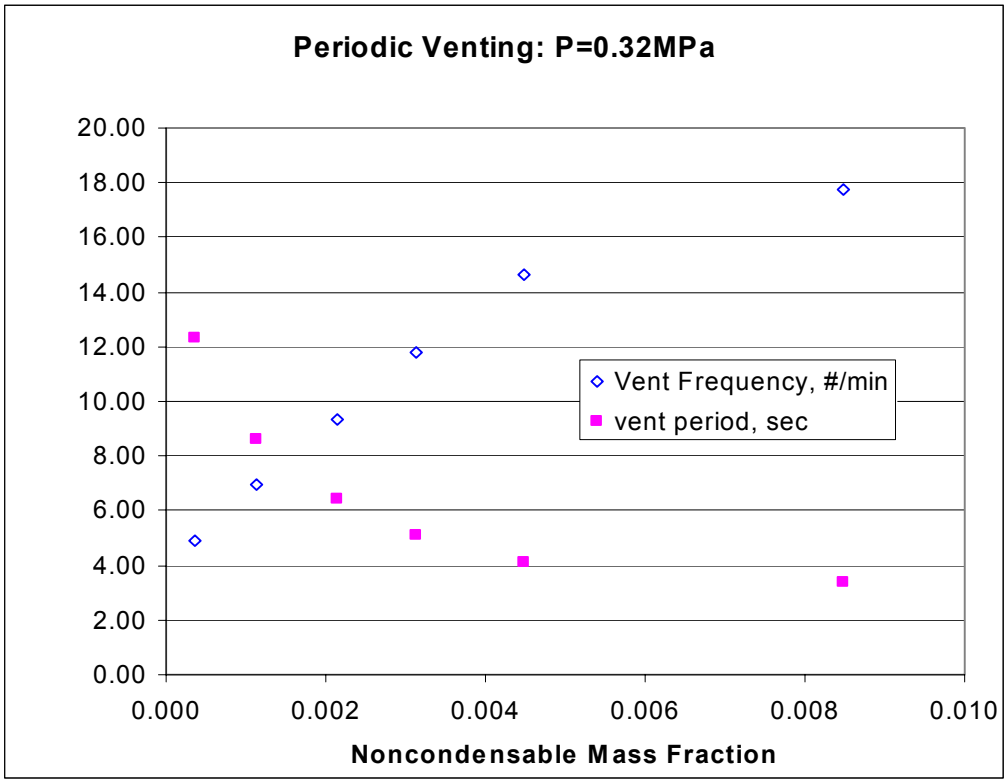

Figure 5.41 Vent Frequency and Vent Period for P=0.32MPa

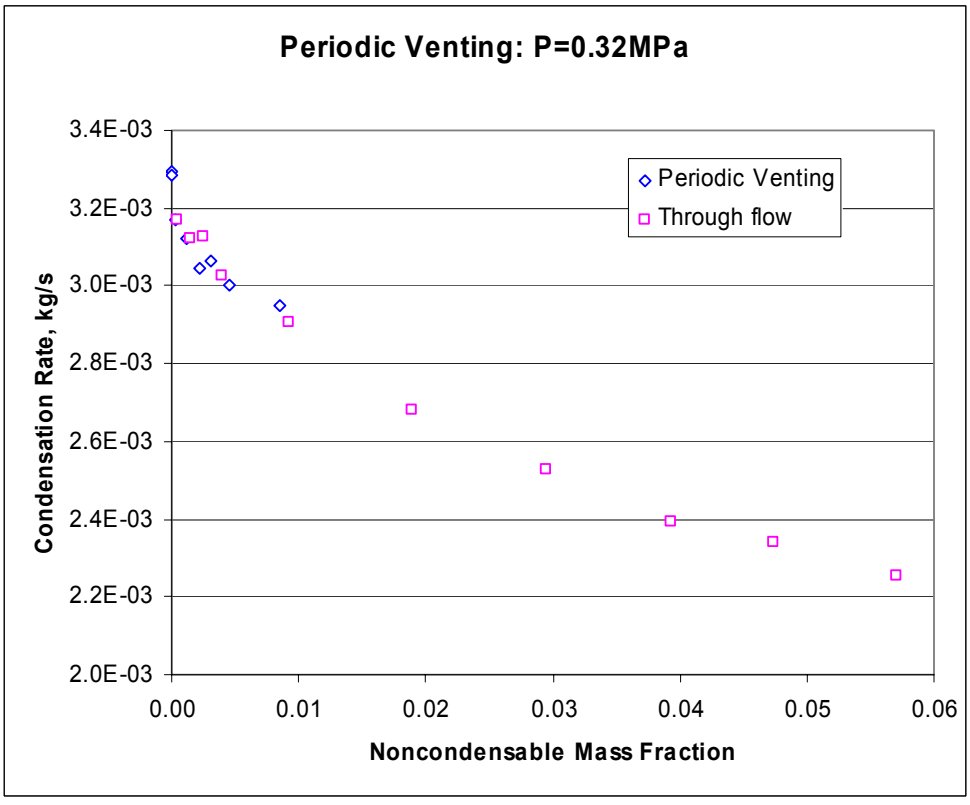

Figure 5.42 Condensation Rate P=0.32MPa

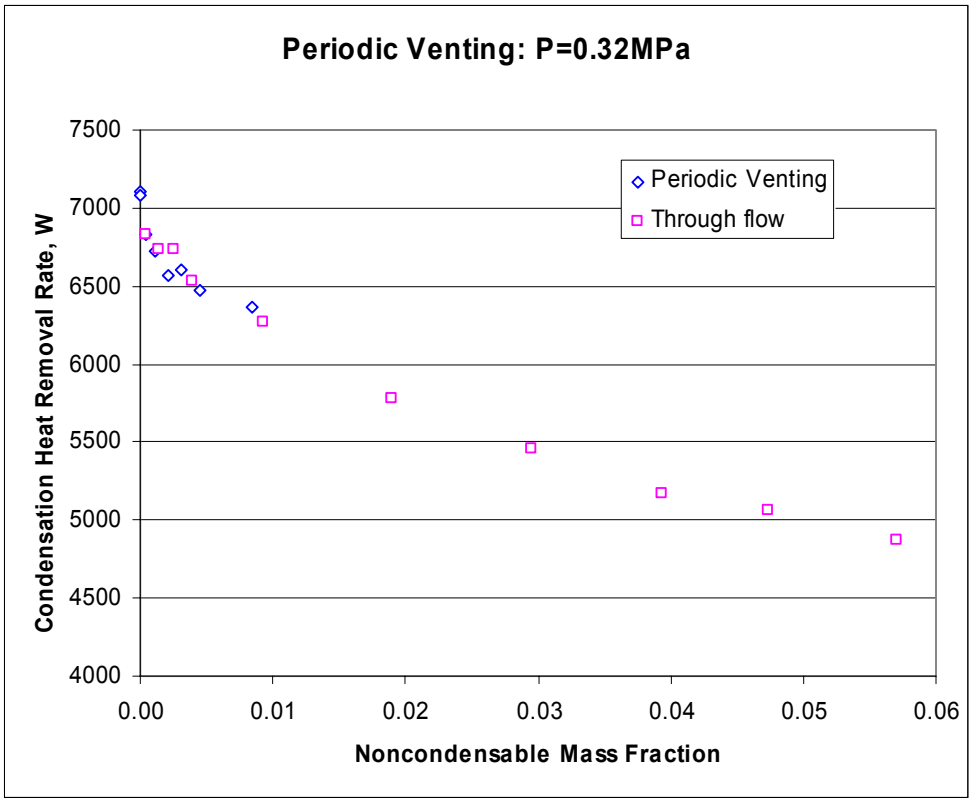

Figure 5.43 Condensation Heat Transfer Rate P=0.32MPa

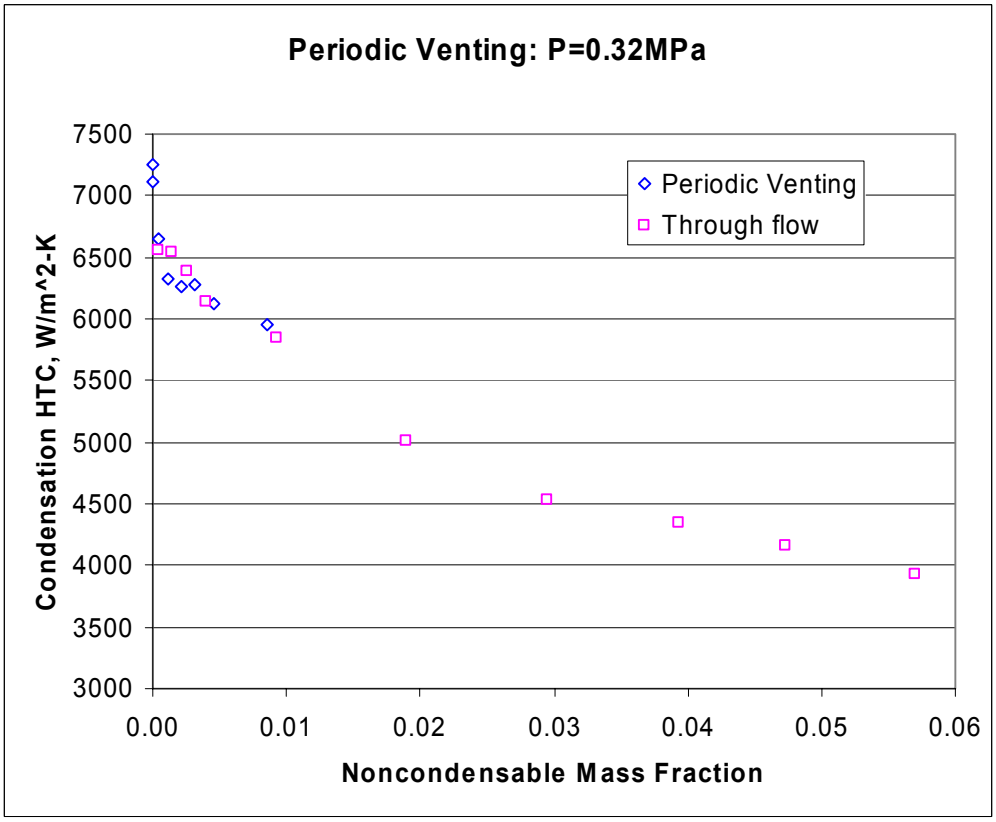

Figure 5.44 Condensation Heat Transfer Coefficients P=0.32MPa-

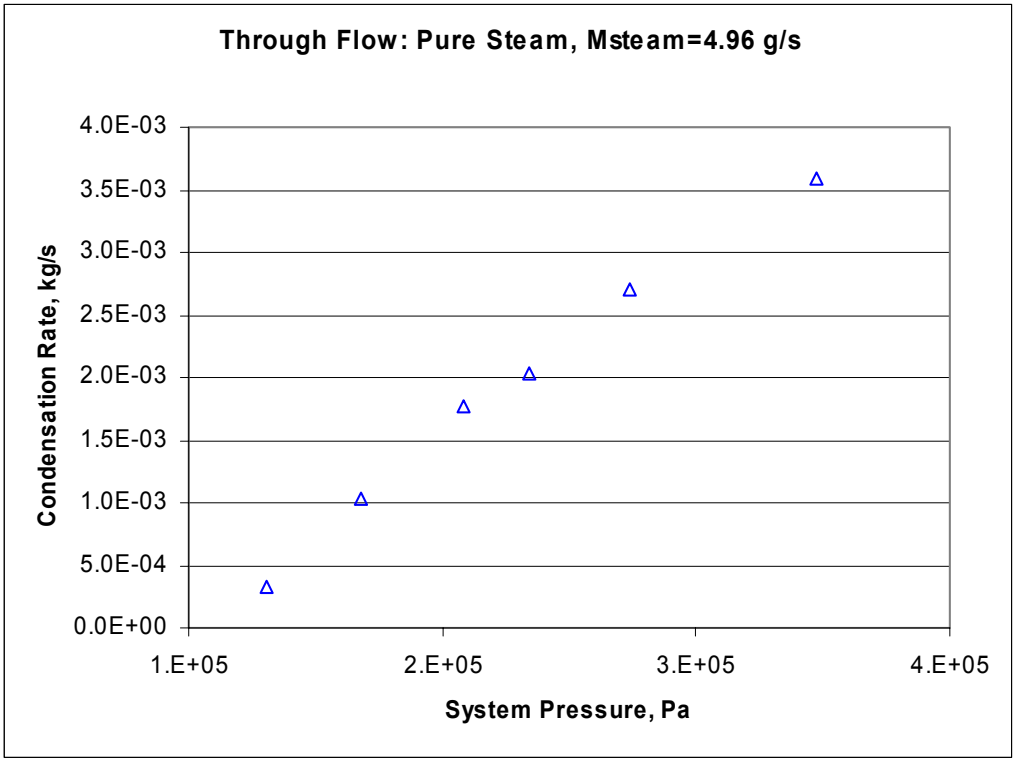

Figure 5.45 Through Flow: Condensation Rate for Pure Steam

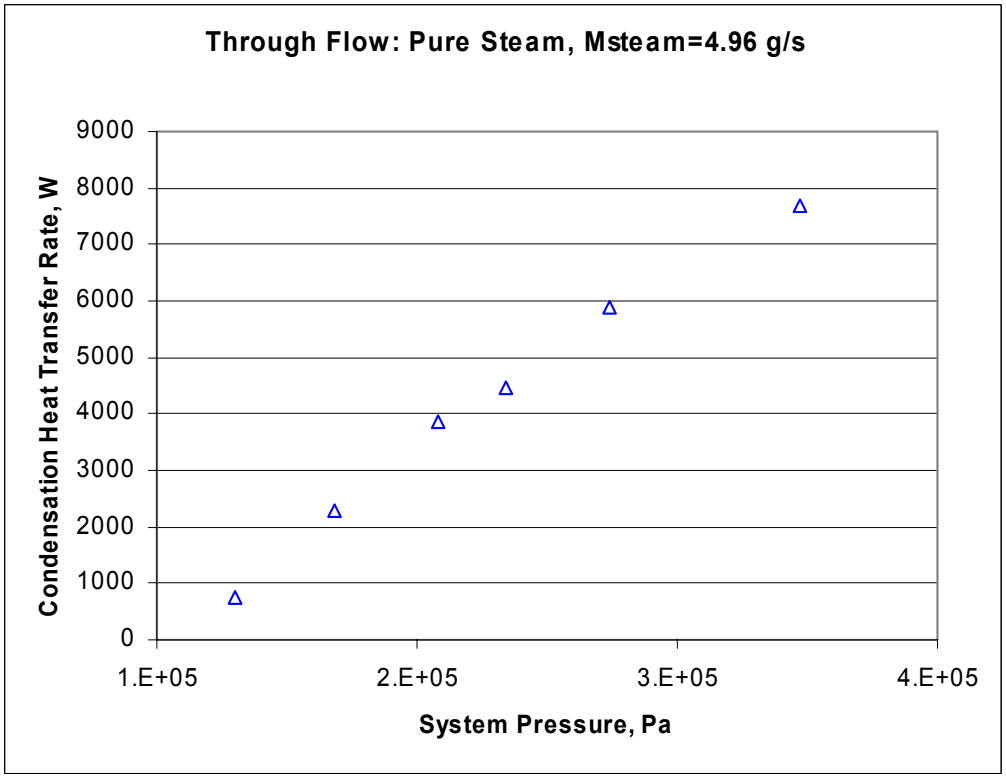

Figure 5.46 Through Flow: Condensation Heat Transfer Rate for Pure Steam

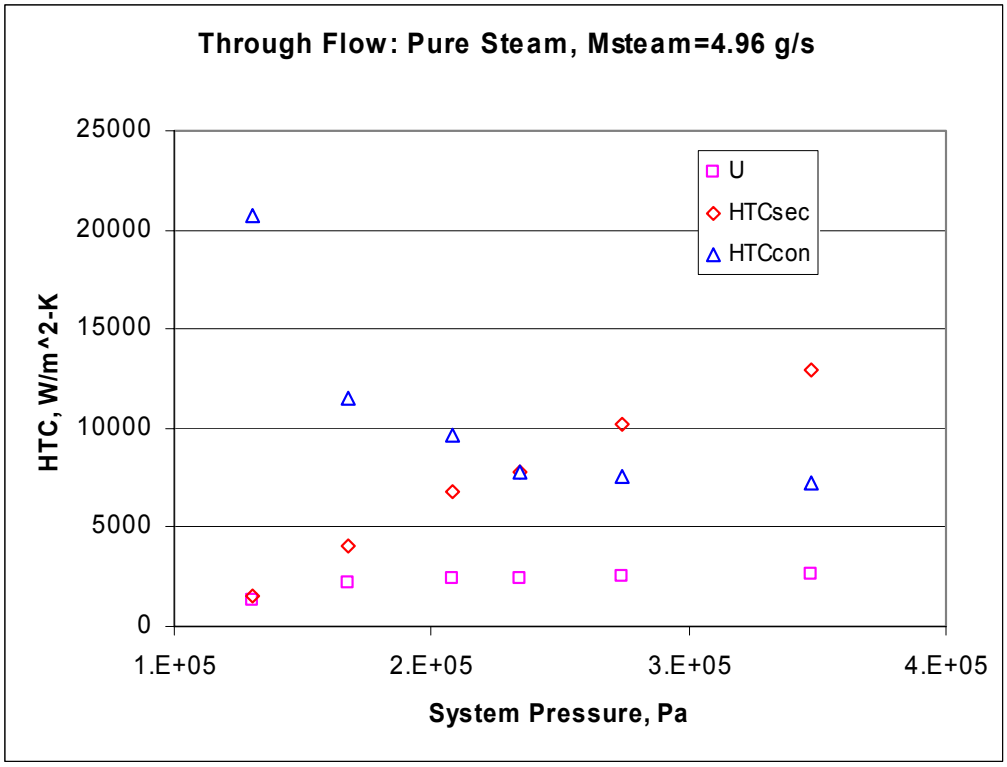

Figure 5.47 Through Flow: Heat Transfer Coefficient for Pure Steam

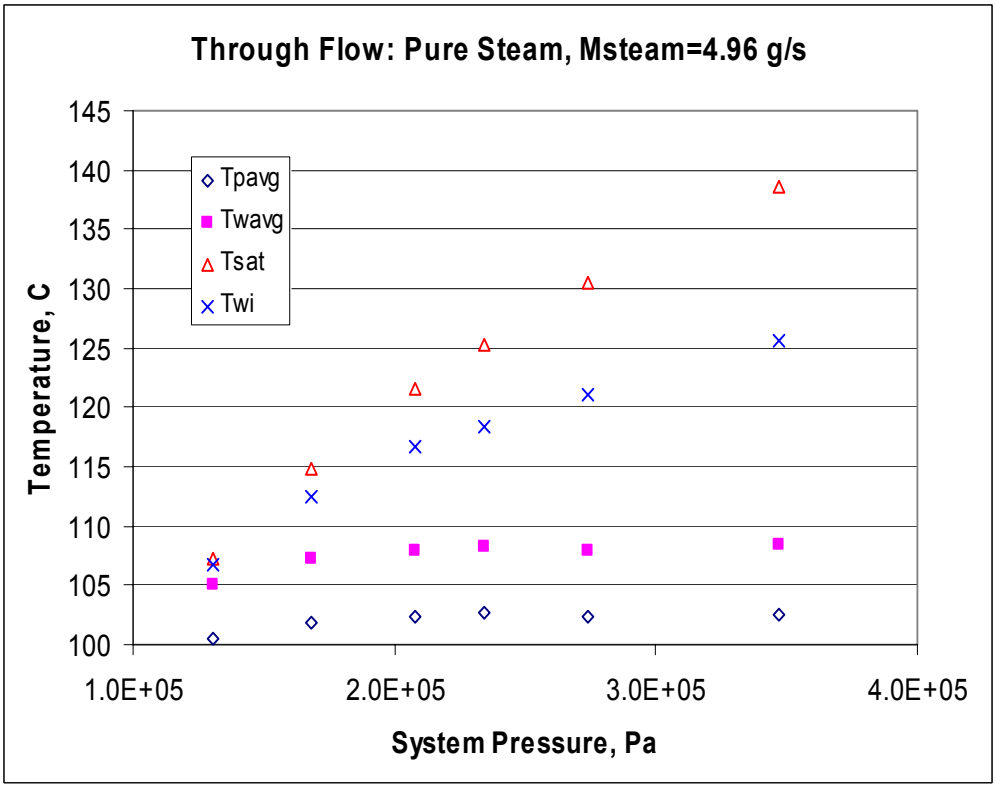

Figure 5.48 Through Flow: Temperatures

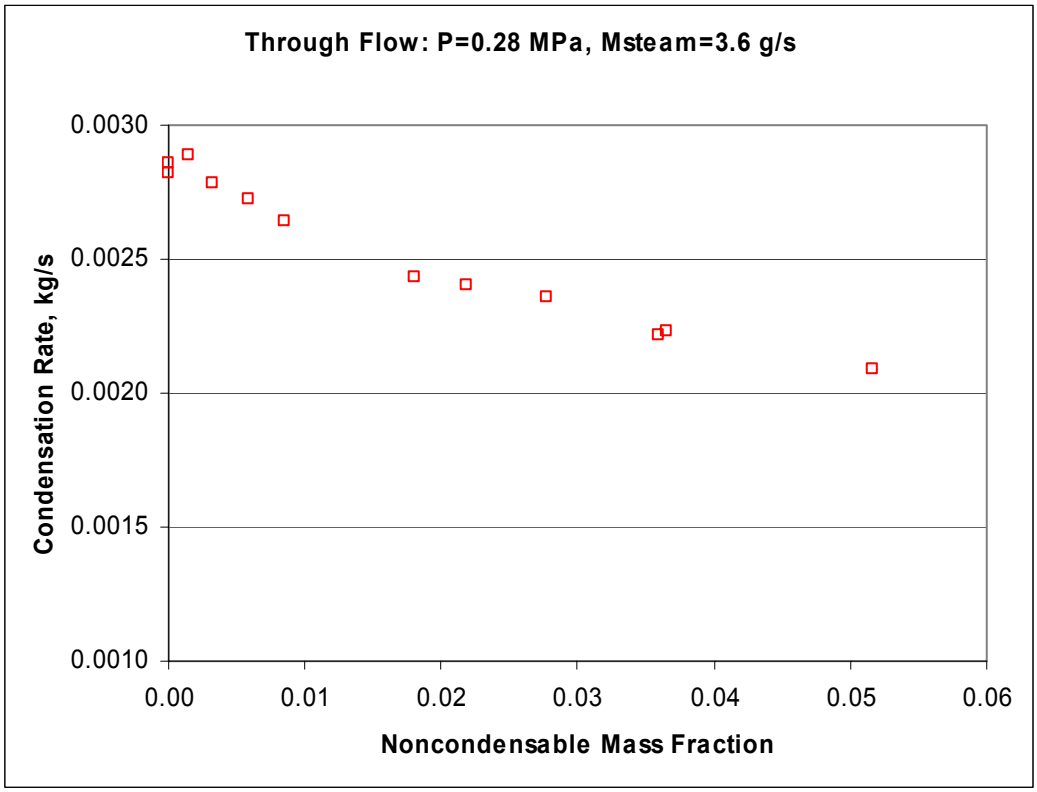

Figure 5.49 Through Flow: Condensation Rate at P=0.28 MPa, Msteam=3.6 g/s

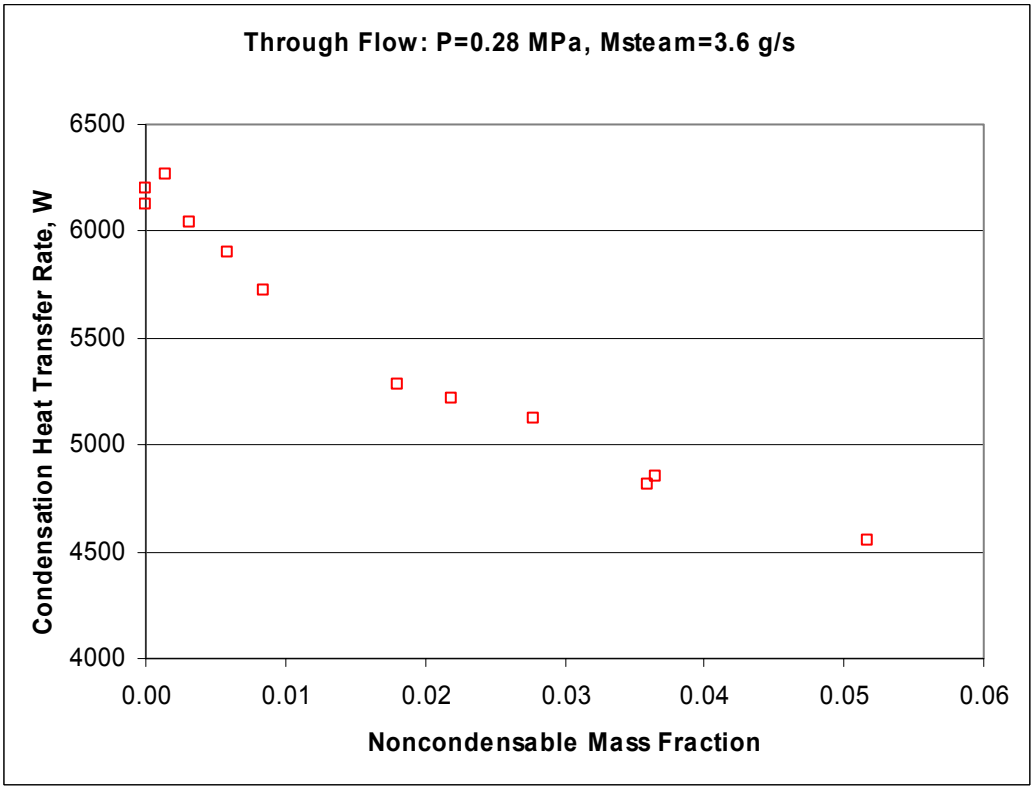

Figure 5.50 Through Flow: Condensation Heat Transfer Rate at P=0.28 MPa, Msteam=3.6 g/s

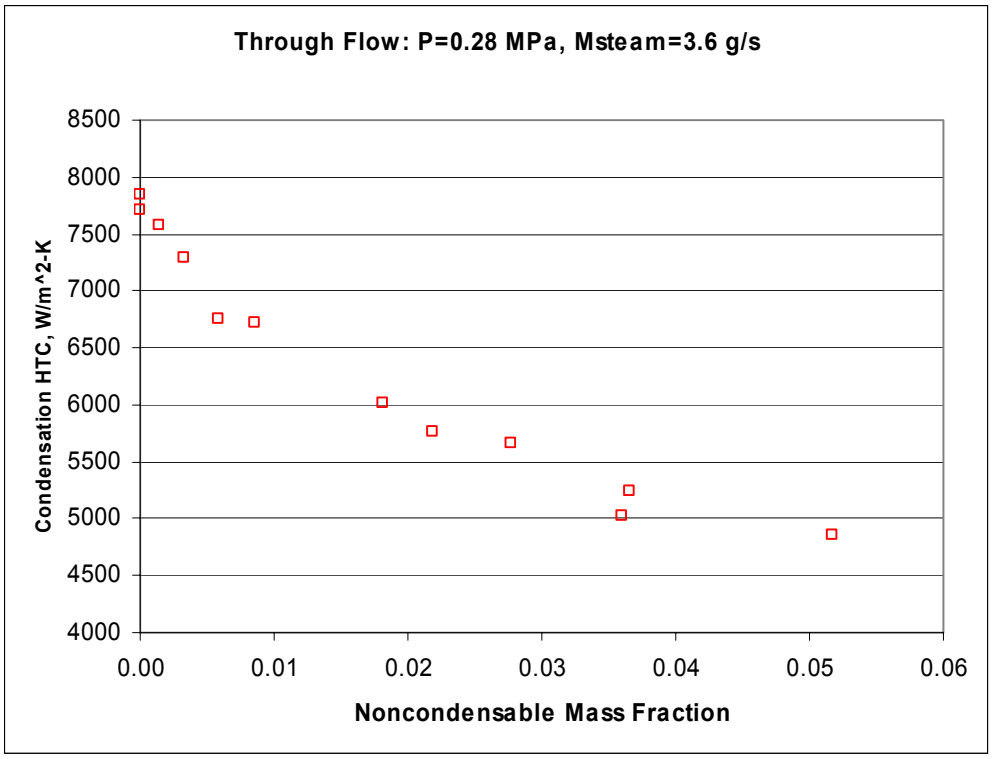

Figure 5.51 Through Flow: Condensation HTC at P=0.28 MPa, Msteam=3.6 g/s

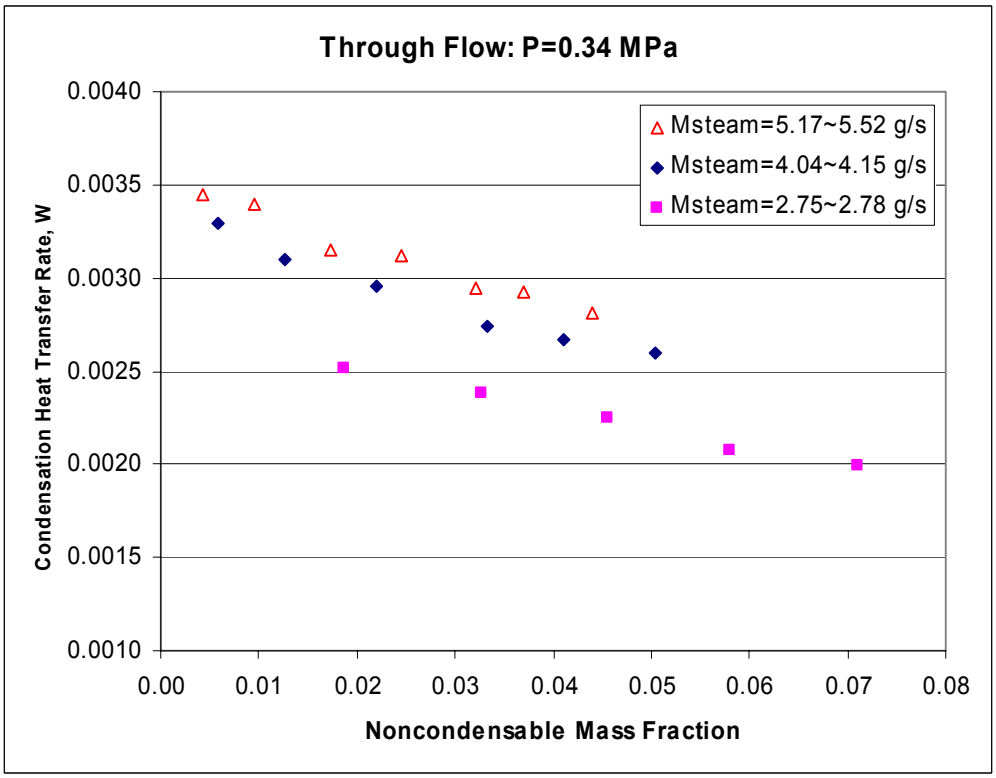

Figure 5.52 Through Flow: Condensation Rate at P=0.34 MPa

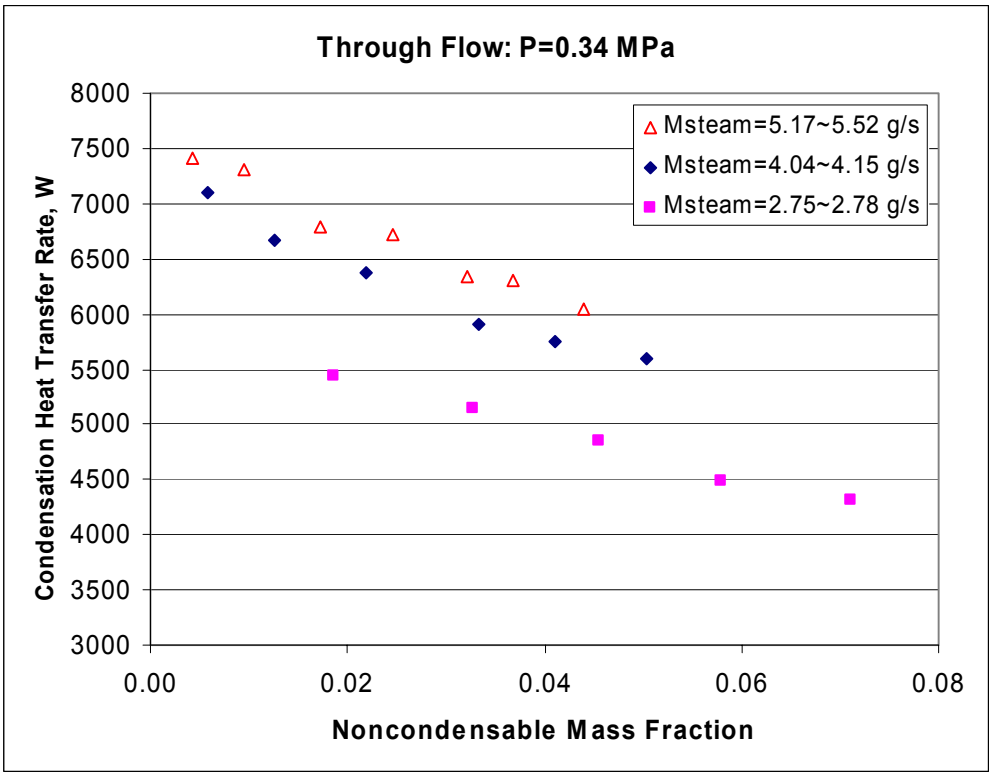

Figure 5.53 Through Flow: Condensation Heat Transfer Rate at P=0.34 MPa

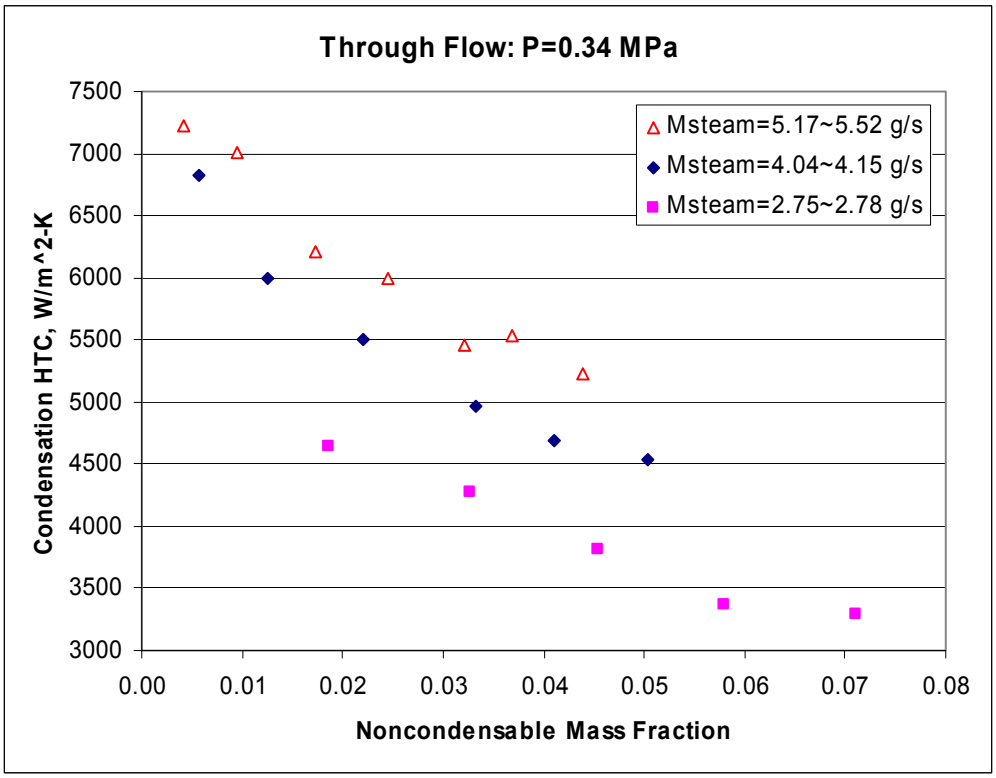

Figure 5.54 Through Flow: Condensation HTC at P=0.34 MPa

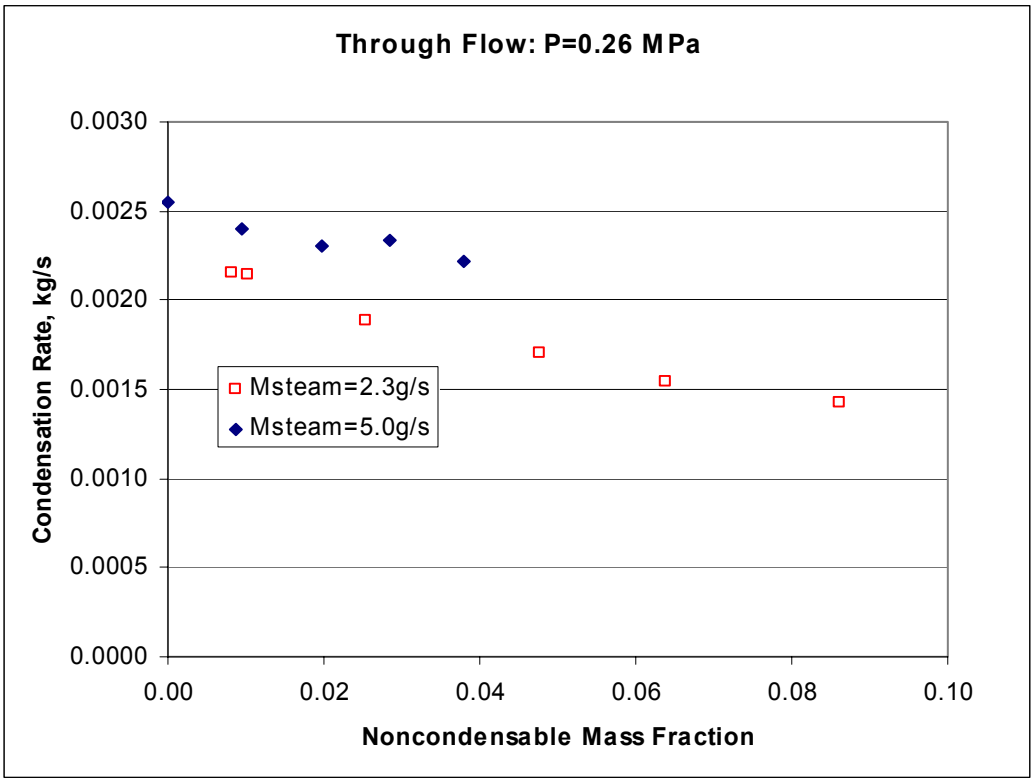

Figure 5.55 Through Flow: Condensation Rate at P=0.26 MPa

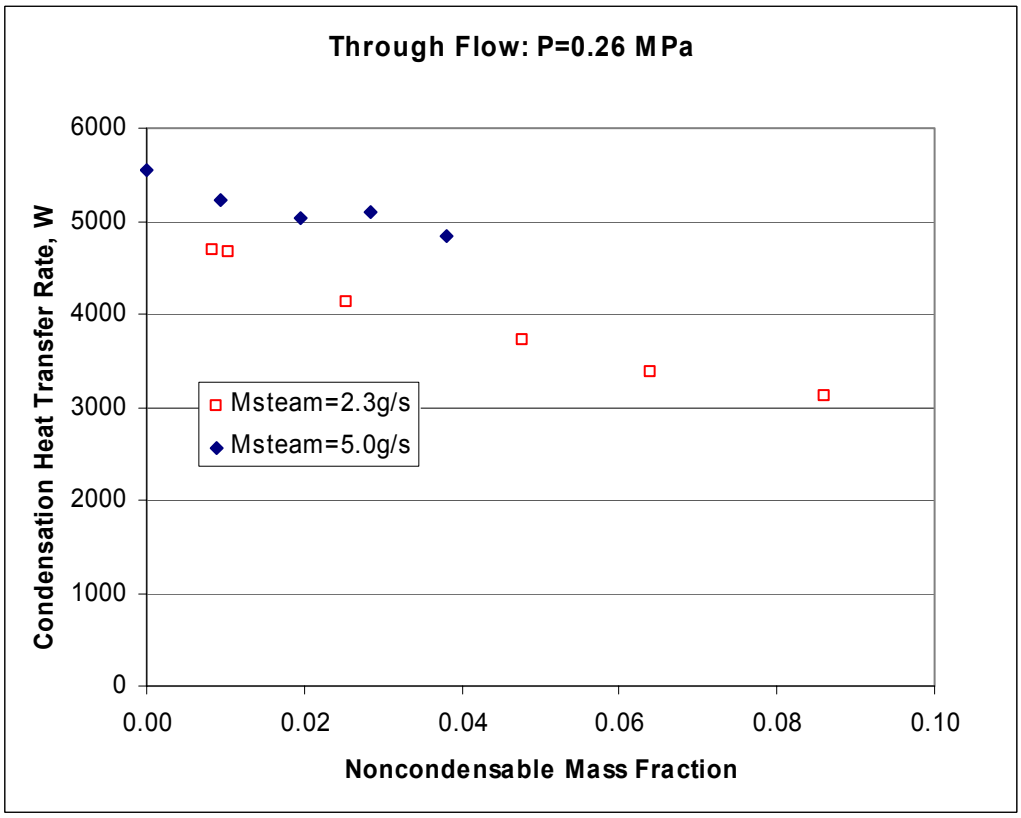

Figure 5.56 Through Flow: Condensation Heat Transfer Rate at P=0.26 MPa

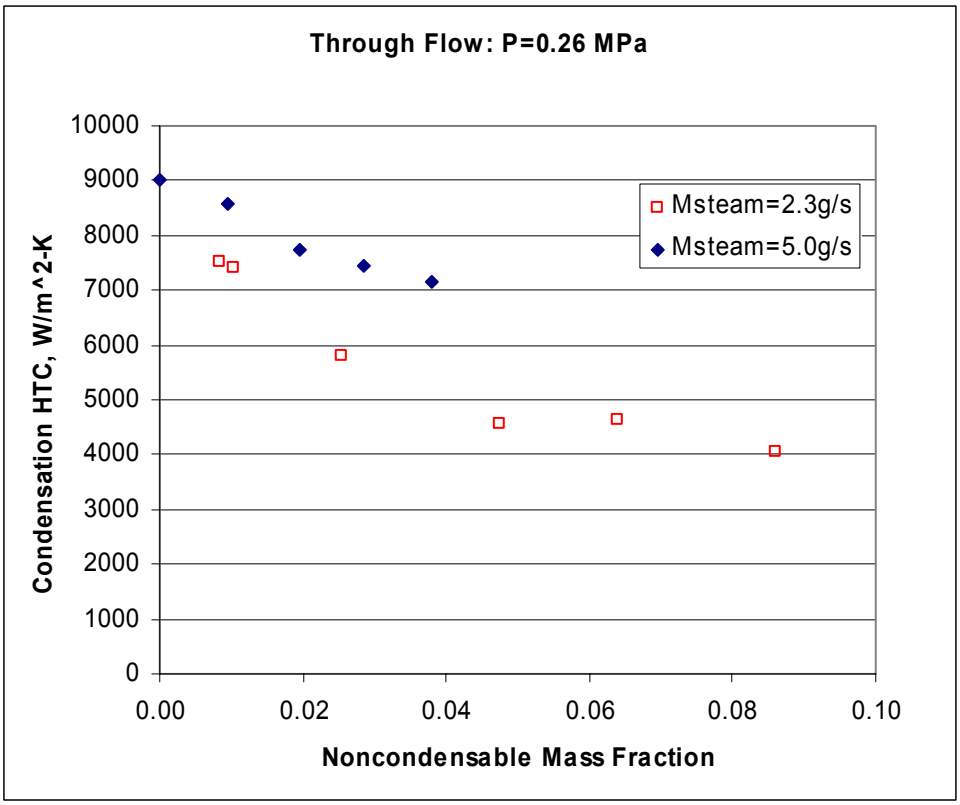

Figure 5.57 Through Flow: Condensation HTC at P=0.26 MPa

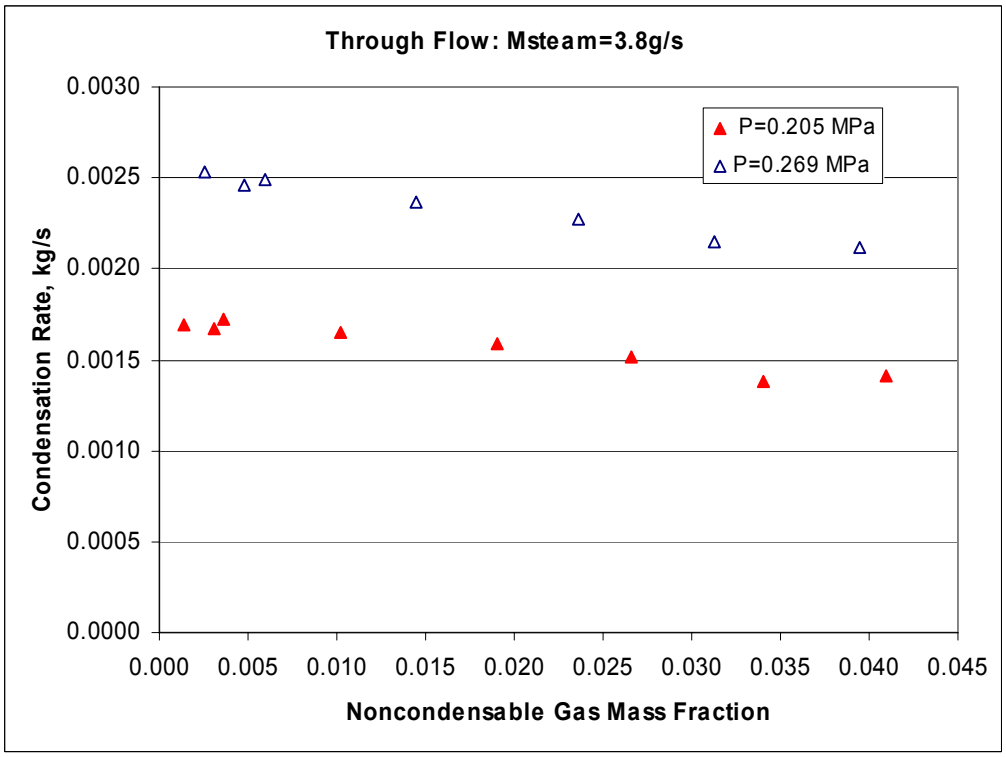

Figure 5.58 Through Flow: Condensation Rate at Msteam=3.8 g/s

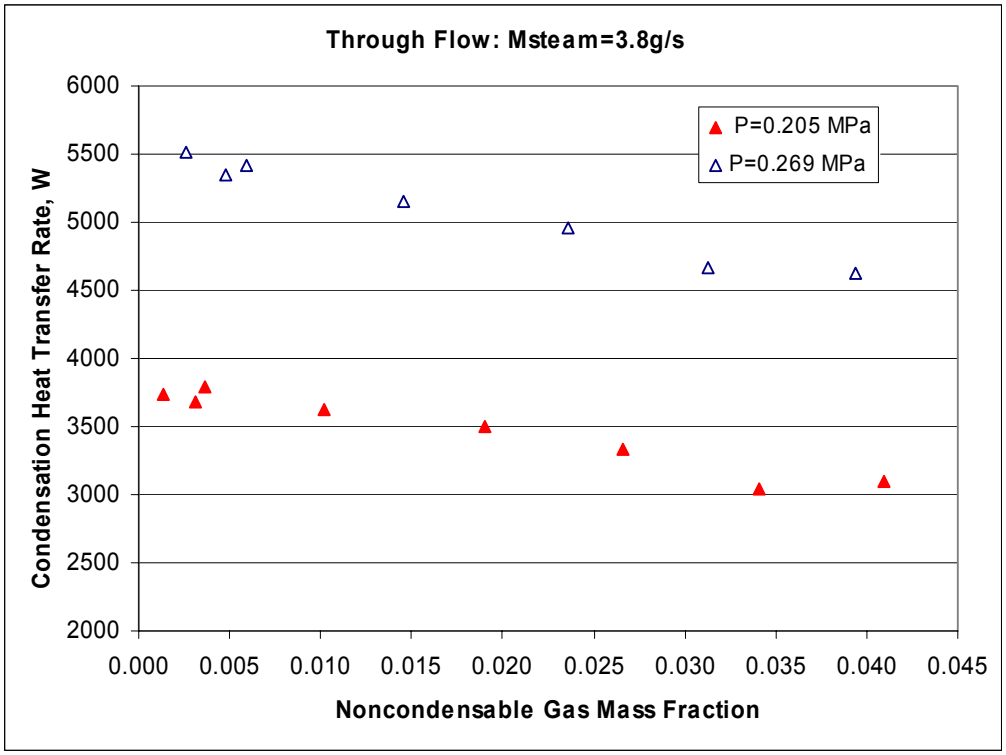

Figure 5.59 Through Flow: Condensation Heat Transfer Rate at Msteam=3.8 g/s

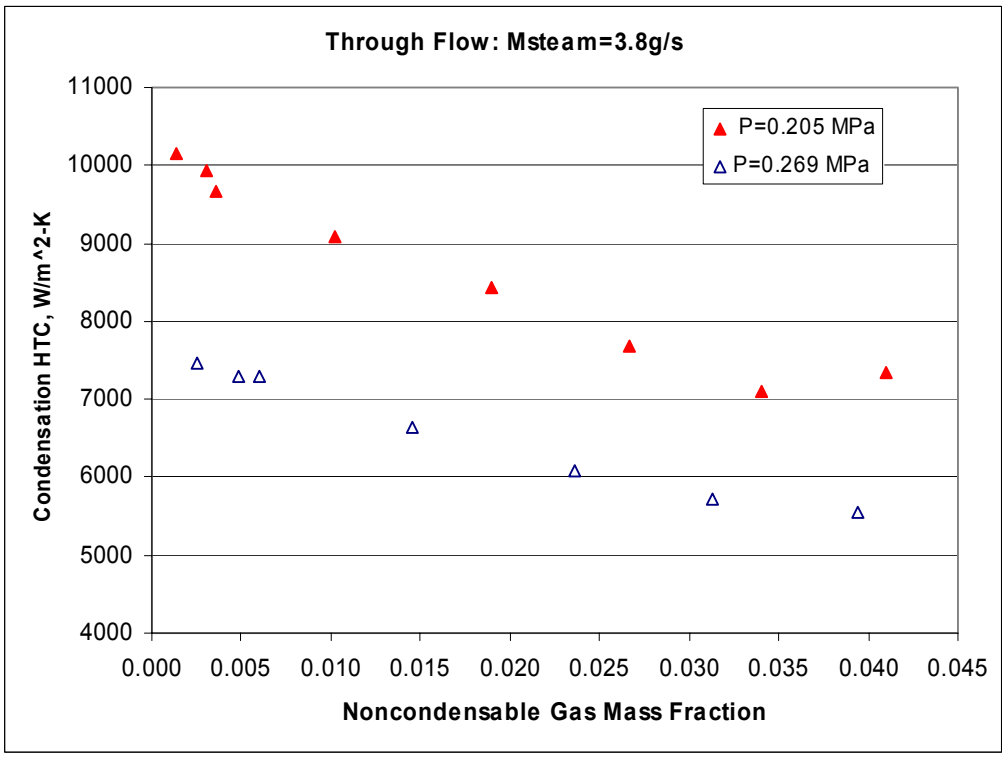

Figure 5.60 Through Flow: Condensation HTC at Msteam=3.8 g/s

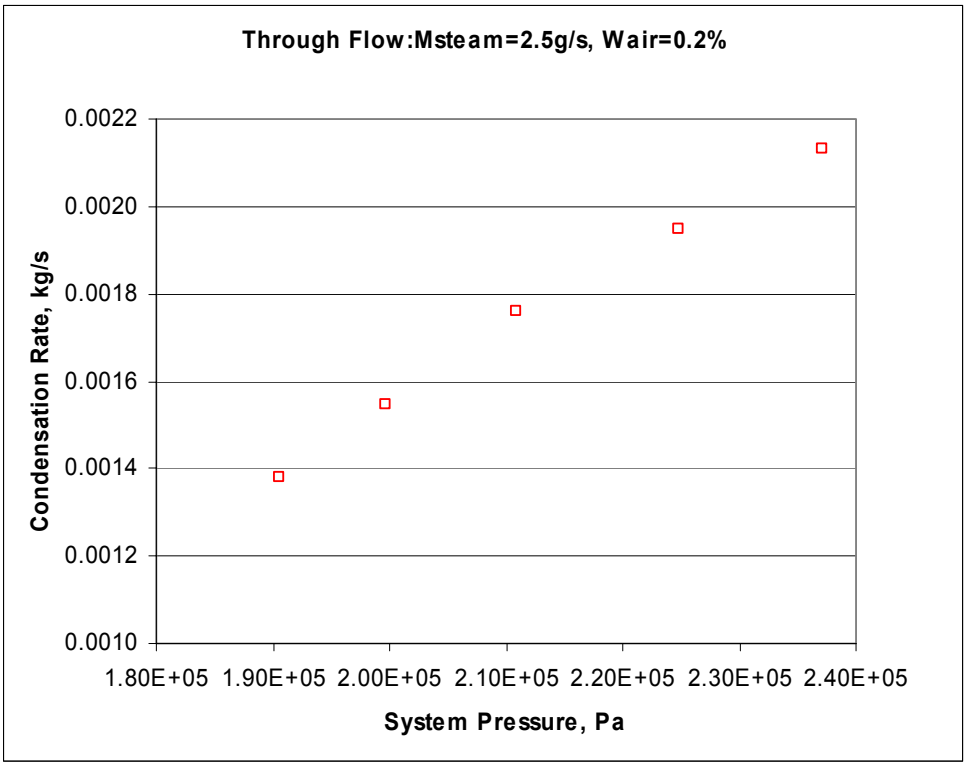

Figure 5.61 Through Flow: Condensation Rate at Msteam=2.5 g/s, Wair=0.2%

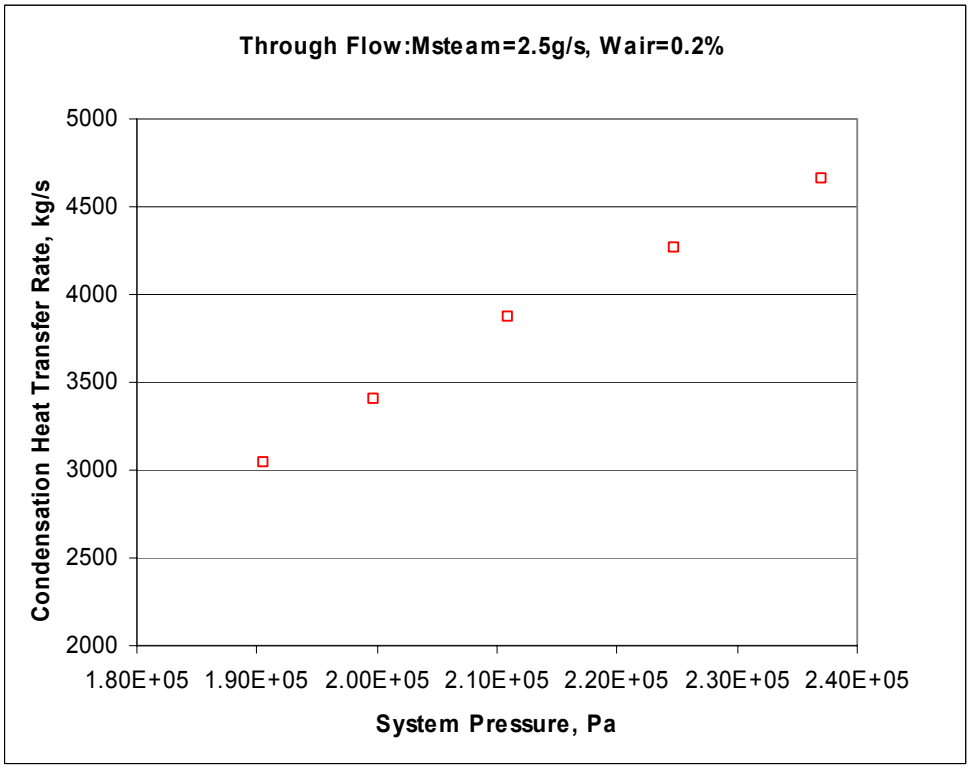

Figure 5.62 Through Flow: Condensation Heat Transfer Rate at Msteam=2.5 g/s, Wair=0.2%

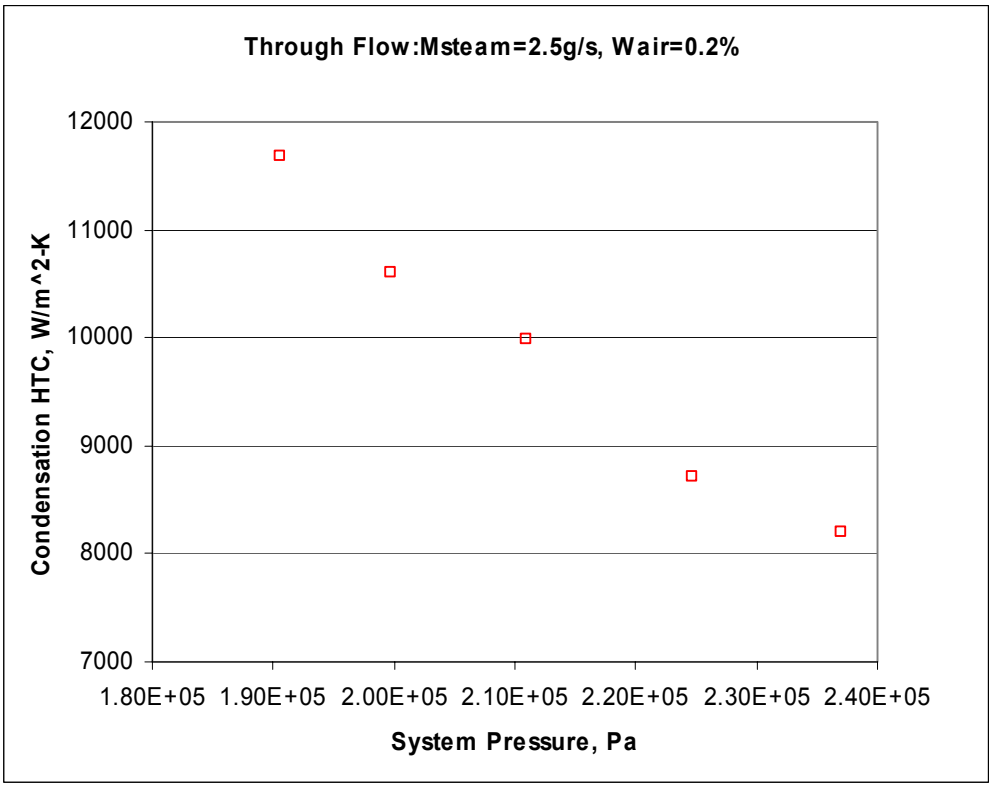

Figure 5.63 Through Flow: Condensation HTC at Msteam=2.5 g/s, Wair=0.2%

6. ANALYTICAL MODELING

6.1 Introduction

Analytical modeling has been developed since first year of the research. At first year, a condensation model was developed for forced downflow of steam and non-condensable gas in vertical tube based on the self-similar velocity profile assumption. First the model was tested for pure steam condensation and the predicted heat transfer results were compared with the experimental data. Then the model was tested for condensation in the presence of non-condensable gas, air, and results of the predictions were compared to the published experimental data [6.1]. The agreement was fairly good. At second year the condensation model was tested with various interfacial friction factor correlations and turbulent models. The iteration based analytical interfacial friction factor results on heat transfer were compared with the heat transfer results from the existing correlations for the interfacial friction factor [6.2]. Recently we obtained the Kuhn's detail experiment data [6.3]. So, some comparisons predicted by second year analysis model are presented in this chapter.

Further study was carried out on the analytical modeling of the film condensation in third year. The analytic model developed in the previous years is based on the self-similar velocity profile assumption. This assumption can be considered as a reasonable one for the engineering purpose. But it may introduce some errors in the entrance region since the entrance region is the developing region of velocity, temperature, and noncondensable fraction. Also, the condensation at the entrance region is most efficient in the condenser tube. So, it is valuable to develop the new model without the self-similar assumption. For this purpose, the full boundary layer model is under developing. The preliminary results are presented.

6.2 Comparison with Kuhn's data

In this section, comparisons between the Kuhn's detail experiment data [6.3] for pure steam cases and analysis predicted by second year model are presented. Detail descriptions for the model developed in second year are described in the second year report [6.2]. Kuhn's

experiment was performed with a 50.8 mm OD, 1.65 mm thickness, 2.37 m long tube with secondary forced flow cooling. The tube is composed of a 50 cm adiabatic entrance length, 2.4 m long condensing section, and a short adiabatic exit section.

Figs. 6.1 ~ 6.4 show the comparison between Kuhn's experimental data run 1.1-1 and analysis model. This case is inlet steam flow rate of 60.2 kg/he, system pressure of 113.9 kPa. The local condensation heat transfer coefficients presented in Fig. 6.1 show very good agreement between test data and analysis. Calculated gas mixture Reynolds number, liquid film Reynolds number, and film thickness from the test data also show good agreement with small bias as shown in Figs. 6.2 ~ 6.4. Figs. 6.5 and 6.6 show the local condensation heat transfer coefficients for test run 1.1-4R1 and 1.4-3, respectively. Inlet steam flow rate(kg/hr)/pressure(kPa) conditions of test run 1.1-4R1 and run 1.4-3 are 60.7/408.1 and 28.3/308.3, respectively. Test run 1.1-4R1 is a representative high pressure case and run 1.4-3 is a representative low steam flow rate case. The agreement between the test data and the predictions for these cases is also satisfactory.

6.3 New Boundary Layer Model

In this section the physical model for the condensation process is described. The governing equations for the mass, momentum, energy, and species concentration balance are presented along with the interface and boundary conditions. The basic assumptions used in the present model are given. The non-condensable effects on the condensation are taken into account through boundary layer analysis of species concentration and energy.

Assumptions:

- The flow is two-dimensional and steady state.
- The cross sectional geometry is circular and axially uniform.
- The condensate film is impermeable to non-condensable gas.
- The wall temperature is known.
- The non-condensable gas is assumed to be locally well mixed and at thermodynamic equilibrium with the vapor.

- The mass exchanged because of phase change at the liquid-gas interface has the properties corresponding to the interphase temperature

Physical Model

Figure 6.7 shows the schematic of the physical model considered for the condensation process with defined coordinate systems. A superheated vapor-gas mixture, corresponding to inlet pressure and temperature conditions, enters the tube and is turbulent. The condenser tube surface is below the vapor saturation temperature. The condensate forms along the tube surface and thus an annular flow regime is realized inside the condenser tube. Along the condensate film interface, a temperature, momentum and concentration boundary layers develop and respective gradients are formed. These gradients are shown later to impede the condensation.

1) Gas Region

Basic balance equations for the mass, momentum, energy and species in steam-gas mixture region are as follows:

Conservation of Mass

$$\frac{\partial \rho \mathrm{rv}}{\partial \mathrm{r}} + \frac{\partial \rho \mathrm{ru}}{\partial \mathrm{x}} = 0 \tag{6.1}$$

Conservation of x-Directional Momentum

$$\frac{\partial \rho \mathrm{u}^2}{\partial \mathrm{x}} + \frac{1}{\mathrm{r}} \frac{\partial \mathrm{r} \rho \mathrm{vu}}{\partial \mathrm{r}} = -\frac{\partial \mathrm{p}}{\partial \mathrm{x}} - \frac{1}{\mathrm{r}} \frac{\partial \mathrm{r}\, \tau}{\partial \mathrm{r}} + \rho g \tag{6.2}$$

Conservation of Energy

$$\frac{\partial \rho C_p \mathrm{u}\, T}{\partial \mathrm{x}} + \frac{1}{\mathrm{r}} \frac{\partial \mathrm{r} \rho C_p \mathrm{vT}}{\partial \mathrm{r}} = -\frac{1}{\mathrm{r}} \frac{\partial \mathrm{r}\, q}{\partial \mathrm{r}} \tag{6.3}$$

Conservation of Species

$$\frac{\partial \rho \mathrm{u}\, W}{\partial \mathrm{x}} + \frac{1}{\mathrm{r}} \frac{\partial \mathrm{r} \rho \mathrm{vW}}{\partial \mathrm{r}} = -\frac{1}{\mathrm{r}} \frac{\partial \mathrm{r}\, j}{\partial \mathrm{r}} \tag{6.4}$$

To complete the above balance equations, we need the constitutive relations for shear stress, heat flux, diffusion mass flux as follows:

Shear Stress

$$\tau = -\left(\mu + \mu^t\right)\frac{\partial \mathrm{u}}{\partial \mathrm{r}} \tag{6.5}$$

Heat Flux

$$q = -\left(k + k^t\right)\frac{\partial \mathrm{T}}{\partial \mathrm{r}} \tag{6.6}$$

Diffusion Mass Flux

$$j = -\rho\left(D + D^t\right)\frac{\partial \mathrm{W}}{\partial \mathrm{r}} \tag{6.7}$$

2) Film Region

For the liquid film, the force balance in the control volume depicted in Fig. 6.7 can be described as follows:

$$\tau_L = \left[\left(\rho_L - \rho_g\right)g - \frac{dp}{dx}\right]\left(\delta - y\right) + \tau_i \tag{6.8}$$

For laminar film, the velocity profile in the liquid film can be obtained from the above equation.

$$u_L(y) = \frac{\left(\rho_L - \rho_g\right)g}{\mu_L} G\left(\delta y - \frac{y^2}{2}\right) + \frac{\tau_i}{\mu_L} y \tag{6.9}$$

$$\text{where, } G = 1 - \frac{1}{\left(\rho_L - \rho_g\right)g}\frac{dp}{dx}$$

The first term in the right hand side of above equation is the parabolic velocity distribution, which is exactly same with Nusselt analysis for no interfacial shear. The second term is the linear velocity distribution due to the interfacial shear. For high interfacial shear, the second term is dominant. So the velocity distribution is almost linear.

The liquid flow rate can be calculate from the velocity profile as follows:

$$\mathrm{m}_L = \int_{R-\delta}^{\mathrm{R}} \mathrm{u}_\mathrm{L}(\mathrm{r})\, 2\pi \mathrm{r} \mathrm{dr} = 2\pi \int_0^{\delta} \mathrm{u(y)}\, (\mathrm{R} - \mathrm{y}) \mathrm{dy} \tag{6.10}$$

The liquid flow rate must be balanced with the sum of the condensation flow rate at each axial node.

$$\mathrm{m}_L = \sum \left(m_c\right)_i \tag{6.11}$$

From eqs. (6.10) and (6.11) the mass balance in liquid film can be expressed with respect to the film thickness as follows:

$$\frac{\left(\rho_L - \rho_g\right)g}{3\nu_L} G\delta^3 + \frac{\tau_i}{2\nu_L}\delta^2 - \frac{m_L}{2\pi R} = 0 \tag{6.12}$$

Conservation of Energy

$$\frac{\partial \rho_L C_{pL} \mathrm{u}_\mathrm{L}\ T_L}{\partial \mathrm{x}} + \frac{1}{\mathrm{r}} \frac{\partial \mathrm{r} \rho_L C_{pL} \mathrm{v}_\mathrm{L} \mathrm{T}_\mathrm{L}}{\partial \mathrm{r}} = -\frac{1}{\mathrm{r}} \frac{\partial \mathrm{r}\ q_L}{\partial \mathrm{r}} \tag{6.13}$$

The constitutive relations for heat flux in the liquid is as follows:

$$q_L = -\left(k_L + k_L{}^t\right) \frac{\partial \mathrm{T}_L}{\partial \mathrm{r}} \tag{6.14}$$

3) Interfacial Jump Condition

We need the interface jump condition at the liquid-gas interface.

Mass

$$m_c^{"} = m_L^{"} \tag{6.15}$$

Momentum

$$\mu_L \left.\frac{\partial \mathrm{u}_L}{\partial \mathrm{r}}\right|_i = \mu_G \left.\frac{\partial \mathrm{u}_G}{\partial \mathrm{r}}\right|_i \tag{6.16}$$

Energy

$$-k_L \frac{\partial \mathrm{T}_L}{\partial \mathrm{r}}\bigg|_i = -k_G \frac{\partial \mathrm{T}_G}{\partial \mathrm{r}}\bigg|_i + m_c^{"} h_{fg} \tag{6.17}$$

Species

$$m_c^{"} W_i - \rho_G D \frac{\partial W}{\partial \mathrm{r}}\bigg|_i = 0 \tag{6.18}$$

4) Boundary Condition

Boundary conditions at the tube wall, tuber center, and interface can be specified as follows:

At interface:

$$u_{Li} = u_{Gi}\ ,\ T_{Li} = T_{Gi} \tag{6.19}$$

At r = 0 (tube center line),

$$\frac{\partial \mathrm{u}_G}{\partial \mathrm{r}} = \frac{\partial \mathrm{T}_G}{\partial \mathrm{r}} = \frac{\partial W}{\partial \mathrm{r}} = 0 \tag{6.20}$$

At r = R (wall),

$$\mathrm{u}_L = 0, \qquad T_L = Tw \tag{6.21}$$

5) Turbulent Model

Turbulent Eddy Diffusivity

It is important to choose the appropriate turbulent transport model. In this analysis, three different models for the eddy diffusivity of momentum are considered.

The first is the Prandtl-Nikuradze model (Seban [6.4], Rohsenow et al. [6.5]) which divides the flow regions into three different regions: laminar sub-layer, buffer region, and turbulent core region.

$$\frac{\varepsilon_m}{\nu_g} = 0 \qquad for \quad 0 \le y^+ \le 5 \tag{6.22a}$$

$$\frac{\varepsilon_m}{\nu_g} = \frac{y^+ - 5}{5} \qquad for \quad 5 \le y^+ \le 30 \tag{6.22b}$$

$$\frac{\varepsilon_m}{\nu_g} = \frac{y^+}{2.5} \qquad for \quad 30 \le y^+ \tag{6.22c}$$

From above equation, there is a discontinuity between buffer region and turbulent core region. To make it continuous, the equation for turbulent core region was modified slightly as follows:

$$\frac{\varepsilon_m}{\nu_g} = 5 - \frac{y^+ - 30}{2.5}\cdot \qquad for \quad 30 \le y^+ \tag{6.22d}$$

The second is Reichardt model (given in Burmeister [6.6]) which is applicable to all regions of the turbulent pipe flow.

$$\begin{aligned} \frac{\varepsilon_m}{\nu_g} &= \frac{R^+}{2.5}\cdot\frac{1}{6}\left[1-\left(\frac{r}{R}\right)^2\right]\left[1+2\left(\frac{r}{R}\right)^2\right] \\ &= \frac{y^+}{2.5}\cdot\frac{1}{6}\left[1+\frac{r}{R}\right]\left[1+2\left(\frac{r}{R}\right)^2\right] \end{aligned} \tag{6.23}$$

In eq. (6.22c), the eddy diffusivity of momentum increases linearly from the wall whereas it increases initially but stays almost constant near the pipe center in eq. (6.23). This model was adopted in the present analysis for three regions in the gas core and is given below.

$$\frac{\varepsilon_m}{\nu_g} = 0 \qquad for \quad 0 \le y^+ \le 5 \tag{6.24a}$$

$$\frac{\varepsilon_m}{\nu_g} = \frac{y^+ - 5}{5} \qquad for \quad 5 \le y^+ \le 26 \tag{6.24b}$$

$$\frac{\varepsilon_m}{\nu_g} = \frac{21}{5} - \frac{y^+ - 26}{2.5}\cdot\frac{1}{6}\left[1+\frac{r}{R}\right]\left[1+2\left(\frac{r}{R}\right)^2\right] \qquad for \quad 26 \le y^+ \tag{6.24c}$$

The third is the method applied by Chen & Ke [6.7]. They divided the eddy diffusivity of momentum into two parts for the mixture region. One is the outer region and the other is the interface region. For the outer region, they used the turbulent core region correlation of Prandtl-Nikuradze model as in eq. (6.22c). For the interface region, Mills & Chung[6.8] model was used.

$$\frac{\varepsilon_m}{\nu_g} = 6.47\text{X}10^{-4}\,\frac{g\rho_g}{\sigma}\left(\frac{\nu_g}{u^*}\right)^2(\delta^+ - y^+)^2\,\text{Re}_g^{\,1.678}. \tag{6.25}$$

For this case, the boundary between the interface region and the outer region is determined by the intersection of each line.

Turbulent Thermal Diffusivity

Turbulent Prandtle number is defined as follows:

$$\text{Pr}_t \equiv \frac{\nu^t}{\alpha^t} = \frac{\mu^t C_{pG}}{k^t} \tag{6.26}$$

From the above equation, the turbulent thermal diffusivity can be calculated with the assumption of $\text{Pr}_t = 1$ and with the turbulent thermal diffusivity calculated previously.

$$k^t = \frac{\mu^t C_{pG}}{\text{Pr}_t} \tag{6.27}$$

Turbulent Mass Diffusivity

Turbulent Schmitt number is defined as follows:

$$Sc_t \equiv \frac{\nu^t}{D^t} = \frac{\mu^t}{\rho_G D^t} \tag{6.28}$$

From the above equation, the turbulent mass diffusivity can be calculated with the assumption of $Sc_t = 1$ and with the turbulent thermal diffusivity calculated previously.

$$D^t = \frac{\mu^t}{\rho_G Sc_t} \tag{6.29}$$

6) Mixture Property

Noncondensable gas mass fraction is defined as

$$W = \frac{\rho_a}{\rho_G} = \frac{\rho_a}{\rho_a + \rho_v}. \tag{6.30}$$

Then the mixture density can be calculated with the noncondensable gas mass fraction and steam density as follows:

$$\rho_G = \rho_a + \rho_v = \frac{\rho_v}{1-W} \tag{6.31}$$

Vapor density is a function of temperature and vapor partial pressure.

$$\rho_v = \rho_v(T_G, P_v) \tag{6.32}$$

It must be noted that vapor assumed as superheated except at the interface, where vapor is saturated. Vapor partial pressure can be calculated from Gibbs-Dalton ideal gas mixture equation As follows:

$$\frac{P_v(j)}{P_{TOT}} = \frac{1-W(j)}{1-W(j)\left(1-\frac{M_v}{M_a}\right)} \tag{6.33}$$

By rearranging the above equation, we can calculate the noncondensable gas mass fraction with vapor partial pressure.

$$W(j) = \frac{P_{TOT} - P_v(j)}{P_{TOT} - P_v(j)\left(1-\frac{M_v}{M_a}\right)} \tag{6.34}$$

Viscosity, thermal conductivity, and specific heat for the mixture can be calculated as follows [6.9]:

$$\mu_G = \sum_{i=1}^{2} \frac{x_i \mu_i}{\sum_{j=1}^{2} x_j \phi_{ij}} \tag{6.35}$$

Here, x is mole fraction.

$$\phi_{ij} = \frac{1}{\sqrt{8}}\left(1+\frac{M_i}{M_j}\right)^{-0.5}\left[1+\left(\frac{\mu_i}{\mu_j}\right)^{0.5}\left(\frac{M_j}{M_i}\right)^{0.25}\right]^2 \tag{6.36}$$

$$k_G = \sum_{i=1}^{2} \frac{x_i k_i}{\sum_{j=1}^{2} x_j \phi_{ij}} \tag{6.37}$$

$$Cp_G = \sum_{i=1}^{2} \frac{x_i Cp_i}{\sum_{j=1}^{2} x_j \phi_{ij}} \tag{6.38}$$

Film properties are evaluated at the film temperature, which is the arithmetic mean of the inside wall temperature and interface temperature.

$$\mathrm{T}_f = \frac{\mathrm{Tw} + \mathrm{Ti}}{2} \tag{6.39}$$

7) Pressure Drop

In the boundary layer model, we can calculate the pressure field. But the calculation of the pressure field requires more iterations to match mass and momentum balances and more computing time. Since the accurate calculation of the velocity field is not the main focus of this analysis, we can use the general pressure drop correlation.

$$\frac{\mathrm{dp}}{\mathrm{dx}} = -\frac{f_o}{2R}\frac{1}{2}\rho_{\mathrm{G}}\mathrm{u}_{\mathrm{Gavg}}{}^2 \tag{6.39}$$

Here, the friction factor is calculated with Blasius correlation for turbulent or with general laminar correlation.

$$\mathrm{f}_0 = \frac{0.079}{\mathrm{Re}_{\mathrm{G}}^{.25}} \qquad \text{for turbulent} \tag{6.40}$$

$$= \frac{16}{\mathrm{Re}_{\mathrm{g}}} \qquad \text{for laminar.} \tag{6.41}$$

6.4 Solution Methodology

The governing equations presented in the previous section are descritized with numerical Finite Volume Method (FVM) [6.10]. The gas region momentum, energy, species equations and film region energy equation are parabolic partial differential equations. So, the marching scheme along x-direction (axial direction) is used. For the descretization, numerical implicit scheme and staggered grid method are used. The solution procedure is summarized as follows:

1) Specify Inlet and Boundary Conditions :

- Win, TGin, mv, Ptot_in, uGin, vGin

- Tw

2) Initialize the variables and parameters

- Assume interface Wi

- Calculate interface Pvi and TGi using Wi

- Calculate mixture properties using TGin, Win, Pv

- Assume interface condensation mass flux, $m_c^{"}$ => vGi

- Assume interfacial shear, τ_i

3) Calculate film thickness, δ from film mass balance

4) Solve uL(j) from film force balance => uLi

5) Solve uG(j) from gas momentum balance => new

6) Solve vG(j) from gas mass balance => new vGi

7) Go to 3) and repeat until vGi, τ_i , uG(j), vG(j) converge

8) Solve TL(j) from film energy balance => qLi

9) Solve TG(j) from gas energy balance => qGi_sensible

10) Solve W(j) from gas species balance => qGi_sensible

- Calculate new $m_c^{"}$ and vGi

- Calculate Pv(j) using W(j)

- Calculate new TGi to satisfy interfacial energy balance

- Calculate new Wi using new TGi

- Calculate mixture and film properties using TG(j), W(j), Pv(j), TGi, Wi

11) Go to 3) and repeat until TG(j),TL(j), W(j), Ti, Wi, qi converge

In Fig. 6.8, the calculation procedure is summarized.

6.5 Results and Discussion

The developed model was run for the sample case as follows:
-2inch Dia., 1.8m long condenser
-Variable wall temperature
-Inlet velocity = 45m/s, P=3bar, Win=1%

Figs. 6.9 ~ 6.19 shows the analysis results of the model. From the gas axial velocity profile in Fig. 6.9, the velocity development from the inlet constant velocity is clearly shown. From Fig. 6.10, the radial velocity profile shows positive value at interface due to the condensation and negative value at core region due to the axial velocity development. At the entrance region, the interfacial radial velocity is large positive value due to large condensation rate and most of core region shows relatively large negative value due to initial velocity development. But at the exit region, the interfacial radial velocity is small due to small condensation rate and negative radial velocity region in minimum since the axial velocity is already fully developed. These axial and radial velocity profiles are compared with the results of the FLUENT code, which will be shown later.

Fig. 6.11 shows the gas temperature distribution. Constant inlet temperature is developed showing the unrealistic trend. The interface temperature decreases to the saturation temperature. But at the vicinity of the interface, temperature increases although there is no heat source.

Fig. 6.12 shows the noncondensable gas concentration. Constant input concentration is developed with axial length. At the entrance region, the noncondensable gas concentration at the interface is very high due to the high condensation rate but the thickness of the noncondensable gas boundary layer is very thin. At the exit region, the noncondensable gas concentration at the interface is relatively low comparing with the entrance region but the noncondensable gas concentration boundary layer thickness is very thick.

Fig. 6.13 presents the liquid film axial velocity. As commented in section 6.3, the velocity profile is almost linear due to the high interfacial shear. The interfacial liquid velocity increases with the axial direction.

Fig. 6.14 shows the liquid temperature distribution. Inlet temperature is given as constant and the wall temperature is given as it decreases with the axial direction. Since the film thickness is very small, the temperature profile is almost linear.

Figs. 6.15 and 6.16 shows the mixture density and vapor density profiles at an axial location. Near the interface, the vapor temperature and the vapor partial pressure are lower than the core region. So the density near the interface is smaller than that at the core region. However, mixture density near the interface is greater than at the core region since the high noncondensable mass concentration (Eq. 6.31).

Mixture Reynolds number is presented in Fig, 6.17, which is showing the gradual decrease due to the condensation. Interfacial shear and condensation heat transfer coefficient are shown in Figs. 6.18 and 6.19, respectively. The general trend shows the decrease with axial length, which is physically correct since mixture Reynolds number, condensation rate, and interfacial velocity are all big at the entrance region. However, the result shows the oscillation of the interfacial shear and the condensation heat transfer coefficient near the exit region. This result indicates that our new model has some problem. We need to inspect the model carefully for the problem identification and solution.

FLUENT code is used to check the velocity profile of the gas region. FLUENT is a commercial CFD (Computational Fluid Dynamics) code widely used in the fluid and heat transfer for the area. For the velocity profile comparison in the tube, single phase steam condition without condensation is simulated. The tube radius and tube length are 0.0254m and 1.8m, respectively. Inlet constant velocity is set to 10m/s.

As shown in Fig. 20, the radial velocity is negative at entrance region. In velocity developing region, center line axial velocity increases. To increase the center line axial velocity, the radial velocity must be negative (toward to centerline). This is same trend as predicted by boundary layer model for the condensation in Fig. 10. In figure 10, the radial velocity at the interface is not zero since the condensation. Axial velocity in Fig. 21 also shows the similar trend with the results predicted by boundary layer model as presented in Fig. 9.

From the comparison between FLUENT and boundary layer mode, it can be concluded that the velocity field is well analyzed by the boundary layer model. For the further validation of the model, it needs to find the error source of the unrealistic temperature field and the fluctuations of the interfacial shear and condensation heat transfer coefficients.

6.6 References

6.1. S. T. Revankar, and D. Pollock, Analytical and Experimental Study of the Effects of Non-Condensable in a Passive Condenser System for the Advanced Boiling Water Reactor, PU/NE-01-3, May 2001.

6.2. S. T. Revankar, and S. Oh, Analytical and Experimental Study of the Effects of Non-Condensable in a Passive Condenser System for the Advanced Boiling Water Reactor, PU/NE-02-10, Sep. 2002.

6.3.Kuhn S. Z., 1995, "Investigation of Heat Transfer from Condensing Steam-Gas Mixtures and Turbulent Films Flowing Downward inside a Vertical Tube," Ph. D. Thesis, Department of Nuclear Engineering, University of California at Berkeley.

6.4. W.M. Rohsenow, J.H. Webber and A.T. Ling, "Effect of Vapor Velocity on Laminar and Turbulent-Film Condensation," Trans. ASME, 78, pp. 1637 – 1643, 1956.

6.5. R.A. Seban, Remarks on film condensation with turbulent flow, Trans. ASME 76, 299-303, 1954.

6.6.. L.C. Burmeister, *Convective Heat Transfer*, Wiley, New York, 1993.

6.7. S.L. Chen and M.T. Ke, "Forced Convective Film Condensation Inside Vertical Tubes," International Journal of Multiphase Flow 19, pp.1045-1060, 1993.

6.8. A.F. Mills and D.K. Chung, Heat Transfer Across Turbulent Falling Films, Int. J. Heat Mass Transfer 16, 694-696, 1973.

6.9. B.R. Bird, W.E. Stewart, E.N. Lightfoot, *Transport Phenomena*, John Wiley & Sons, INC., 1960.

6.10. S.V. Patankar, *Numerical Heat Transfer and Fluid Flow*, Taylor and Francis, 1980.

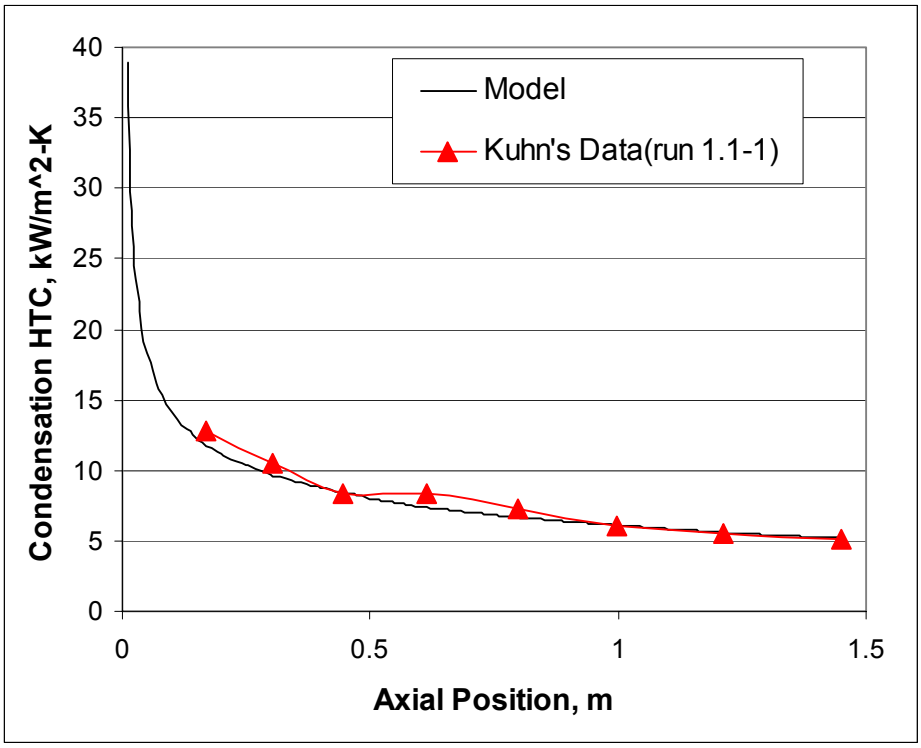

Figure 6.1 Condensation HTC Comparison with Kuhn's Data (run 1.1-1)

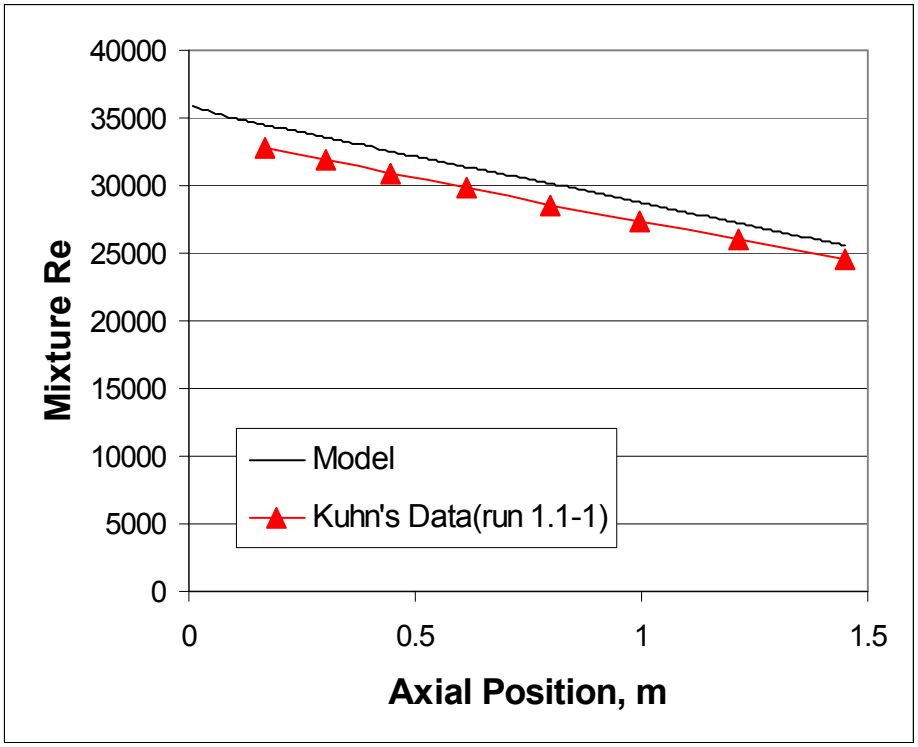

Figure 6.2 Mixture Re Comparison with Kuhn's Data (run 1.1-1)

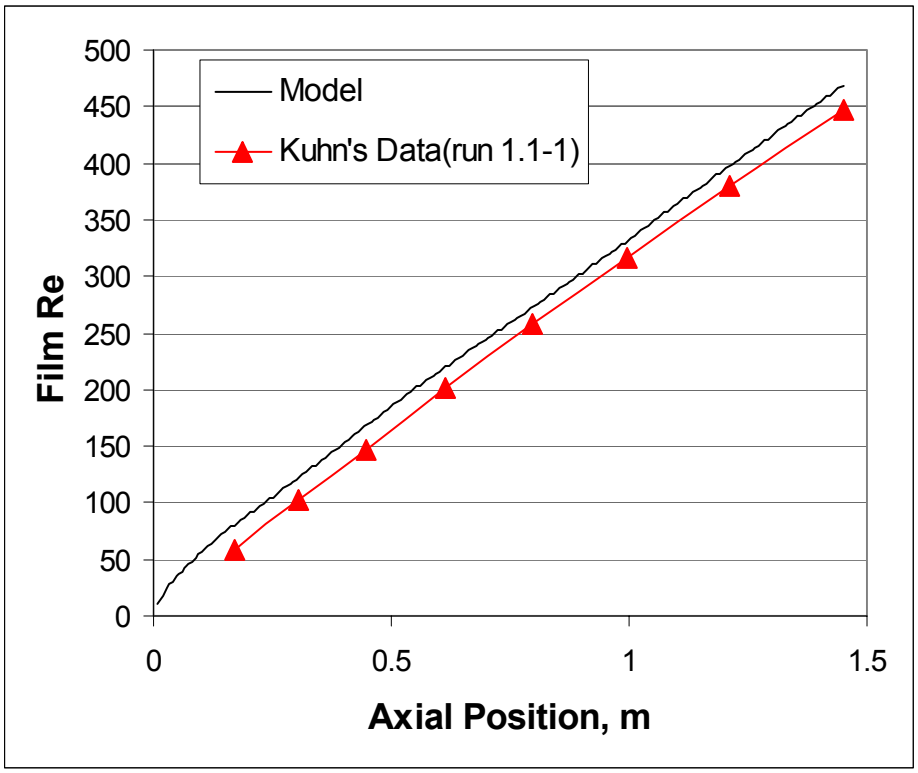

Figure 6.3 Film Re Comparison with Kuhn's Data (run 1.1-1)

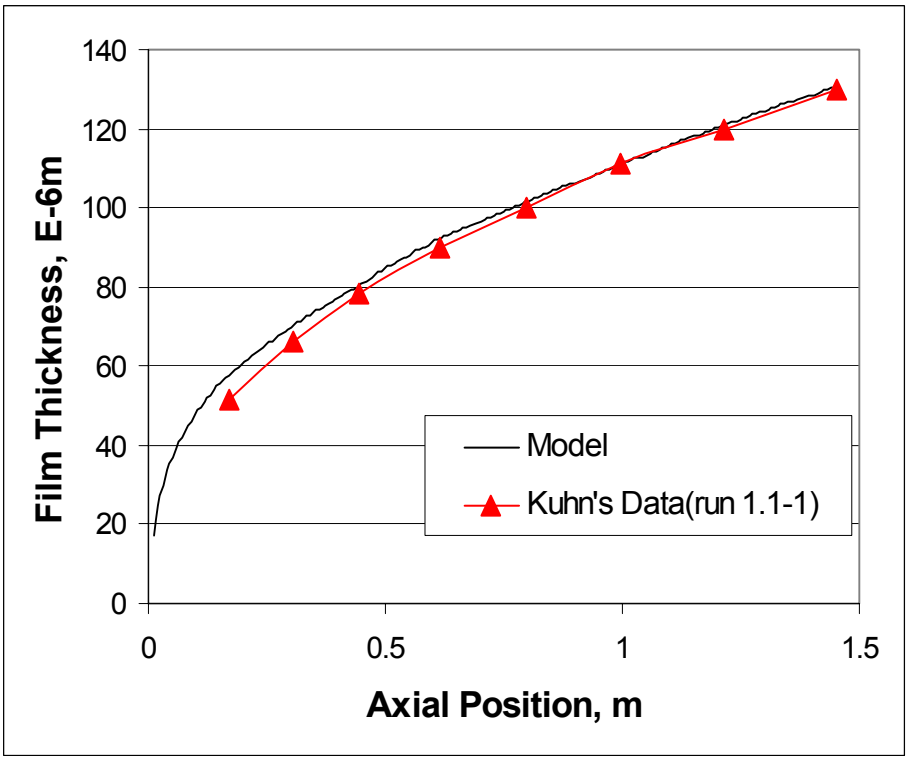

Figure 6.4 Film Thickness Comparison with Kuhn's Data (run 1.1-1)

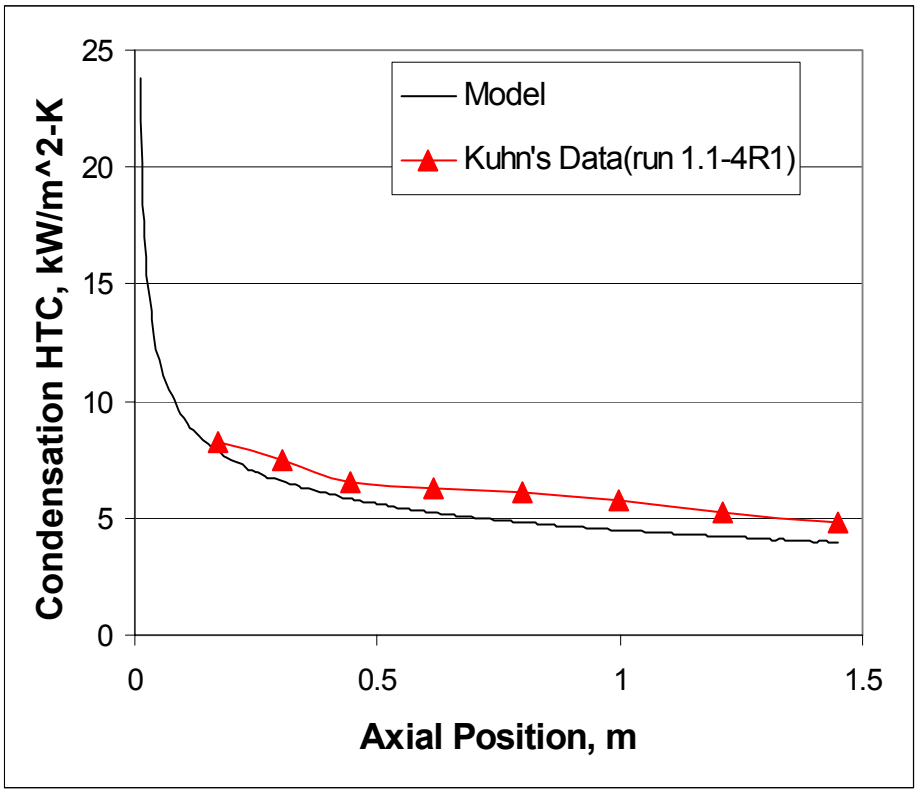

Figure 6.5 Condensation HTC Comparison with Kuhn's Data (run 1.1-4R1)

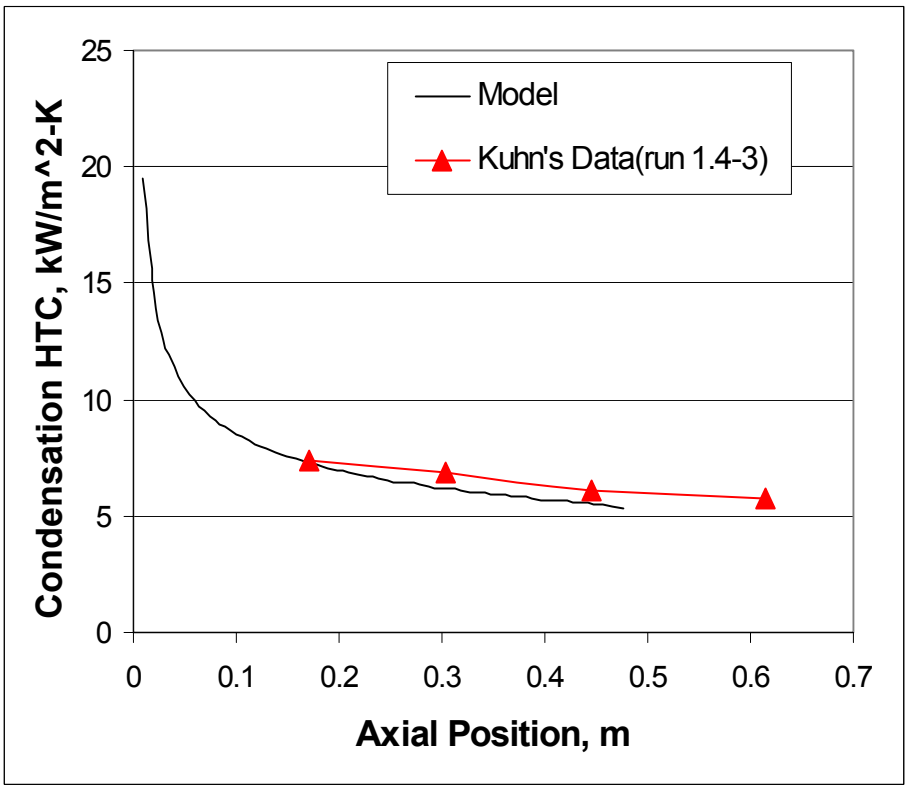

Figure 6.6 Condensation HTC Comparison with Kuhn's Data (run 1.4-3)

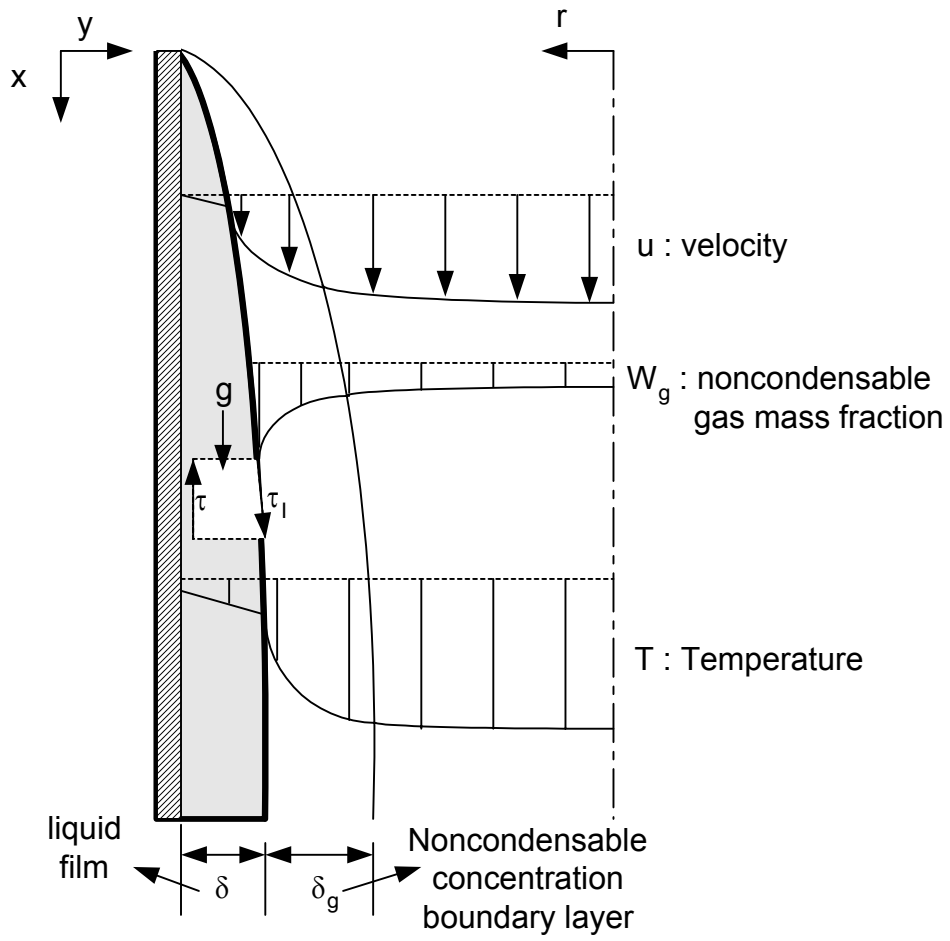

Figure 6.7 Physical Model

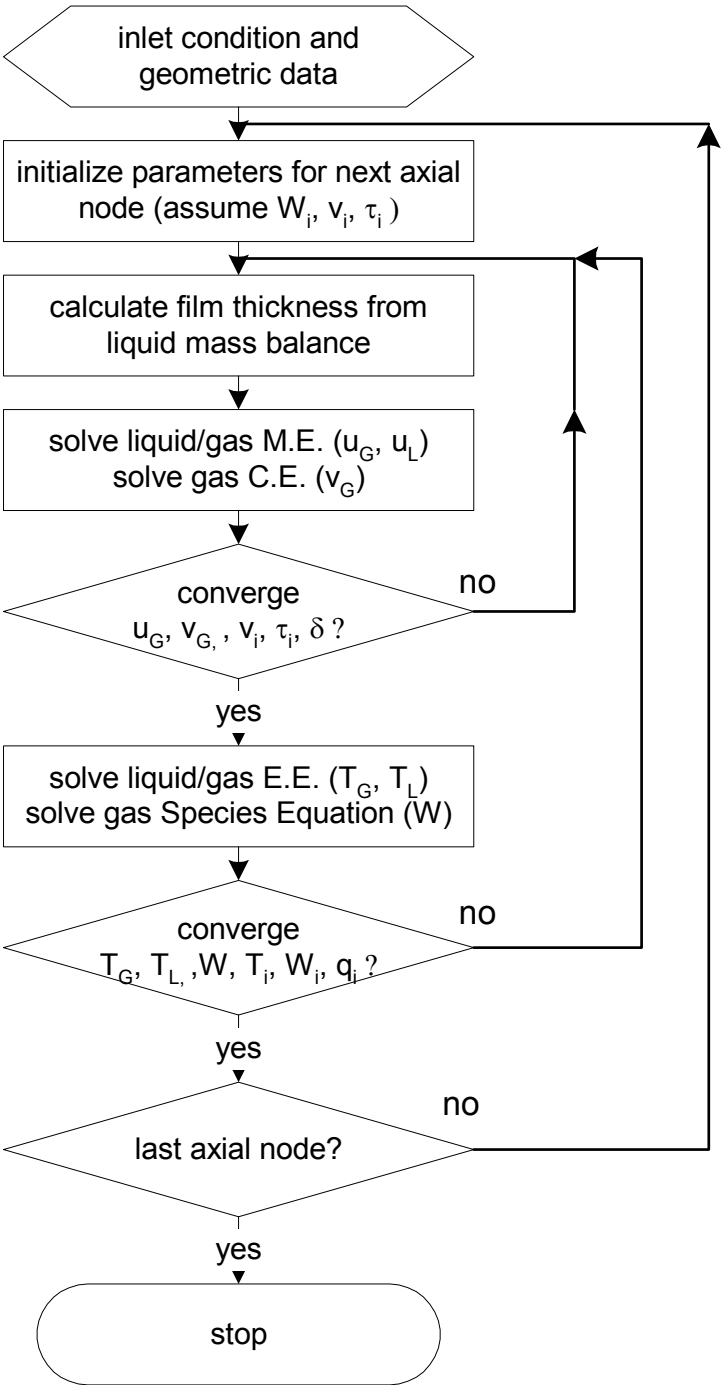

Figure 6.8 Flow Cart of the Calaculation Procedure

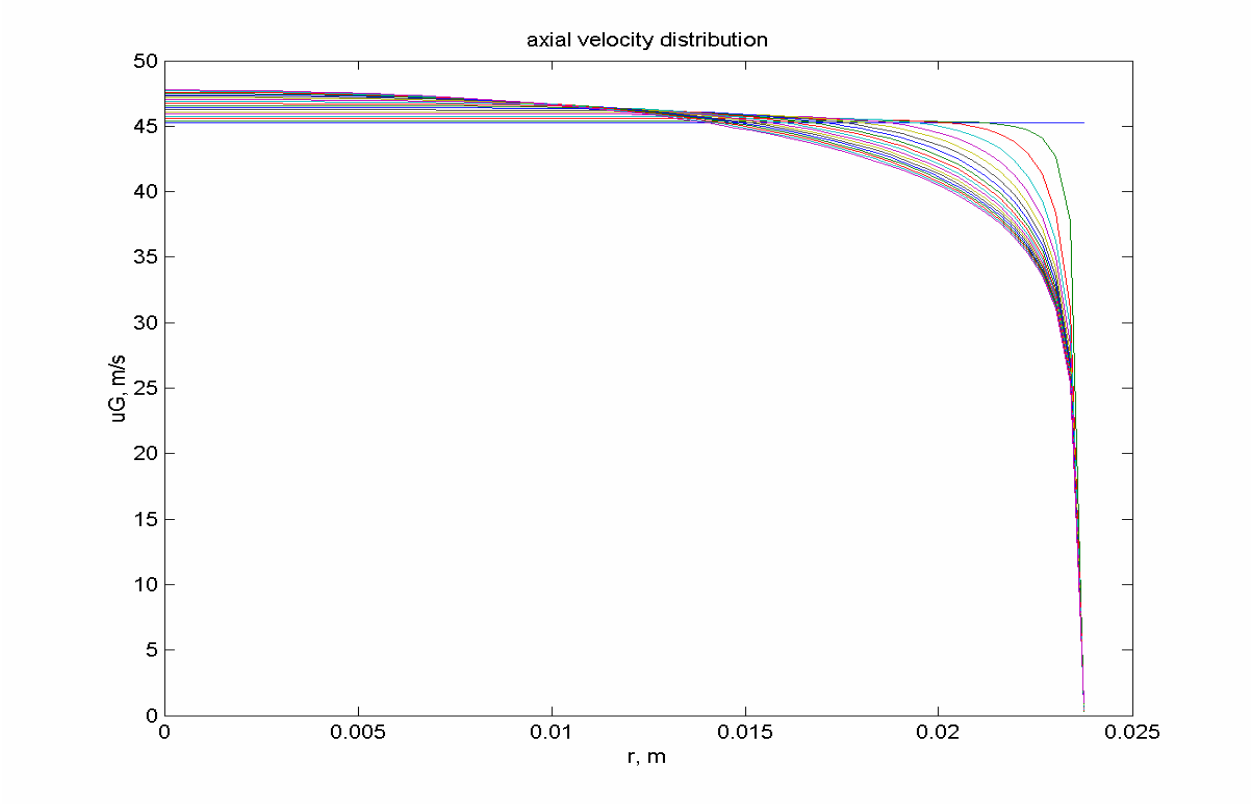

Figure 6.9 Gas Axial Velocity

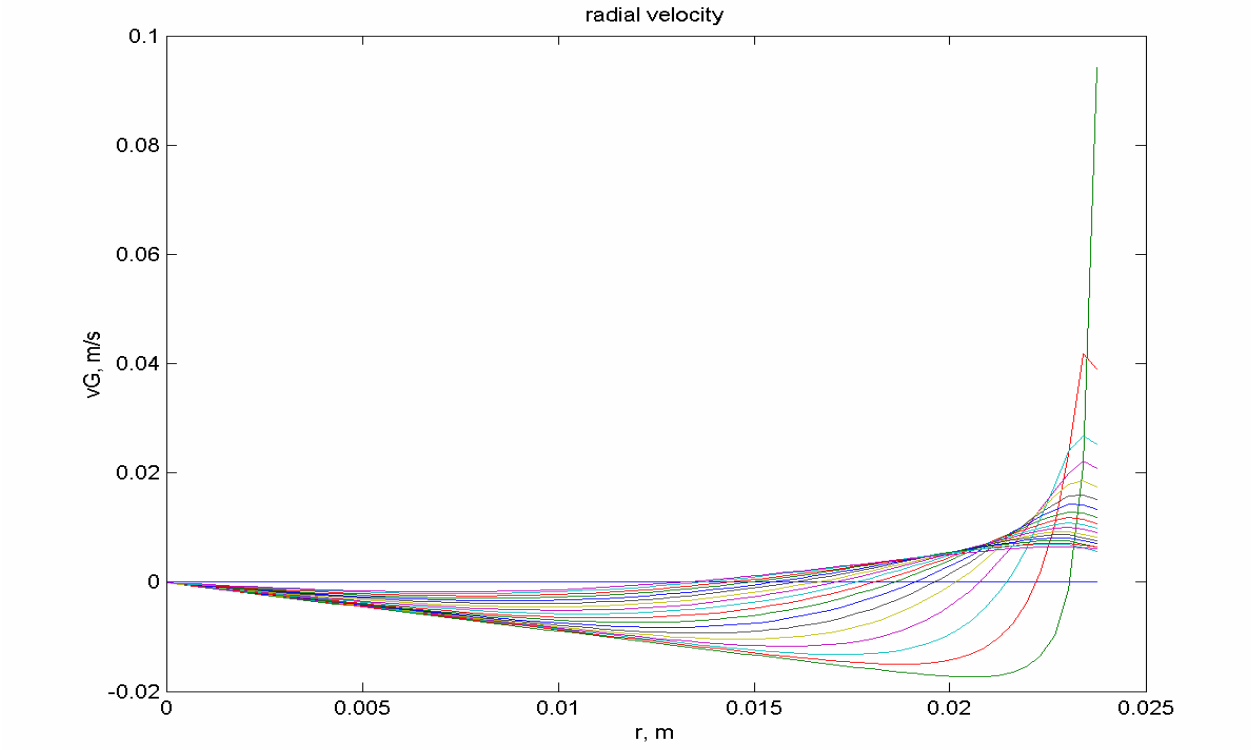

Figure 6.10 Gas Radial Velocity

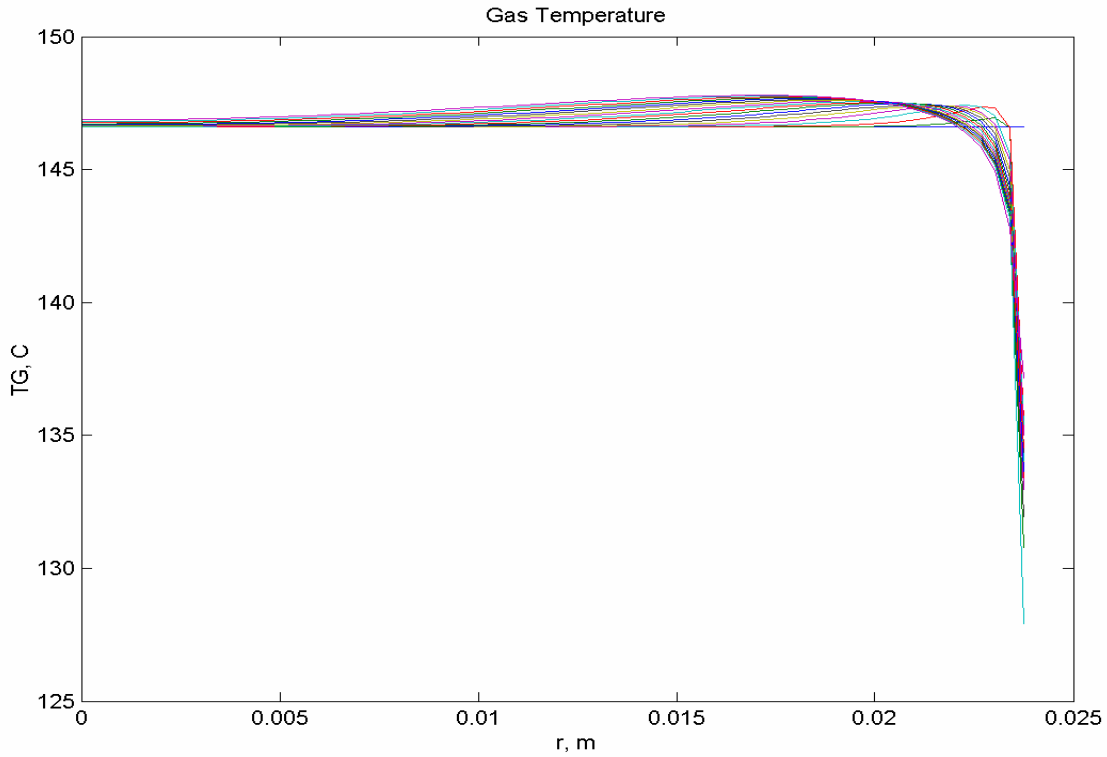

Figure 6.11 Gas Temperature

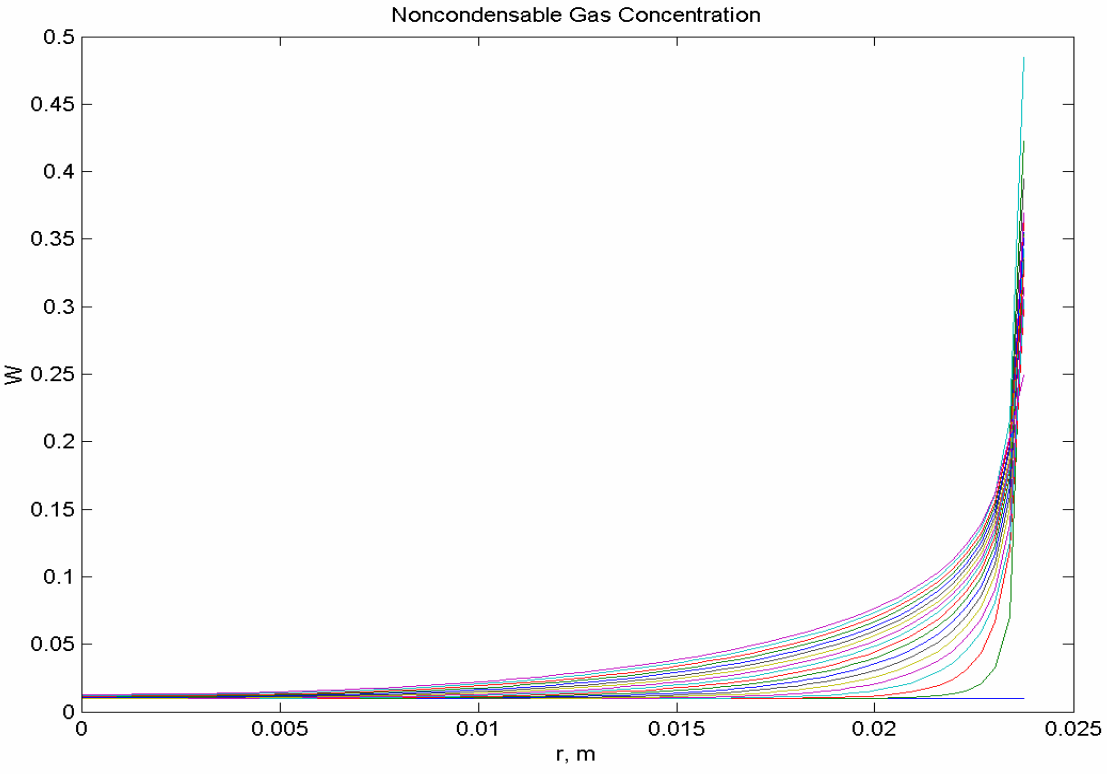

Figure 6.12 Noncondensable Gas Concentration

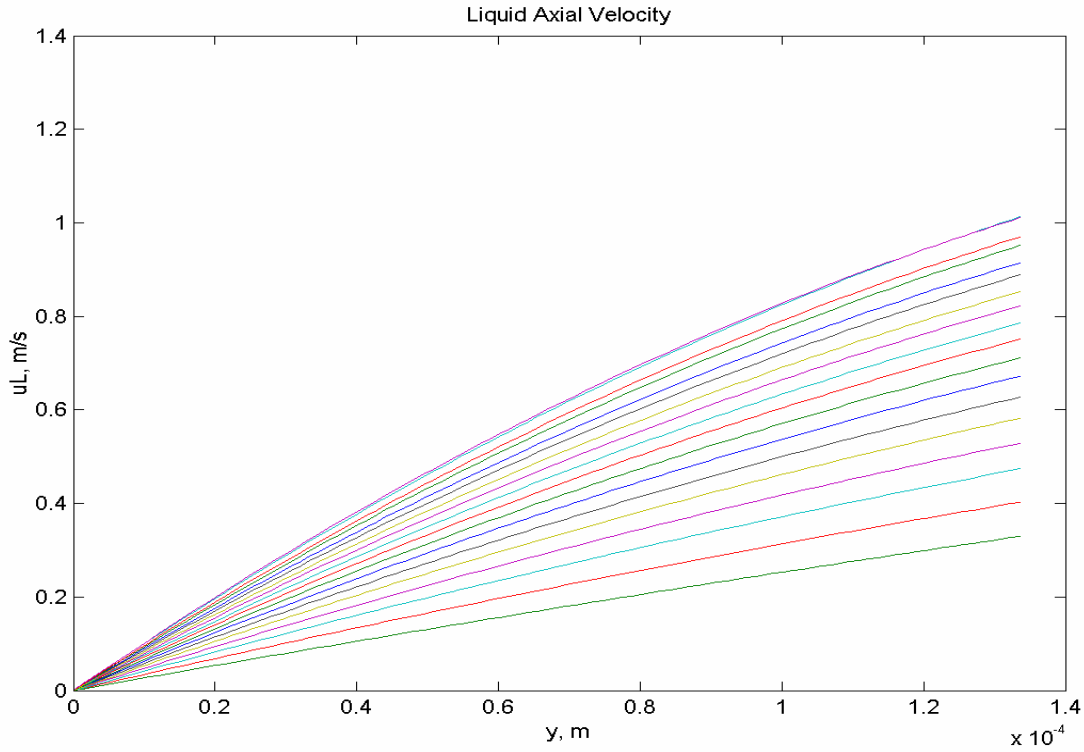

Figure 6.13 Liquid Axial Velocity

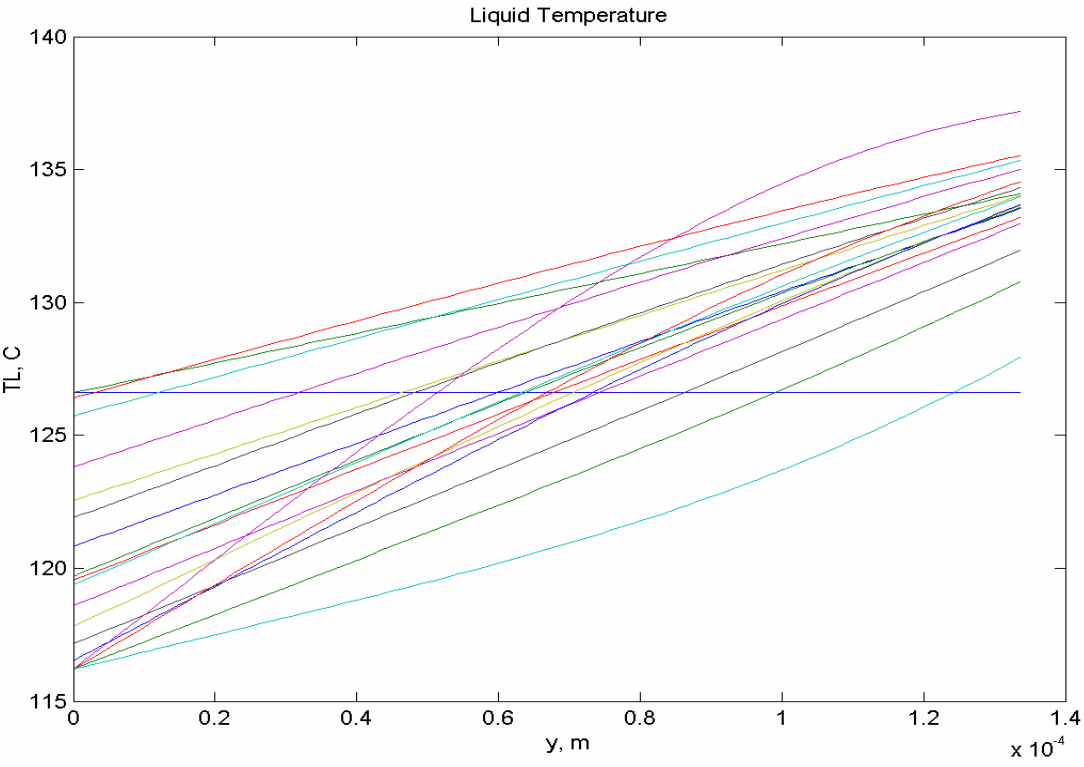

Figure 6.14 Liquid Temperature

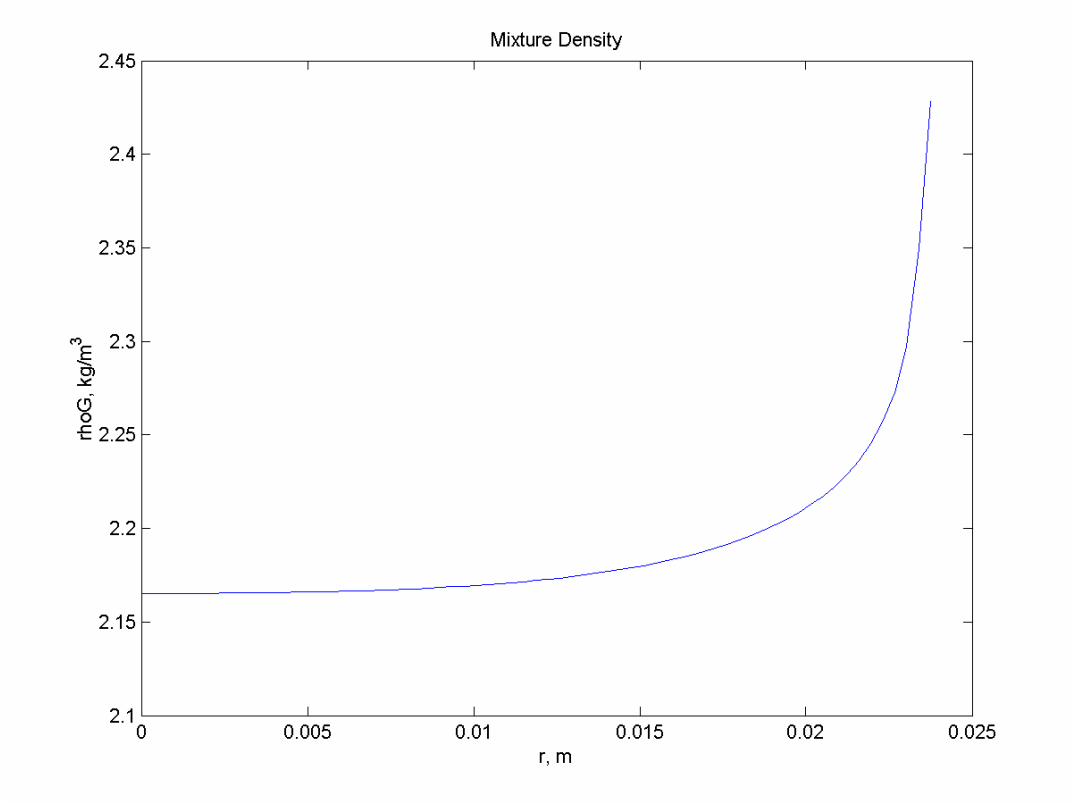

Figure 6.15 Mixture Density

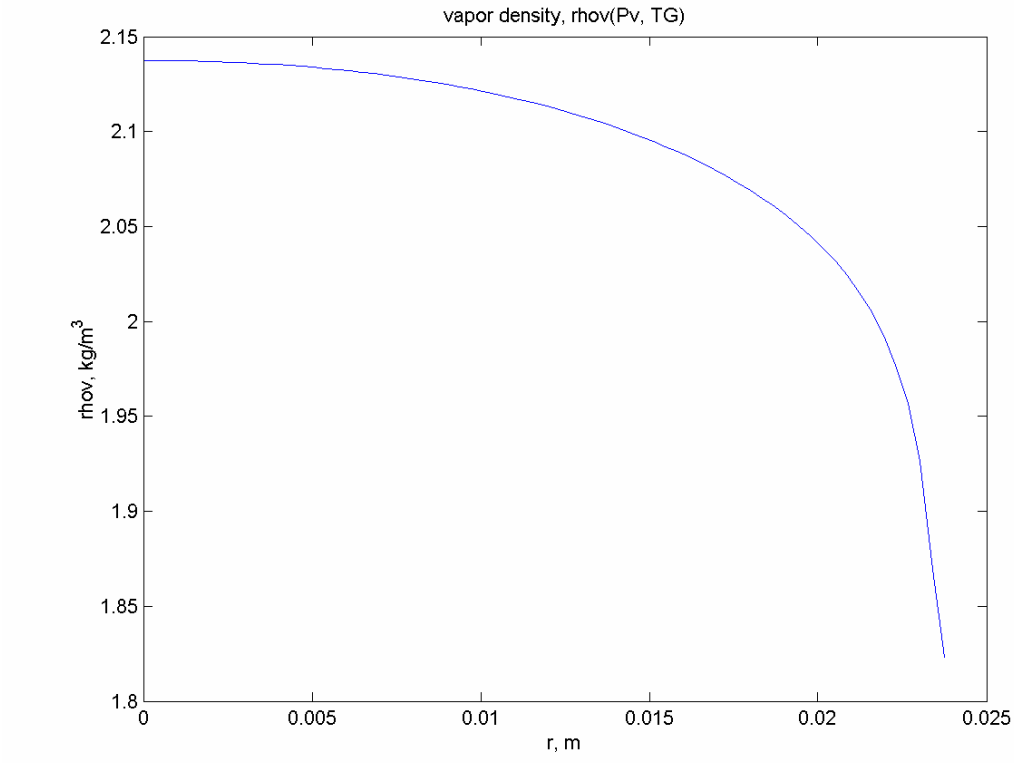

Figure 6.16 Vapor Density

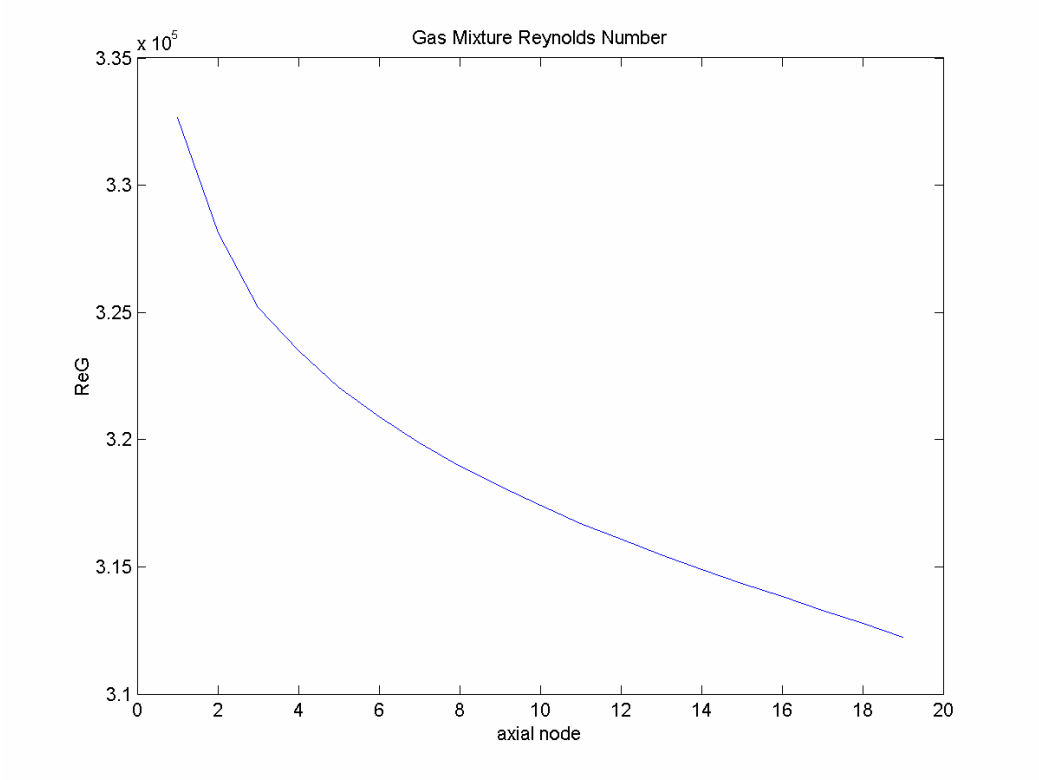

Figure 6.17 Mixture Reynolds Number

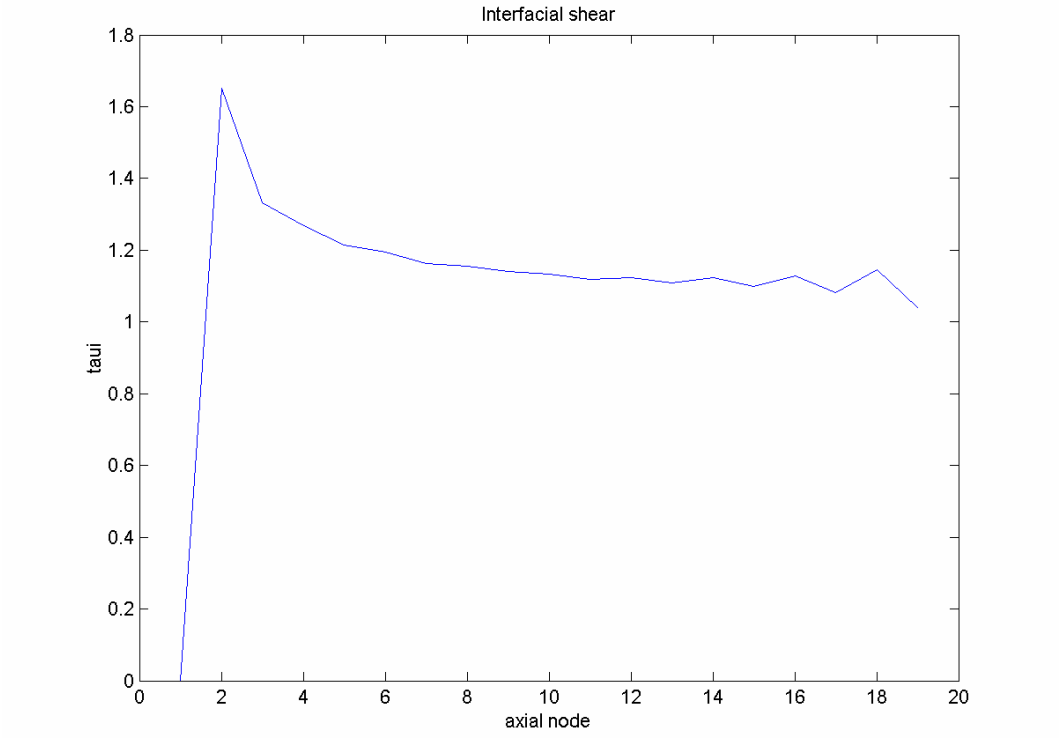

Figure 6.18 Interfacial Shear

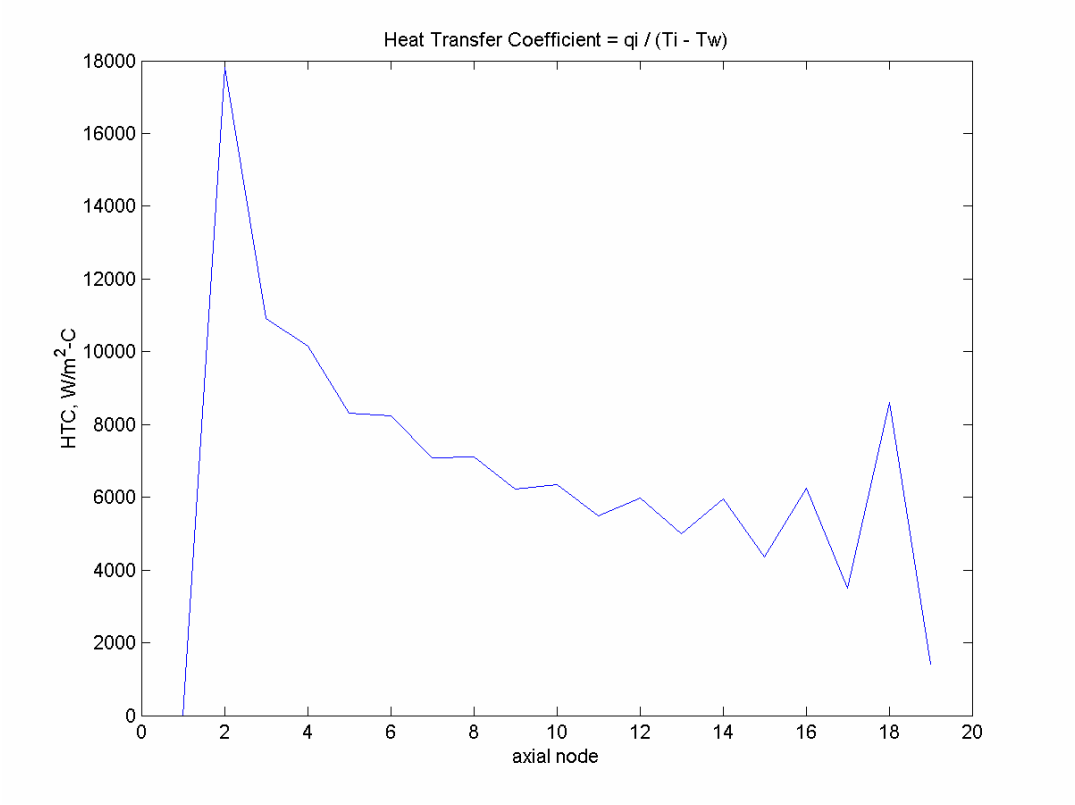

Figure 6.19 Condensation HTC

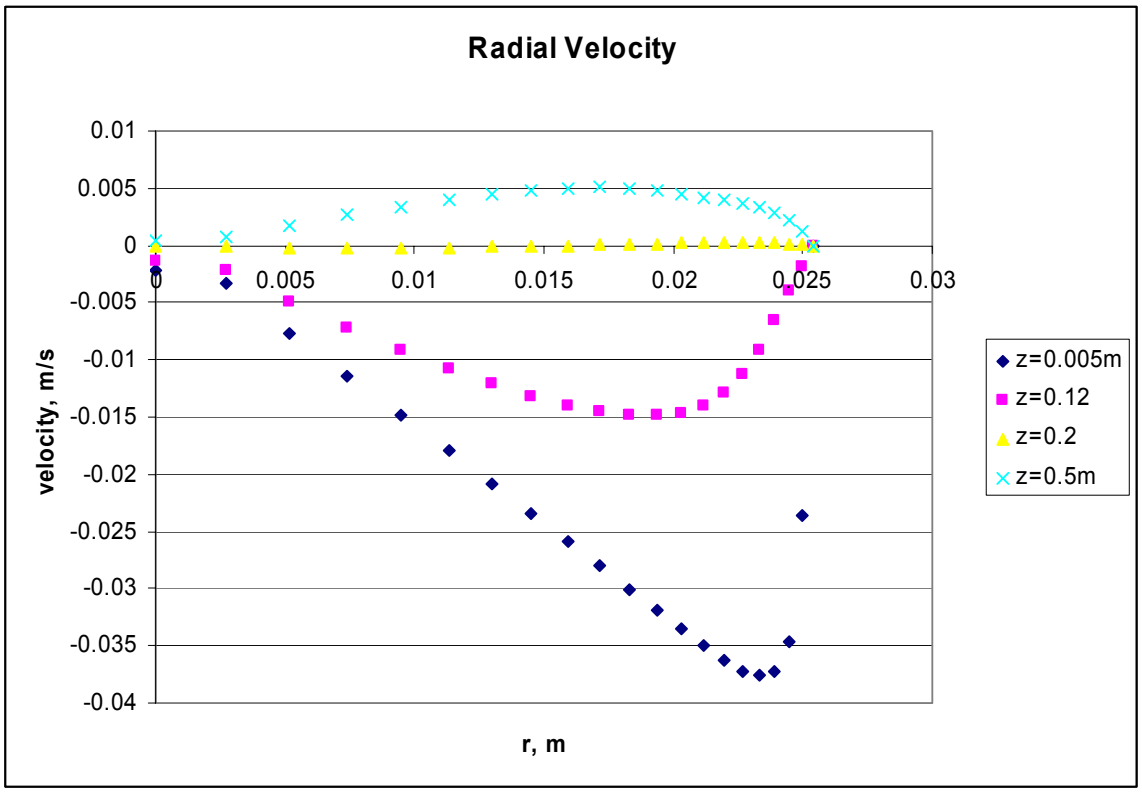

Figure 6.20 FLUENT Results: Radial Velocity

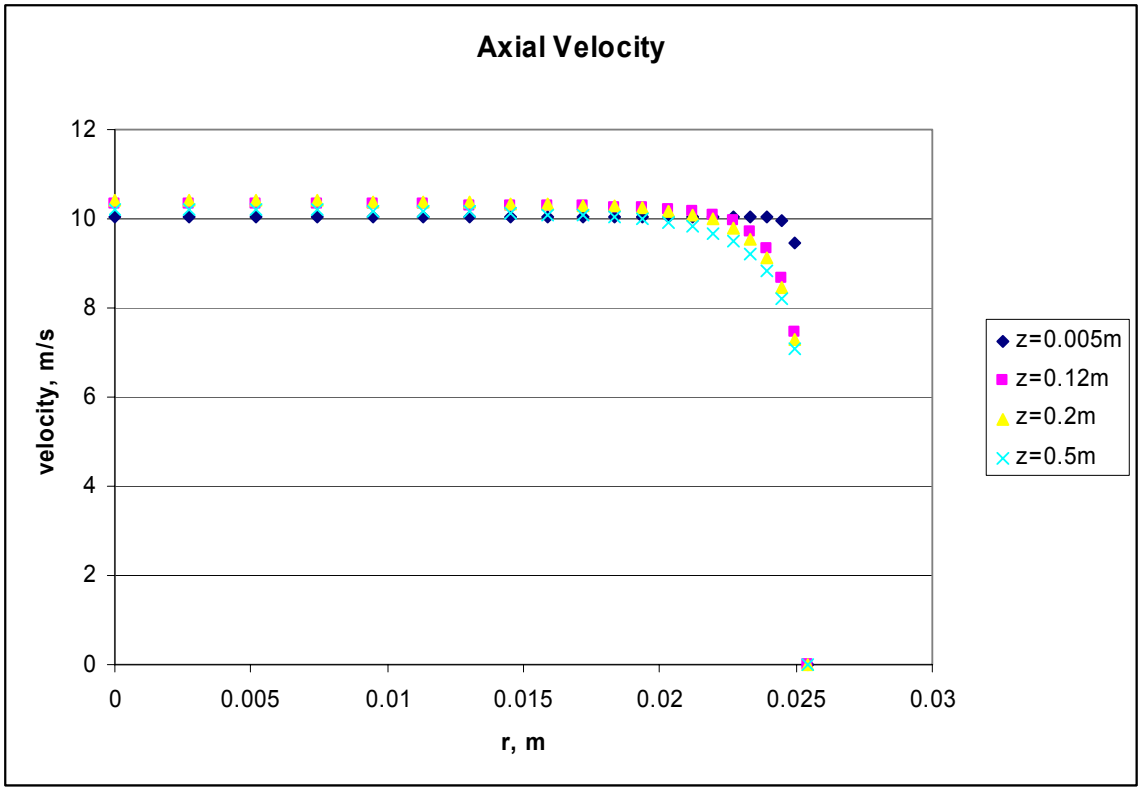

Figure 6.21 FLUENT Results: Axial Velocity

7. ASSESSMENT OF RELAP5 CODE

7.1 Introduction

Assessment of RELAP5 code against the experimental data is one of the main objectives of this research. For the assessment of RELAP5 code, we used the RELAP5/MOD3.3 beta version[7.1]. The RELAP5 computer code is a light water reactor transient analysis code developed for the U. S. Nuclear Regulatory Commission (NRC) for use in rulemaking, licensing audit calculations, evaluation of operator guidelines, and as a basis for a nuclear plant analyzer. RELAP5 is a highly generic code that, in addition to calculating the behavior of a reactor coolant system during a transient, can be used for simulation of a wide variety of hydraulic and thermal transients in both nuclear and nonnuclear systems involving mixture of steam, water, noncondensable, and solute.

RELAP5/MOD3.3 beta version has two wall film condensation models, the default and the alternative model. The default model uses the maximum of the Nusselt[7.2] (laminar) and Shah[7.3] (turbulent) correlations with a diffusion calculation (by Colburn-Hougen[7.4]) when noncondensable gases are present. The alternative model uses the Nusselt model with UCB (University of California at Berkeley) multipliers (Vierow and Schrock[7.5]), which is considering the effects of the noncondensable gases and the interfacial shear.

Using the RELAP5/MOD3.3 beta code, the experimental loop with secondary pool boiling section is simulated. For the assessment of RELAP5 code, experiment conditions are analyzed with the default and the UCB condensation model.

7.2 RELAP5 Nodalization

The RELAP5 nodalization of the experiment is shown in Fig. 7.1.

The condenser tube test section is modeled as a PIPE component 301 with 19 meshes. The condenser tube wall is modeled as a heat structure component 1301 with 5 radial meshes. The secondary side pool boiling section is modeled as an ANNULUS component 321. The annulus component 321 has total 39 meshes. 19 meshes correspond to the boiling section of the test

section and 20 meshes correspond to the bubble riser section. RELAP5 calculates the condensation heat transfer rate between the condenser tube inside wall (1301) and the PIPE 301 and the boiling heat transfer rate between the condenser tube outside wall (1301) and the ANNULUS 321.

The steam source is modeled as a time dependent volume component (TDV 202). The steam pressure is set to the value measured at the vortex flow meter from the experiment. The time dependent junction component (TDJ 801) is used to set the steam mass flow rate input.

The air source is modeled as a time dependent volume component (TDV 205). The air flow rate is set to the value measured from the experiment at the time dependent junction component (TDJ 803). Air pressure is set to the same pressure at TDV202. This prevents the air flow to the TDV 202. The steam and air temperatures are set to the test section steam inlet temperature (TS4). So, there is no need to consider the thermal mixing between the air and steam and heat loss in the supply pipe.

The condensate tank is modeled as a PIPE component (306). This component has 21 meshes and level tracking option is used to see the level change in the tank.

The suppression pool is modeled as a time dependent volume component (TDV 204). This component has very big volume to act as a mass sink.

To simulate the different mode of operation between the complete condensation mode without air and the through flow mode with air, the TRIP VALVE components are used. TRIP VALVE 804 is installed between the air supply line (PIPE 311) and the steam supply line (PIPE 302). If no air flow condition is simulated, this valve remains closed. TRIP VALVE 808 is installed between the condensate tank (PIPE 306) and the vent line (PIPE 305). For the complete condensation mode, the valve remains closed. For the through flow condition, this valve is opened and vent the air and noncondensed steam to the suppression pool.

The secondary steam blowdown tank is modeled as a single volume component (SV 221).

7.3 RELAP5 Analysis Results

For the comparison between the experimental data and the core analysis results, the code outputs are integrated for the entire condenser tube length. For the calculation of the average condensation heat transfer coefficient, the following equation is used instead of the arithmetic mean of local condensation heat transfer coefficient.

$$h_{c,avg} = \frac{Q_{TOT}}{A_i\left(T_{SAT,avg} - T_{Wi,avg}\right)} \tag{7.1}$$

Here, A_i is the total heat transfer area of the condenser tube inside. Total heat transfer rate from the condenser tube to the secondary pool, Q_{TOT}, average steam saturation temperature, $T_{SAT,avg}$, and average tube inside wall temperature, $T_{Wi,avg}$ are calculated as follows:

$$Q_{TOT} = \sum_{j=1}^{N} Q_j \tag{7.2}$$

$$T_{SAT,avg} = \frac{1}{N}\sum_{j=1}^{N} T_{SAT,j} \tag{7.3}$$

$$T_{Wi,avg} = \frac{1}{N}\sum_{j=1}^{N} T_{Wi,j} \tag{7.4}$$

Here, N is total number of condenser meshes.

Complete Condensation Mode

For the comparison of the complete condensation mode, trip valve 808 is closed during the simulation. Results are shown in Figs. 7.2 ~ 7.6.

Fig. 7.2 shows the system pressure with the condensation rate. For a given condensation rate, the corresponding system pressure for the default model is very high. It means the default model underestimate the condensation rate. The discrepancy is much more severe at high condensation rate. But for the UCB model, the pressure is very close to the test results although it is slightly higher.

Fig. 7.3 presents the same plot with Fig. 7.2 except change of the x- and y-axis. Fig. 7.4 shows the condensation heat transfer rate with system pressure. For a given system pressure, the condensation heat transfer rate for the default model is very low and it means the default model underestimate the condensation performance. However, the condensation heat transfer rate for the UCB model is very close to the test data although the condensation rate is slightly smaller than the test data. This difference is due to the facts that the total heat transfer rate from the condenser tube to the secondary pool, Q_{TOT} contains the condensation heat plus sensible heat transfer.

Fig. 7.5 presents the condensation HTC with system pressure. Default model shows small HTC but the trend is very similar to the test data. However, the condensation HTC from UCB model shows very small dependency with system pressure. This result can be more easily described with Fig. 7.6, inside wall temperature data. From Fig. 7.6, inside wall temperature for the default model is almost same with test data. It means the temperature difference between the saturation and inside wall is same between the test and default model. So the condensation HTC follows the trend of the condensation heat transfer rate. However, the inside wall temperature for the UCB model is higher than test data at high pressure condition. Then the temperature difference is smaller than test data. Since condensation rate is similar to the test data, the condensation HTC is higher than the test data at high pressure condition.

Through Flow Mode

For the comparison of the through flow mode with noncondensable gas, trip valve 808 is opened during the simulation. The representative case for the through flow mode, P=0.28 MPa and Msteam=3.6 g/s is selected and the results are shown in Figs. 7.7 ~ 7.10.

Fig. 7.7 shows the condensation rate with noncondensable gas mass fraction. Default model underestimate especially at the low gas fraction region. UCB model predict very well at low gas fraction region. But as gas fraction increases, the condensation rate decreases very rapidly comparing test data. Fig. 7.8 presents the condensation heat transfer rate with noncondensable gas mass fraction. This figure shows the similar trend with Fig. 7.7.

Condensation HTC is plotted in Fig. 7.9. This plot shows more evident trend of UCB model, which has large negative slope with gas fraction. This large slope can be explained by the inside wall temperature in Fig. 7.10.

From the previous comparison, the default model and the UCB model show quite different results. It must be also noted that the trends of the condensation rate and condensation heat transfer rate are also quite different with those of the condensation heat transfer coefficient. So, it can be concluded that we should compare the results comprehensively instead of comparing the heat transfer coefficients only. Generally, the UCB model shows better result than the default model as an aspect of the condensation rate and condensation heat transfer rate. However the trend of the condensation heat transfer coefficient for the UCB model shows large discrepancy with teat data for the complete condensation mode without noncondensable gas and through flow mode with noncondensable gas.

7.4 References

7.1 NUREG/CR-5535/Rev 1, "RELAP5/MOD3.3 Beta Code Manual," May 2001.

7.2 W.A. Nusselt , "The Surface Condensation of Water Vapor," Ziesrhift Ver Deut. Ing., 60 pp. 541-546 & pp. 569-575, 1916.

7.3 M.M. Shah, "A General Correlation for Heat Transfer During Film Condensation Inside Pipes," Int. J. Heat Mass Transfer Vol. 22, 547-556, 1979.

7.4 A.P. Colburn, O.A. Hougen, "Design of Cooler Condensers for Mixture of Vapors with Non-condensable Gases," Industrial and Engineering Chemistry Vol. 26, 1178-1182, 1934.

7.5 K.M. Vierow, V.E. Schrock, "Condensation in a Natural Circulation Loop with Noncondensable Gases: Part I – Heat Transfer," Proc. of the Int. Conf. on Multiphase Flow, 183-186, 1991.

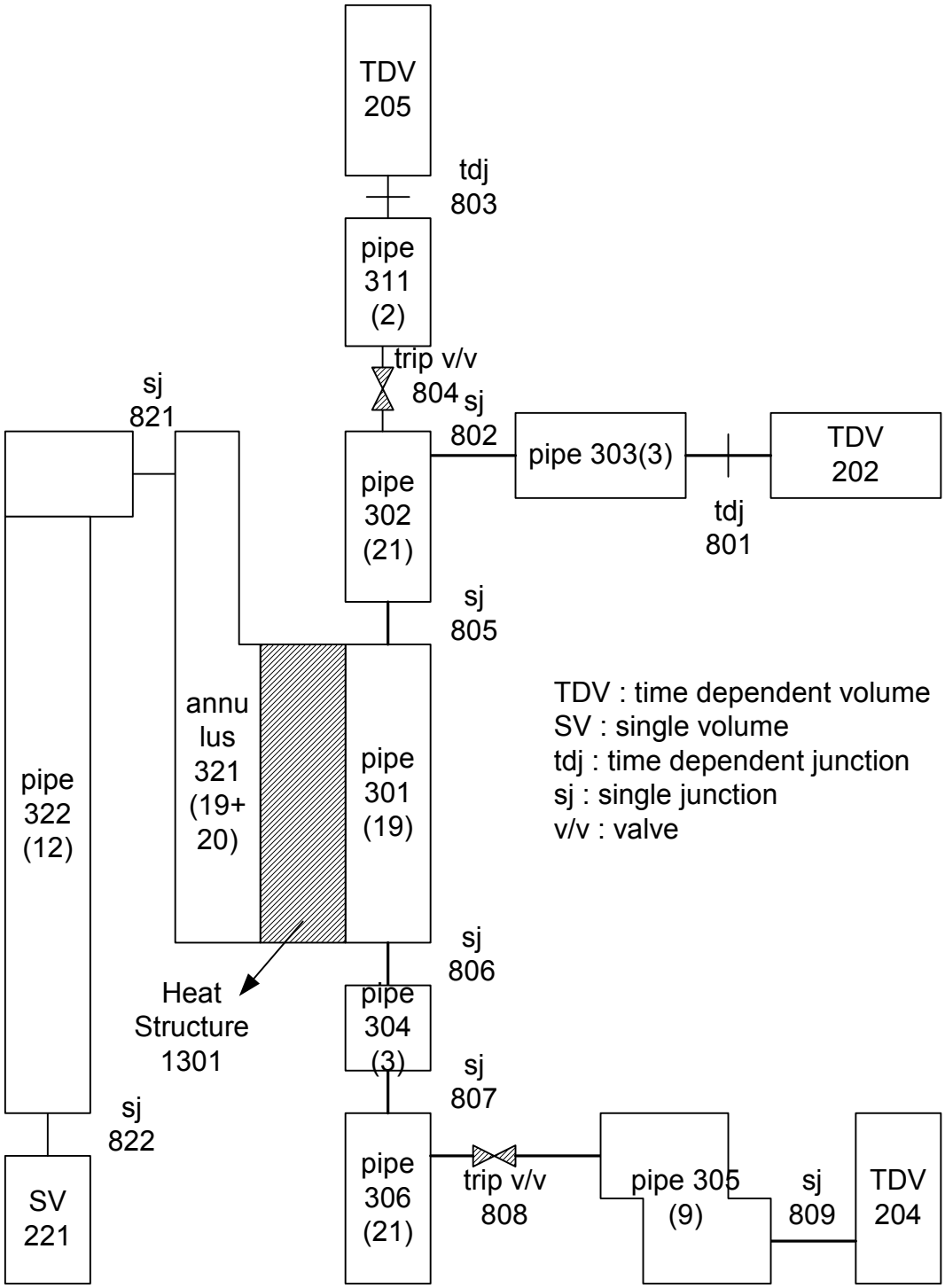

Figure 7.1 RELAP5 Nodalization

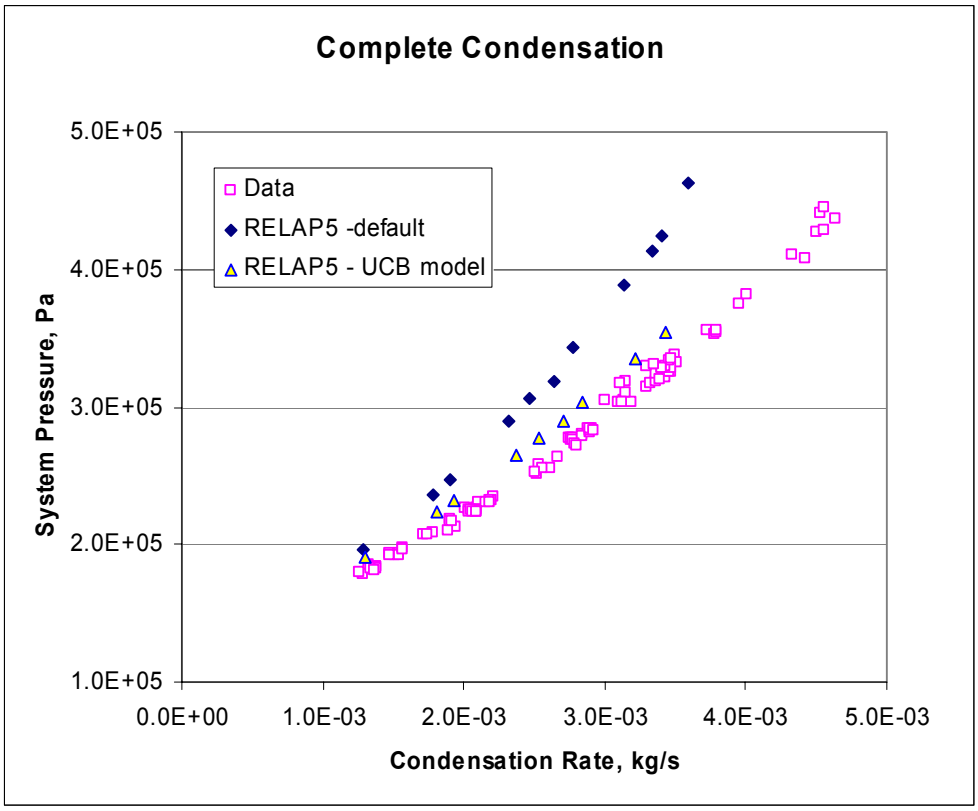

Figure 7.2 Comparison of System Pressure for Complete Condensation

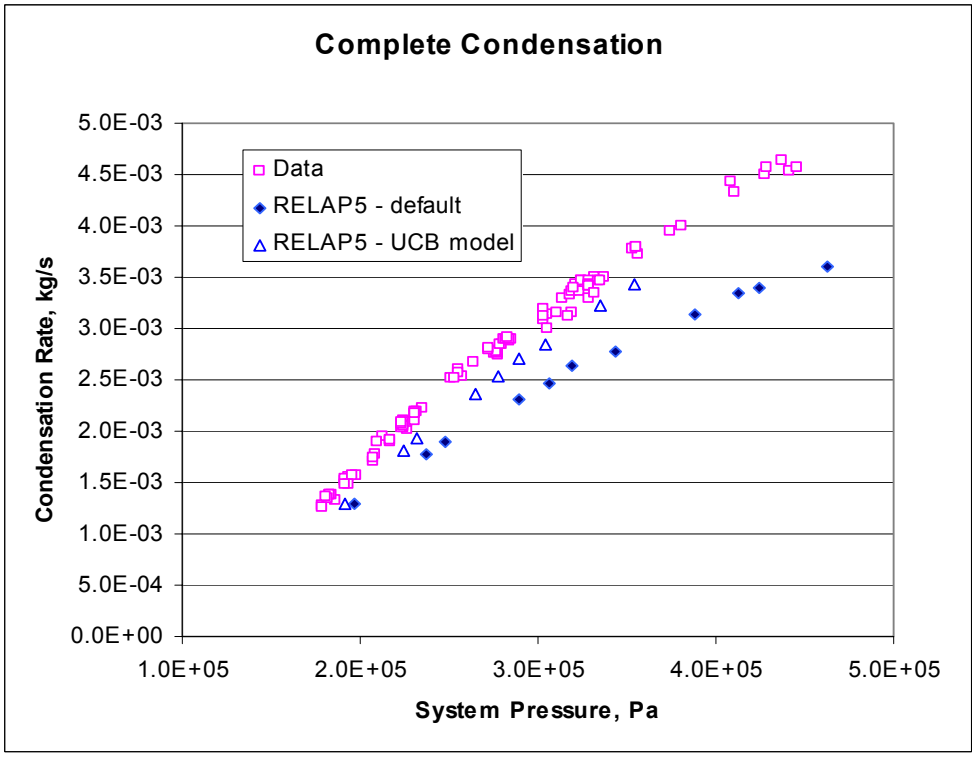

Figure 7.3 Comparison of Condensation Rate for Complete Condensation

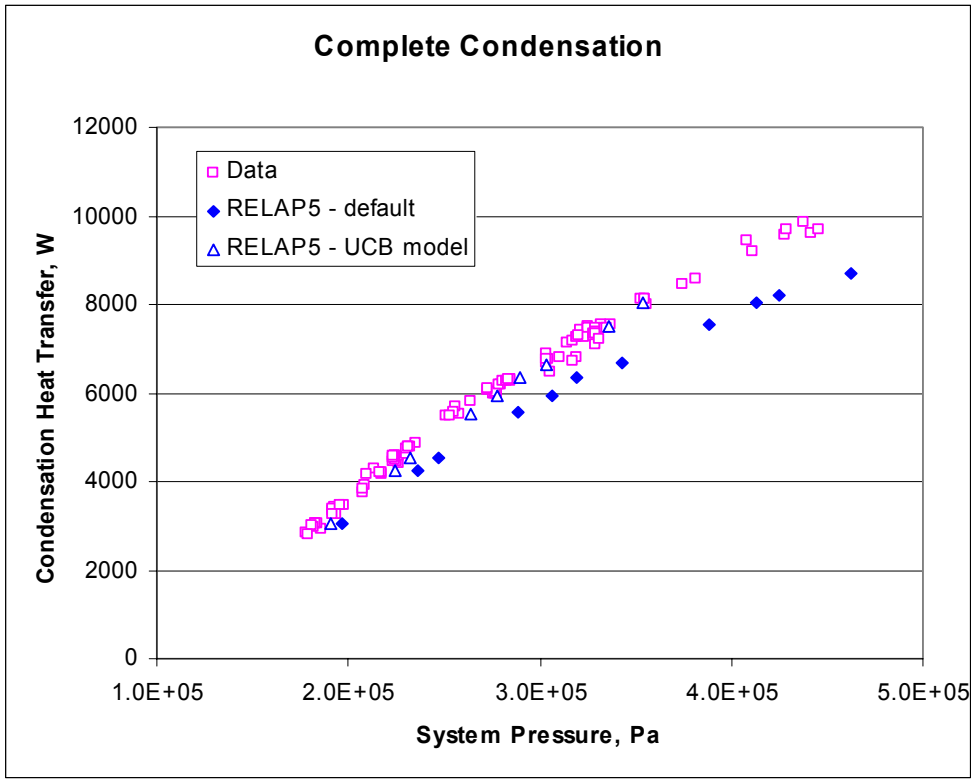

Figure 7.4 Comparison of Condensation Heat Transfer Rate for Complete Condensation

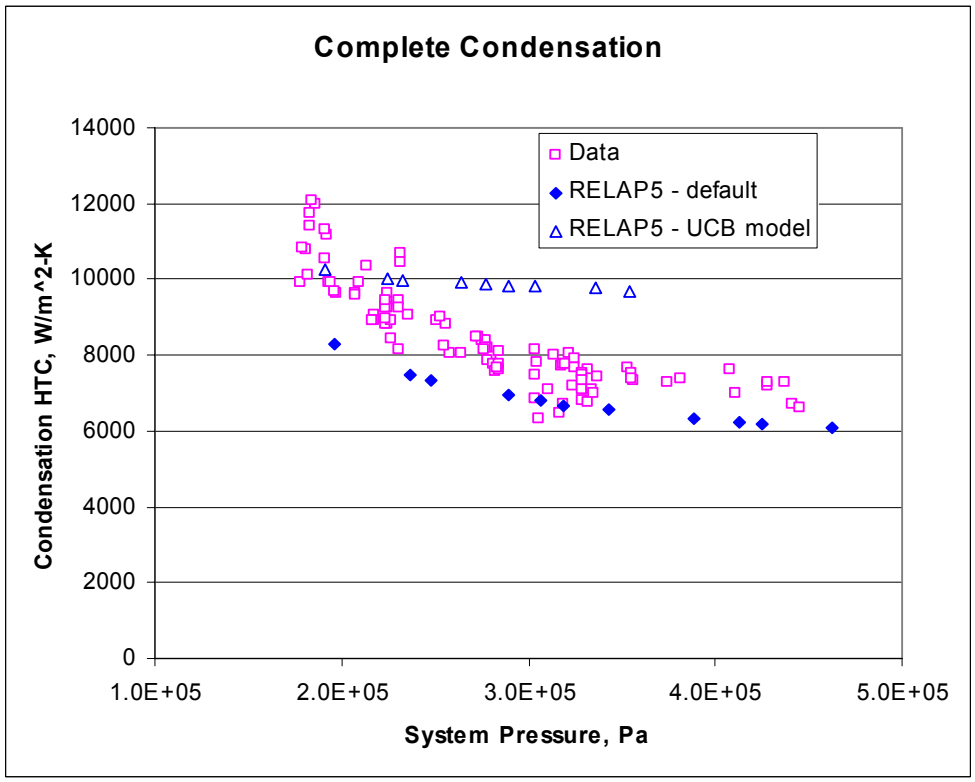

Figure 7.5 Comparison of Condensation HTC for Complete Condensation

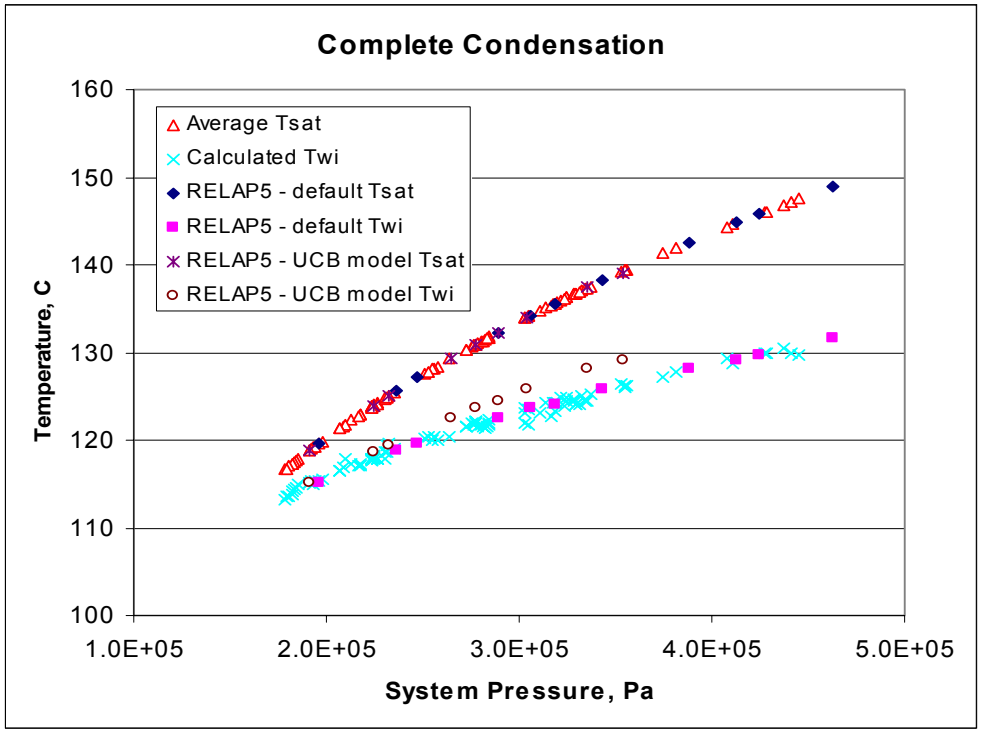

Figure 7.6 Comparison of Temperatures for Complete Condensation

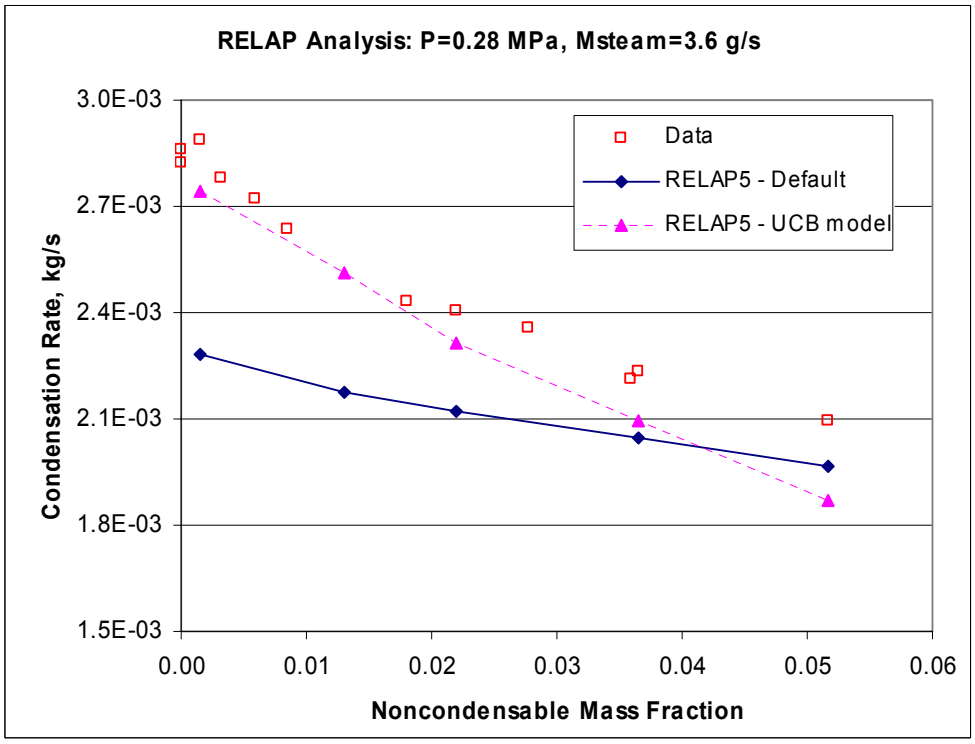

Figure 7.7 Comparison of Condensation Rate for Through Flow

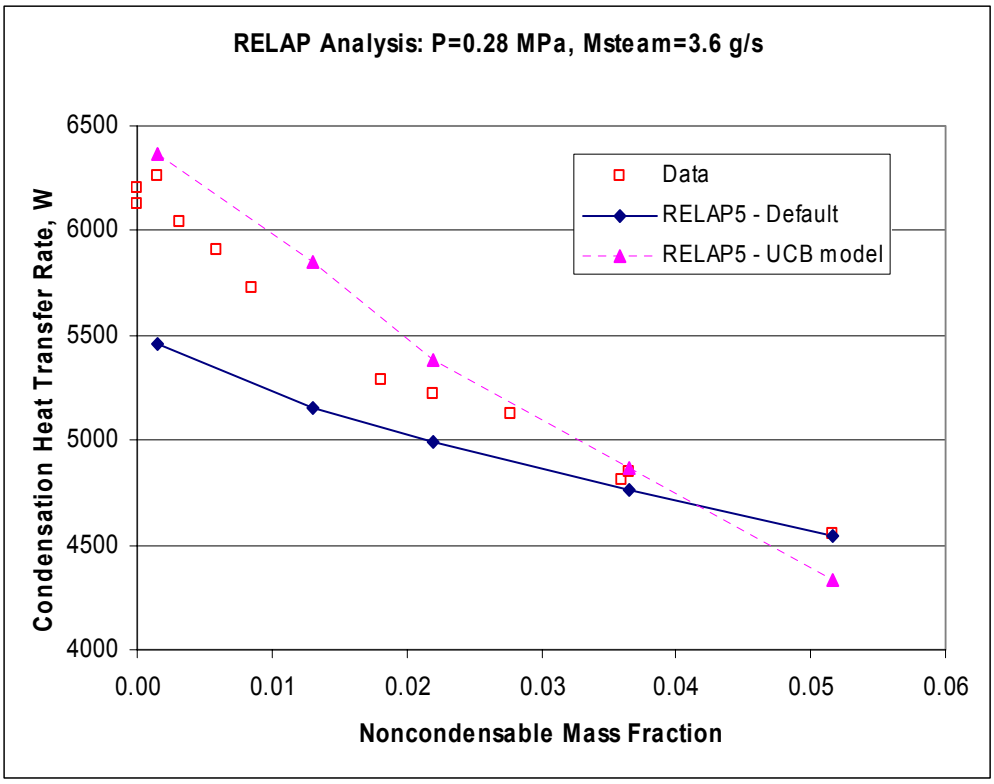

Figure 7.8 Comparison of Condensation Heat Transfer Rate for Through Flow

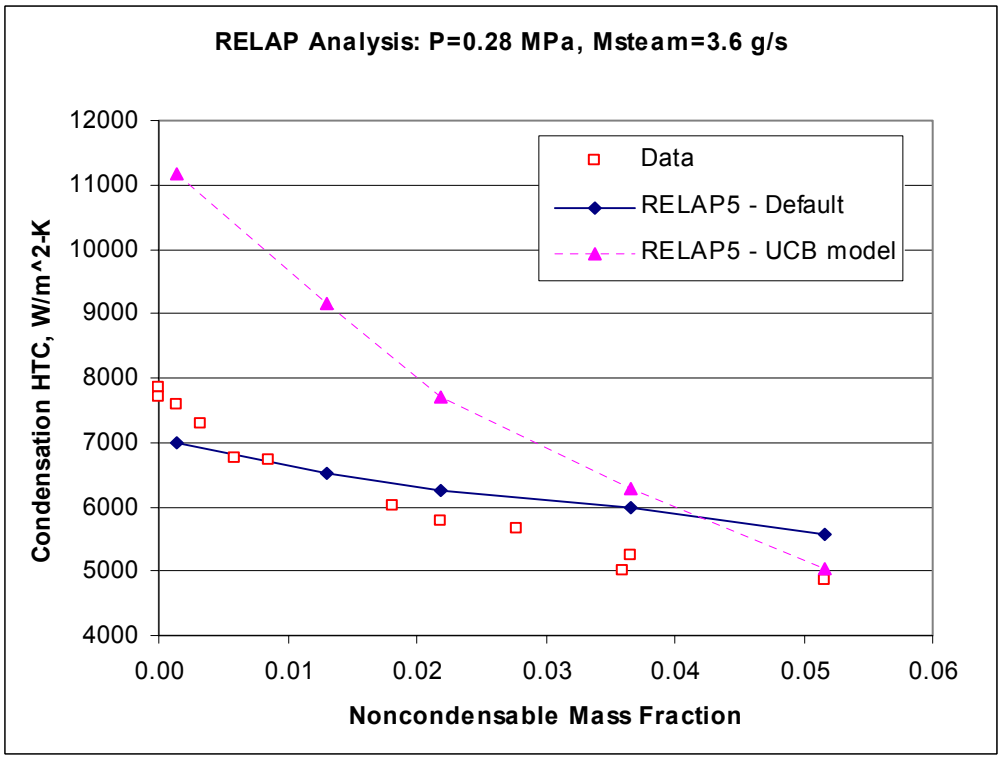

Figure 7.9 Comparison of Condensation HTC for Through Flow

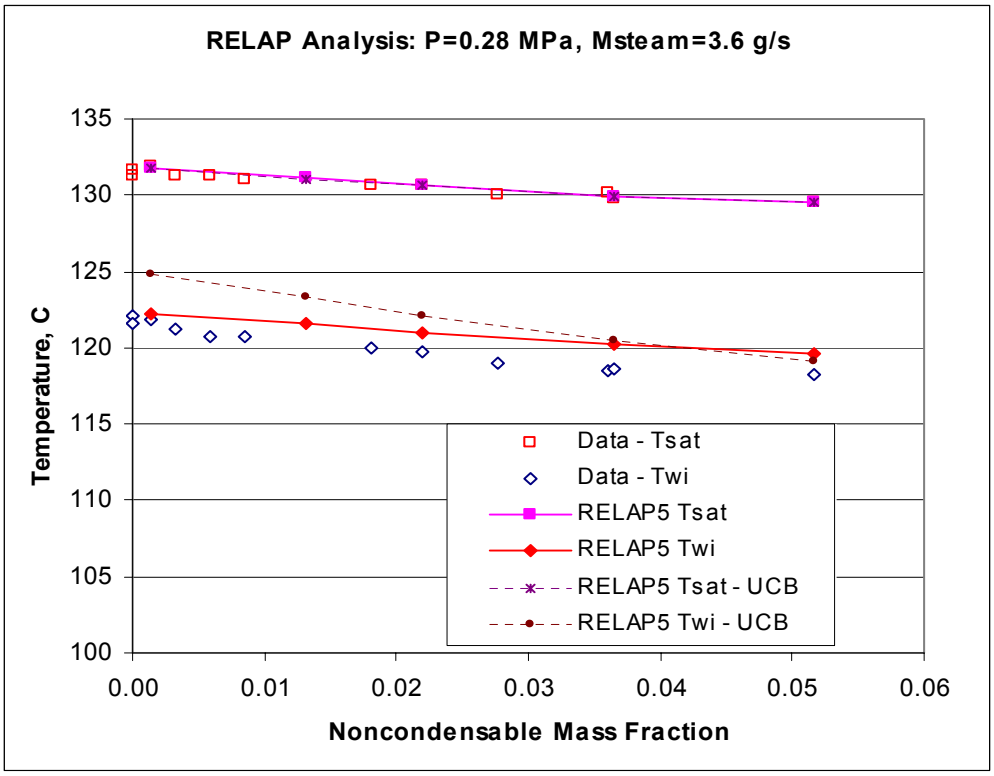

Figure 7.10 Comparison of Temperatures for Through Flow

8. ACCOMPLISHMENTS FOR THIRD YEAR

Here the accomplishments of the third year are summarized.

- Condensation tests were carried out for the complete condensation conditions for 2.54 cm diameter condenser for pure steam with pool boiling cooling on the secondary side. The data showed that system pressure increases as inlet steam flow rate increases at complete condensation mode. However, condensation heat transfer coefficient decreases as inlet steam flow rate (i.e., system pressure) increases at this mode. Generally, the condensation rate increases and the condensation heat transfer coefficient decreases as system pressure increases.

- Condensation tests were carried out for the periodic venting conditions with small amount of noncondensable gas. As the noncondensable mass fraction increases, vent frequency increases and vent period decreases. Therefore, through flow mode and continuous condensation mode can be considered as one of the limiting condition of the periodic venting mode. It suggests the possibility of combining all three PCCS operation modes into one universal condensation heat transfer model.

- Condensation tests were carried out for the through flow condition. Condensation heat transfer coefficient decreases as the noncondensable gas mass fraction increases, inlet steam flow rate decreases, and system pressure increases.

- Data have been obtained for various non-condensable gas concentrations (0.% ~ 10%), inlet steam flow rate (1 ~ 7 g/s) and operating pressures (180 ~ 450 kPa) for three operational mode of the PCCS.

- Kuhn's experiment data were compared with the condensation model developed in the second year. The agreement was very good.

- A new condensation model has been developed for forced downflow of steam and non-condensable gas in vertical tube, which does not use the self-similar velocity profile assumption since this assumption may not be applicable in the entrance region. The velocity profile predicted by new model was compared with the analysis of the FLUENT commercial code. The trend of the velocity profile is very similar between two results. But, new model shows unrealistic temperature profile and fluctuation of condensation heat transfer coefficient. Those problems are required to be examined carefully.

- Assessment of the condensation model in RELAP5 code was performed by comparison with experimental data. Default model and UCB model in RELAP5 show quite different results. It must be also noted that the trends of the condensation rate and condensation heat transfer rate are also quite different with those of the condensation heat transfer coefficient. So, it can be concluded that we should compare the results comprehensively instead of comparing the heat transfer coefficients only.

- UCB model shows better result than the default model as an aspect of the condensation rate and condensation heat transfer rate. However, the trend of the condensation heat transfer coefficient for the UCB model shows large discrepancy with teat data for the complete condensation mode without noncondensable gas and through flow mode with noncondensable gas.

- Vent analysis was performed to check the degradation effect of the noncondensable gas for periodic venting condition. System pressure increases partly due to the accumulation of the noncondensable gas mass itself and partly due to the degradation of condensation caused by the noncondensable gas boundary layer.

Appendix A. ERROR ANALYSIS

Consider the function $f(x_1, x_2, ..., x_N)$, which depends on the random variables $x_1, x_2, ..., x_N$. Generally, the values $x_1, x_2, ..., x_N$ are determined by experimentally and then the value of $f(x_1, x_2, ..., x_N)$ is calculated. For this case, the standard error and variance of $f(x_1, x_2, ..., x_N)$ can be calculated by using the following equations as derived by Ref. A.1:

The variance of $f(x_1, x_2, ..., x_N)$ is

$$\sigma_f^2 = V(f) = \overline{\left(f - \overline{f}\right)^2} = \sum_{i=1}^{N}\left(\frac{\partial f}{\partial x_i}\right)^2 \sigma_i^2 \quad + \quad 2\sum_{j>i}^{N}\sum^{N}\left(\frac{\partial f}{\partial x_i}\right)\left(\frac{\partial f}{\partial x_j}\right)\rho_{ij}\sigma_i\,\sigma_j \tag{A.1}$$

where σ_i is the standard error of x_i and ρ_{ij} is the correlation coefficient given by

$$\rho_{ij} = \frac{1}{\sigma_i\,\sigma_j}\overline{(x_i - m_i)(x_j - m_j)}. \tag{A.2}$$

In most practical cases, the random variables are uncorrelated, i.e., ρ_{ij}=0. For this case, the standard error of $f(x_1, x_2, ..., x_N)$ is expressed a simple equation as follows:

$$\sigma_f = \sqrt{\sum_{i=1}^{N}\left(\frac{\partial f}{\partial x_i}\right)^2 \sigma_i^2} \tag{A.3}$$

The condensation heat transfer coefficient can be expressed as follows as eq. (5.11):

$$h_c \;=\; \frac{2k_w m_{con} h_{fg}}{2k_w \pi D_i H_{tube}\left(T_{SAT} - T_{Wo}\right) - m_{con} h_{fg} 1n\left(D_o/D_i\right) D_i} \tag{A.4}$$

From eq. (A.4), the condensation heat transfer coefficient is a function of 9 variables and it can be expressed as follows:

$$h_c \;=\; h_c\left(k_w, m_{con}, h_{fg}, D_i, H_{tube}, T_{SAT}, T_{Wo}, D_o\right) \tag{A.5}$$

k_w is material properties, D_i, D_o, H_{tube} are geometric data and m_{con}, h_{fg}, T_{SAT}, T_{Wo} are variables determined by experiment. Inevitably, the material properties and geometric data have uncertainty. However, it is assumed that uncertainties in those data are negligible. So these are

not considered as variables in this error analysis. But the effect of these data in error analysis will be taken into account in final error value by considering some margin.

Then, the condensation heat transfer coefficient can be expressed as a function of 5 variables.

$$h_c = h_c\left(m_{con}, h_{fg}, T_{SAT}, T_{Wo}\right) \tag{A.6}$$

These 4 variables can be considered as mutually independent, so these are uncorrelated. Therefore, eq. (A.3) can be used for the error analysis.

$$\sigma_{h_c}^2 = \left(\frac{\partial h_c}{\partial m_{con}}\right)^2 \sigma_{m_{con}}^2 + \left(\frac{\partial h_c}{\partial h_{fg}}\right)^2 \sigma_{h_{fg}}^2 + \left(\frac{\partial h_c}{\partial T_{SAT}}\right)^2 \sigma_{T_{SAT}}^2 + \left(\frac{\partial h_c}{\partial T_{Wo}}\right)^2 \sigma_{T_{Wo}}^2 \tag{A.7}$$

The partial derivative terms in above eq. can be derived by eq. (A.4). To simplify the equation, let the numerator and the denominator in eq. (A.4) be X and Y, respectively.

$$X = 2k_w m_{con} h_{fg} \tag{A.8}$$

$$Y = 2k_w \pi D_i H_{tube}\left(T_{SAT} - T_{Wo}\right) - m_{con} h_{fg} 1n\left(D_o / D_i\right) D_i \tag{A.9}$$

$$\frac{\partial h_c}{\partial m_{con}} = \frac{1}{Y}\left[2k_w h_{fg}\right] + \frac{X}{Y^2}\left[h_{fg} 1n\left(D_o / D_i\right) D_i\right] \tag{A.10}$$

$$\frac{\partial h_c}{\partial h_{fg}} = \frac{1}{Y}\left[2k_w m_{con}\right] + \frac{X}{Y^2}\left[m_{con} 1n\left(D_o / D_i\right) D_i\right] \tag{A.11}$$

$$\frac{\partial h_c}{\partial T_{SAT}} = -\frac{X}{Y^2}\left[2k_w \pi D_i H_{tube}\right] \tag{A.12}$$

$$\frac{\partial h_c}{\partial T_{Wo}} = \frac{X}{Y^2}\left[2k_w \pi D_i H_{tube}\right] \tag{A.13}$$

Let the error of the thermocouple be σ_{TC}. The error of the thermocouple has mainly two components: the error of the temperature measurement itself by the thermocouple and the error of the data acquisition system. The total error of the thermocouple is conservatively selected as 1 degree C.

The average temperature at tube outside wall is the arithmetic mean of 5 thermocouple measurements. Therefore, the error of T_{Wo} is

$$\sigma_{T_{Wo}} = \frac{1}{\sqrt{5}}\sigma_{TC} \tag{A.14}$$

As mentioned above, the bulk temperature of steam-air mixture is assumed as the saturation temperature at the steam partial pressure. Therefore, the bulk temperature is a function of the steam partial pressure and it can be read from steam table. So, the error in bulk temperature has two components: error in pressure measurement and error in steam table. It is very hard to quantify the error in steam table and this type of error can be considered as very small value. Instead of neglecting the error in steam table, conservative value of error in pressure measurement will be used.

$$\sigma_{T_{SAT}}^2 = \left(\frac{\partial T_{SAT}}{\partial P_{PARTIAL}}\right)^2 \sigma_{P_{PARTIAL}}^2 \tag{A.15}$$

The partial derivative term, $\frac{\partial T_{SAT}}{\partial P_{PARTIAL}}$, can be obtained from steam table by calculating the change in saturation temperature with small change in pressure. Error in system pressure is 0.5% of total range of pressure gauge per manufacturer's manual.

Condensation mass flow rate can be calculated with the following equation.

$$m_{con} = \frac{\Delta H_{ref}}{\Delta t}\rho_{ref} A_{CT} \tag{A.16}$$

where ΔH_{ref} is the condensate tank level difference converted to the reference temperature (4C) condition, Δt is the measurement time, ρ_{ref} is the density at the reference temperature, and A_{CT} is the cross-sectional area of the condensate tank.

By neglecting the error of Δt, ρ_{ref}, A_{CT} condensation rate is only a function of ΔH_{ref}. The error of the condensation rate is expressed as follows:

$$\sigma_{m_{con}}^2 = \left(\frac{\partial m_{con}}{\partial \Delta H_{ref}}\right)^2 \sigma_{\Delta H_{ref}}^2 \tag{A.17}$$

$$\Delta H_{ref} = H_{mea,initail} - H_{mea,final} \tag{A.18}$$

$$\sigma_{\Delta H_{ref}} = \sqrt{2}\sigma_{H_{mea}} \tag{A.19}$$

The measurement error of the CT level, $\sigma_{H_{mea}}$, is 0.1% span of DP sensor. Then, the final form of the condensation rate error is:

$$\sigma_{m_{con}}^2 = \left(\frac{\rho_{ref} A_{CT}}{\Delta t} \right)^2 2\sigma_{H_{mes}}^2 \tag{A.20}$$

Now calculate the error of the latent heat of condensation, $\sigma_{h_{fg}}$. The latent heat of the condensation is only a function of the steam partial pressure.

$$h_{fg} = h_{fg}(P_{PARTIAL}) \tag{A.21}$$

$$\sigma_{h_{fg}}^2 = \left(\frac{\partial h_{fg}}{\partial P_{PARTIAL}} \right)^2 \sigma_{P_{PARTIAL}}^2 \tag{A.22}$$

Average partial pressure can be calculated by the arithmetic mean of the inlet and outlet partial pressure.

$$P_{PARTIAL} = \frac{P_{PARTIAL,in} + P_{PARTIAL,out}}{2} \tag{A.23}$$

For the pure steam case, i.e., m_{air}=0,

$$P_{PARTIAL} = P_{TOT} \tag{A.24}$$

$$\sigma_{P_{PARTIAL}}^2 = \sigma_{P_{TOT}}^2 \tag{A.25}$$

For the noncondensable gas case,

$$P_{PARTIAL,in} = P_{TOT} \frac{1 - W_{air,in}}{1 - W_{air,in}\left(1 - M_{h2o} / M_{air}\right)} \tag{A.26}$$

$$P_{PARTIAL,out} = P_{TOT} \frac{1 - W_{air,out}}{1 - W_{air,out}\left(1 - M_{h2o} / M_{air}\right)} \tag{A.27}$$

$$W_{air,in} = \frac{m_{air}}{m_{air} + m_{v,in}} \tag{A.28}$$

$$W_{air,out} = \frac{m_{air}}{m_{air} + m_{v,out}} = \frac{m_{air}}{m_{air} + m_{v,in} - m_{con}} \tag{A.29}$$

Let, $X1 = \left(1 - M_{h2o} / M_{air}\right)$

$$P_{PARTIAL} = \frac{P_{TOT}}{2}\left\{\frac{1-\dfrac{m_{air}}{m_{air}+m_{v,in}}}{1-\dfrac{m_{air}}{m_{air}+m_{v,in}}X1} + \frac{1-\dfrac{m_{air}}{m_{air}+m_{v,in}-m_{con}}}{1-\dfrac{m_{air}}{m_{air}+m_{v,in}-m_{con}}X1}\right\} \tag{A.30}$$

$$P_{PARTIAL} = \frac{P_{TOT}}{2}\left\{\frac{m_{v,in}}{m_{air}(1-X1)+m_{v,in}} + \frac{m_{v,in}-m_{con}}{m_{air}(1-X1)+m_{v,in}-m_{con}}\right\} \tag{A.31}$$

Let, $X2 = 1 - X1 = M_{h2o} / M_{air}$

$$P_{PARTIAL} = \frac{P_{TOT}}{2}\left\{\frac{m_{v,in}}{m_{air}X2+m_{v,in}} + \frac{m_{v,in}-m_{con}}{m_{air}X2+m_{v,in}-m_{con}}\right\} \tag{A.32}$$

Then, the partial pressure is a function of the system total pressure, the air inlet flow rate, the steam inlet flow rate, and the condensation rate.

$$P_{PARTIAL} = P_{PARTIAL}(P_{TOT}, m_{air}, m_{v,in}, m_{con}) \tag{A.33}$$

$$\sigma^2_{P_{PARTIAL}} = \left(\frac{\partial P_{PARTIAL}}{\partial P_{TOT}}\right)^2 \sigma^2_{P_{TOT}} + \left(\frac{\partial P_{PARTIAL}}{\partial m_{air}}\right)^2 \sigma^2_{m_{air}} + \left(\frac{\partial P_{PARTIAL}}{\partial m_{v,in}}\right)^2 \sigma^2_{m_{v,in}} + \left(\frac{\partial P_{PARTIAL}}{\partial m_{con}}\right)^2 \sigma^2_{m_{con}} \tag{A.34}$$

Let, $Y1 = m_{air}X2 + m_{v,in}$, $Y2 = m_{air}X2 + m_{v,in} - m_{con}$

$$\frac{\partial P_{PARTIAL}}{\partial P_{TOT}} = \frac{1}{2}\left\{\frac{m_{v,in}}{Y1} + \frac{m_{v,in}-m_{con}}{Y2}\right\} \tag{A.35}$$

$$\frac{\partial P_{PARTIAL}}{\partial m_{air}} = \frac{P_{TOT}}{2}\left\{-\frac{m_{v,in}X2}{Y1^2} - \frac{(m_{v,in}-m_{con})X2}{Y2^2}\right\} \tag{A.36}$$

$$\frac{\partial P_{PARTIAL}}{\partial m_{v,in}} = \frac{P_{TOT}}{2}\left\{\frac{1}{Y1} - \frac{m_{v,in}}{Y1^2} + \frac{1}{Y2} - \frac{m_{v,in}-m_{con}}{Y2^2}\right\} \tag{A.37}$$

$$\frac{\partial P_{PARTIAL}}{\partial m_{con}} = \frac{P_{TOT}}{2}\left\{-\frac{1}{Y2} + \frac{m_{v,in}-m_{con}}{Y2^2}\right\} \tag{A.38}$$

The error of the system total pressure measurement is 0.1% of span, the error of air flow meter is 5% of span, and the error of steam flow rate measured by vortex flow meter is 1%.

Now we got all the data to calculate the error of the condensation heat transfer coefficient in Eq. (A.7). With the same method we can calculate the error of the overall heat transfer coefficient and the secondary heat transfer coefficient.

Overall HTC can be calculated by:

$$U = \frac{m_{con} h_{fg}}{A_i \left(T_{SAT} - T_P \right)} \tag{A.39}$$

By neglecting the geometric error,

$$U = U\left(m_{con}, h_{fg}, T_P, T_{SAT} \right) \tag{A.40}$$

$$\sigma_U^2 = \left(\frac{\partial U}{\partial m_{con}} \right)^2 \sigma_{m_{con}}^2 + \left(\frac{\partial U}{\partial h_{fg}} \right)^2 \sigma_{h_{fg}}^2 + \left(\frac{\partial U}{\partial T_P} \right)^2 \sigma_{T_P}^2 + \left(\frac{\partial U}{\partial T_{SAT}} \right)^2 \sigma_{T_{SAT}}^2 \tag{A.41}$$

$$\frac{\partial U}{\partial m_{con}} = \frac{h_{fg}}{A_i \left(T_{SAT} - T_P \right)} \tag{A.42}$$

$$\frac{\partial U}{\partial h_{fg}} = \frac{m_{con}}{A_i \left(T_{SAT} - T_P \right)} \tag{A.43}$$

$$\frac{\partial U}{\partial T_P} = \frac{m_{con} h_{fg}}{A_i \left(T_{SAT} - T_P \right)^2} \tag{A.44}$$

$$\frac{\partial U}{\partial T_{SAT}} = -\frac{m_{con} h_{fg}}{A_i \left(T_{SAT} - T_P \right)^2} \tag{A.45}$$

Error of the secondary HTC are:

$$h_{\sec} = \frac{m_{con} h_{fg}}{A_o \left(T_{Wo} - T_P \right)} \tag{A.46}$$

$$h_{\sec} = h_{\sec}\left(m_{con}, h_{fg}, T_P, T_{Wo} \right) \tag{A.47}$$

$$\sigma_{h_{\sec}}^2 = \left(\frac{\partial h_{\sec}}{\partial m_{con}} \right)^2 \sigma_{m_{con}}^2 + \left(\frac{\partial h_{\sec}}{\partial h_{fg}} \right)^2 \sigma_{h_{fg}}^2 + \left(\frac{\partial h_{\sec}}{\partial T_P} \right)^2 \sigma_{T_P}^2 + \left(\frac{\partial h_{\sec}}{\partial T_{Wo}} \right)^2 \sigma_{T_{Wo}}^2 \tag{A.48}$$

$$\frac{\partial h_{\sec}}{\partial m_{con}} = \frac{h_{fg}}{A_o \left(T_{Wo} - T_P \right)} \tag{A.49}$$

$$\frac{\partial h_{\sec}}{\partial h_{fg}} = \frac{m_{con}}{A_o \left(T_{Wo} - T_P \right)} \tag{A.50}$$

$$\frac{\partial h_{\sec}}{\partial T_P} = \frac{m_{con} h_{fg}}{A_o \left(T_{Wo} - T_P \right)^2} \tag{A.51}$$

$$\frac{\partial h_{\sec}}{\partial T_{Wo}} = -\frac{m_{con} h_{fg}}{A_o \left(T_{Wo} - T_P \right)^2} \tag{A.52}$$

We have all the data for the error calculation of overall and secondary HTC except the error of average secondary pool temperature, T_P. The average temperature at secondary pool is the arithmetic mean of 3 thermocouple measurements. Therefore, the error of T_P is

$$\sigma_{T_P} = \frac{1}{\sqrt{3}}\sigma_{TC} \tag{A.53}$$

Most of the relative error of the experiment are within 6 ~ 11%. The maximum relative error in the condensation heat transfer coefficient is conservatively selected as 20 %.

Reference

A.1 Nicholas Tsoulfanidis, Measurement and Detection of Radiation, Hemisphere Publishing Co., 1976.

Appendix B. VENT ANALYSIS

If small amount of noncondensable gas is added at a steady state complete condensation mode, the pressure is increase. This increase in pressure comes from two sources. One is due to the addition of the noncondensable gas itself. Since it is not condensable, the gas is accumulated in the system and it makes one part of the pressure increase. The other is due to the addition of steam in the system caused by the degradation of the condensation. At a complete condensation condition, all steam is condensed. So there is no actual steam accumulation in the system. As small amount of the noncondensable gas is added in the system, the condensation performance is degraded, i.e., some amount of steam is not condensed. The uncondensed steam acts as a second source of system pressure increase.

In this section, the pressurization caused by the addition of the noncondensable gas is analyzed based on the ideal gas law.

B.1 Pressurization Due to Gas Addition

Let's consider the steam-air mixture as an ideal gas. Then from the ideal gas law,

$$P \cdot v = R \cdot T \tag{B.1}$$

where, P is pressure,

v is specific volume,

$R = \dfrac{\overline{R}}{M}$ is a constant for a particular gas,

$\overline{R}$ is universal gas constant = 8.31434 $\dfrac{J}{mol \cdot K}$,

M is molecular weight,

T is temperature.

The molecular weight of water and air are 18.01 g/mol and 28.97 g/mol, respectively. Eq. (B.1) can be modified as follows:

$$P \cdot V = m \cdot R \cdot T \tag{B.2}$$

$$P \cdot V = n \cdot \overline{R} \cdot T \tag{B.3}$$

where, V is volume,

m is mass,

n = m/M is the number of moles.

From Eq. (B.3), the following equality can be derided.

$$\overline{R} = \left(\frac{P \cdot V}{n \cdot T} \right)_1 = \left(\frac{P \cdot V}{n \cdot T} \right)_2 \tag{B.4}$$

Here, subscript 1 represents initial condition and subscript 2 represents final condition. By rearranging Eq. (B.4),

$$P_2 = \frac{m_2}{m_1} \frac{M_1}{M_2} \frac{T_2}{T_1} \frac{V_1}{V_2} P_1 \tag{B.5}$$

In Eq. (B.5), the initial condition P_1, T_1, V_1 M_1 are given and m_1 can be calculated using Eq. (B.2).

$$m_1 = \left(\frac{P \cdot V}{R \cdot T} \right)_1 \tag{B.6}$$

Final mass is the sum of initial mass and mass addition to the control volume.

$$m_2 = m_1 + \Delta m = m_1 + \left(M_{steam} + M_{air} - M_{conden} \right) \cdot \Delta t \tag{B.7}$$

Here, M_{steam} is inlet steam flow rate, M_{conden} is condensation rate, M_{air} is air flow rate, and Δt is time difference between the initial and final condition. In actual calculation, it is assumed that $M_{steam} = M_{conden}$.

Final volume is the initial volume minus the volume occupied by the condensate water.

$$V_2 = V_1 - \Delta V = V_1 - \frac{M_{conden} \cdot \Delta t}{\rho_f} \tag{B.8}$$

where ρ_f is the density of condensate liquid which is a function of pressure. Final equation for the pressure can be expressed as follows:

$$P_2 = \frac{m_1 + \Delta m}{m_1} \frac{M_1}{M_2} \frac{V_1}{V_1 - \Delta V} \frac{T_2}{T_1} P_1 = \frac{P_1 \cdot V_1 + R_1 \cdot T_1 \cdot \Delta m}{P_1 \cdot V_1} \frac{M_1}{M_2} \frac{V_1}{V_1 - \Delta V} \frac{T_2}{T_1} P_1$$

$$P_2 = \frac{P_1 \cdot V_1 + R_1 \cdot T_1 \cdot \Delta m}{V_1 - \Delta V} \frac{M_1}{M_2} \frac{T_2}{T_1} \tag{B.9}$$

here, T_2=Tsat(P_2), T_1=Tsat(P_1).

Since ρ_f and T1, T2 are function of pressure, the above equation is an implicit function of pressure. So, it needs to iterate to solve the equation.

Eq. (B.9) can be simplified by assuming T_2=T_1,

$$P_2 = \frac{P_1 \cdot V_1 + R_1 \cdot T_1 \cdot \Delta m}{V_1 - \Delta V} \frac{M_1}{M_2} = \frac{P_1 \cdot V_1 + R_1 \cdot T_1 \cdot \left(M_{steam} + M_{air} - M_{conden}\right) \cdot \Delta t}{V_1 - \frac{M_{conden} \cdot \Delta t}{\rho_f}} \frac{M_1}{M_2} \tag{B.10}$$

By assuming V_2=V_1,

$$P_2 = \left(P_1 + \frac{R_1 \cdot T_1}{V_1} \cdot \Delta m \right) \frac{M_1}{M_2} = \left(P_1 + \frac{R_1 \cdot T_1}{V_1} \cdot \left(M_{steam} + M_{air} - M_{conden}\right) \cdot \Delta t \right) \frac{M_1}{M_2} \tag{B.11}$$

In Eqs. (B.9) ~ (B.11), the gas constant, R_1, Molecular weight M_1 and M_2 are mixture properties varied with time. So it needs to estimate these mixture properties.

Mixture Model for the Ideal Gas

There are two models used in conjunction with the mixtures of gases, namely the Dalton model and the Amagat model [B1].

- Dalton Model

In the case of the Dalton model, the properties of each component are considered as each component exists separately at the volume and temperature of the mixture with different pressure.

For the Mixture:

$$P \cdot V = n \cdot \overline{R} \cdot T ,$$

$$n = n_A + n_B \tag{B.12}$$

Subscript A and B represent each component of binary mixture.

For the components:

$$P_A \cdot V = n_A \cdot \overline{R} \cdot T , \tag{B.13}$$

$$P_B \cdot V = n_B \cdot \overline{R} \cdot T \tag{B.14}$$

By substituting Eqs. B.13 and B.14 into B.12,

$$\frac{P \cdot V}{\overline{R} \cdot T} = \frac{P_A \cdot V}{\overline{R} \cdot T} + \frac{P_B \cdot V}{\overline{R} \cdot T} \rightarrow P = P_A + P_B \tag{B.15}$$

- Armagat Model

In the case of the Armagat model, the properties of each component are considered as each component exists separately at the pressure and temperature of the mixture with different volume.

For the Mixture:

$$P \cdot V = n \cdot \overline{R} \cdot T ,$$

$$n = n_A + n_B$$

For the components:

$$P \cdot V_A = n_A \cdot \overline{R} \cdot T , \tag{B.16}$$

$$P \cdot V_B = n_B \cdot \overline{R} \cdot T \tag{B.17}$$

$$\frac{P \cdot V}{\overline{R} \cdot T} = \frac{P \cdot V_A}{\overline{R} \cdot T} + \frac{P \cdot V_B}{\overline{R} \cdot T} \rightarrow V = V_A + V_B \tag{B.18}$$

The mole fraction of component A, y_A is defined as

$$y_A = \frac{n_A}{n} \tag{B.19}$$

Fron Eqs. B.12 ~ B.18, it is evident that

$$\frac{V_A}{V} = \frac{n_A}{n} = \frac{P_A}{P} = y_A \tag{B.20}$$

That is, for each component of a mixture of ideal gases, mole fraction y_A is equal to the volume fraction and the ratio of the partial pressure to the total pressure.

- Mixture Property

Mixture enthalpy per mole:

$$h_{mix} = \frac{n_A \cdot \overline{h_A} + n_B \cdot \overline{h_B}}{n} = y_A \cdot \overline{h_A} + y_B \cdot \overline{h_B} \tag{B.21}$$

Here, $\overline{h_i}$ is enthalpy per mole for pure i-component.

Mixture molecular weight:

$$M_{mix} = y_A \cdot M_A + y_B \cdot M_B \tag{B.22}$$

Mixture gas constant:

$$R_{mix} = \frac{\overline{R}}{M_{mix}} \tag{B.23}$$

Now we can calculate the final pressure P_2 using Eqs. (B.9), (B.22) and (B.23).

B.2 Condensation Degradation Due to the Noncondensable Gas

Pressure calculated in Eq. (B.9) indicates the pressurization due to the air mass addition. From the measurement data during periodic venting, representative pressurization curve can be obtained by appropriate data processing. Figs. B.1 and B.2 show the data processing result. Then, the pressure difference between the pressurization curve obtained from data and the pressurization curve calculated in section B.1 is pressurization due to the uncondensed steam. The uncondensed steam flow rate, i.e., degradation of condensation can be calculated by those two pressurization curve. In Fig. B.3, the solid line (legend – Pideal) is the pressurization curve calculated in section B.1 and the dotted line (legend – Pcorrected) is the pressurization curve obtained from data. Fig. B.4 shows the degradation effect of the noncondensable gas addition.

Here, the degradation is defined the ratio of the uncondensed steam flow rate and average condensation rate.

The data processing procedure is as follows:

- Raw Data
- Remove the very low-pressure data which is representing undershooting : Reduced Data
- Using this reduced data, obtain locally running average pressure data :Average Pressure
- Normalize average pressurization curve for each periodic venting interval
- Fit the normalized curve using second order polynomial and logarithmic function
- Find the uncondensed steam flow rate to match Pideal to Pcorrected

Testdata=0625t6 case shown in Figs. B.1 ~ B.4 is Wair=0.1038%, base pressure P=26.75 psig (Note: unit of Wair in figures is %). This case is relatively low noncondensable gas fraction condition. Testdata=0625t12 case shown in Figs. B.5 ~ B.8 is Wair=0.478%, base pressure P=27.081 psig. This case is relatively high noncondensable gas fraction condition. Generally speaking, the pressurization curve shows logarithmic trend for low noncondensable gas fraction and the curve shows second order polynomial trend for high noncondensable gas fraction. Figs B.9 ~ B.22 show the pressurization curve and degradation effects for various periodic venting data.

Reference

B.1 G. J. Van Wylen, R. E. Sonntag, Fundamentals of Classical Thermodynamics, 2nd Ed., John Wiley and Sons, INC., 1978.

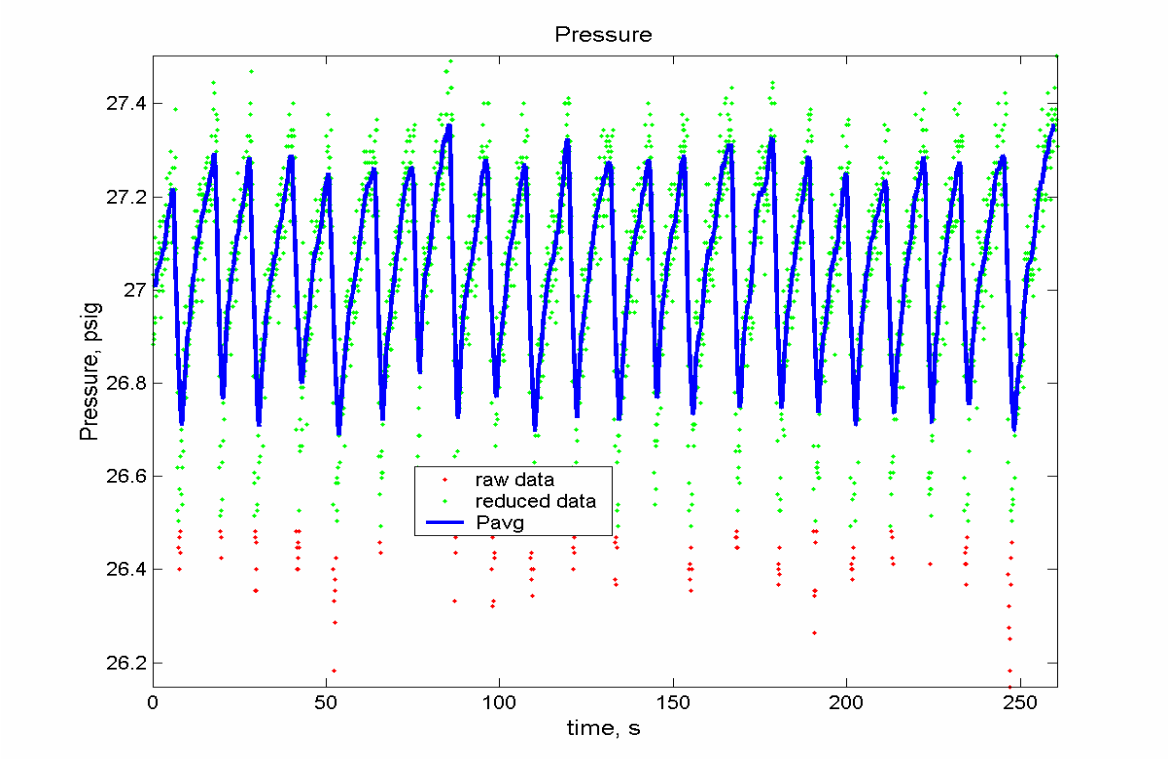

Figure B.1. Pressure: Raw Data, Reduced Data, and Averaged Data for testdata=0625t6

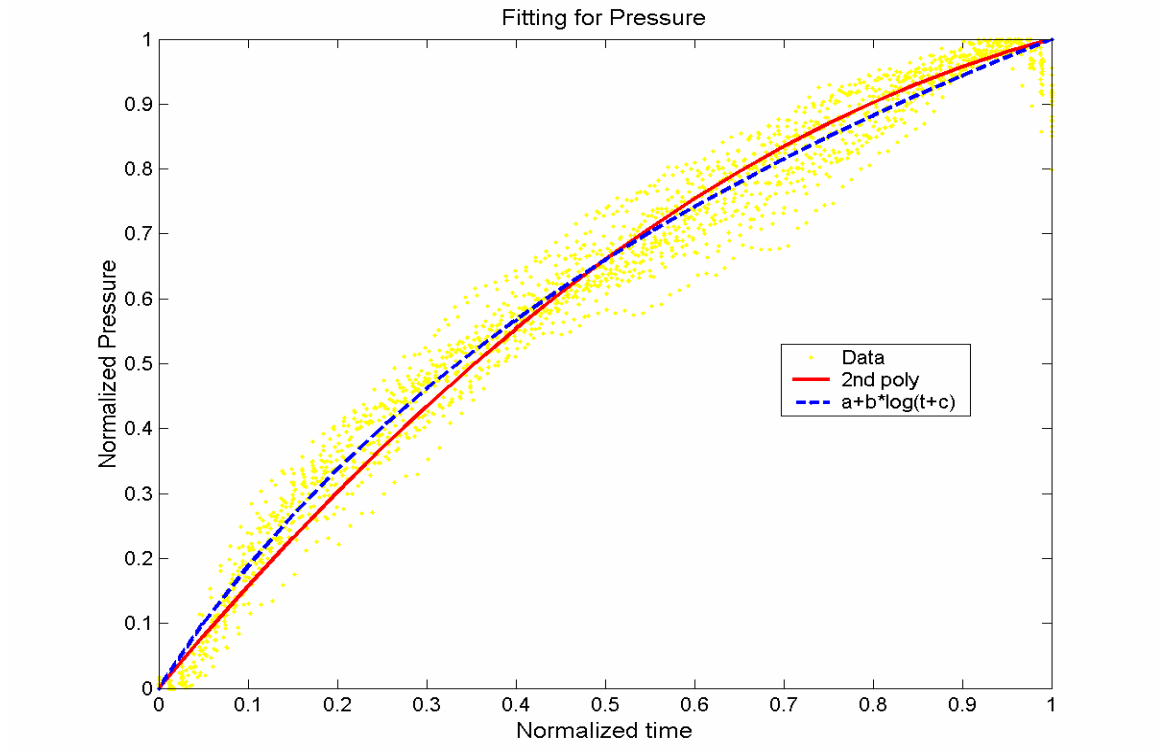

Figure B.2. Data Fitting for the Averaged Pressure for testdata=0625t6

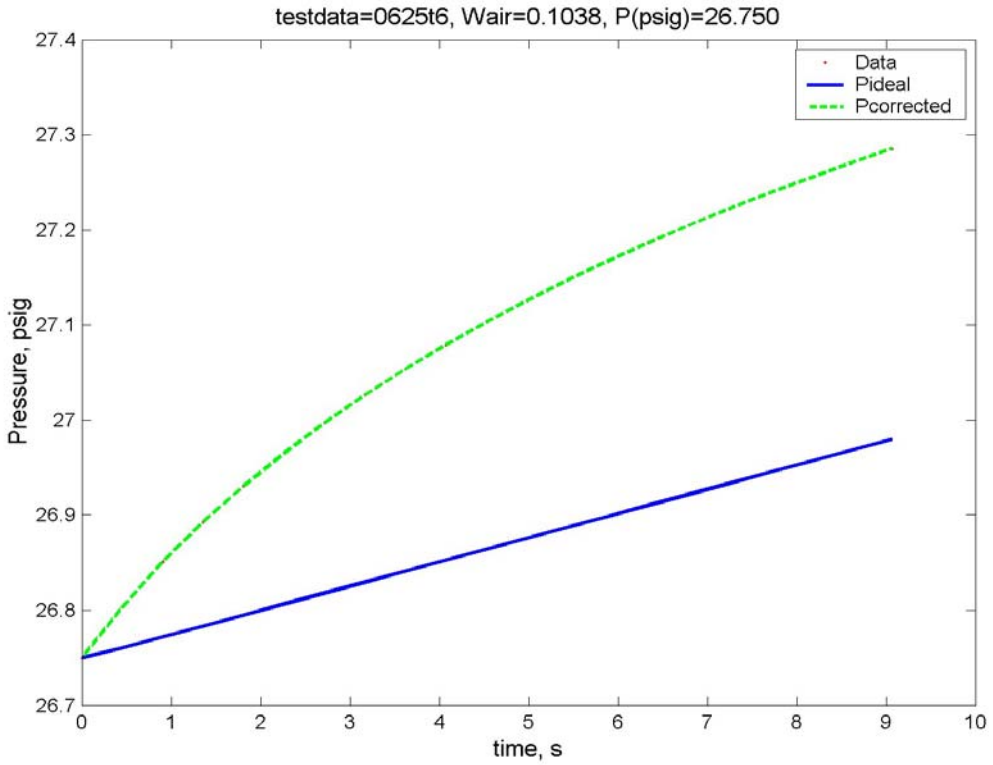

Figure B.3. Pressurization Curves for testdata=0625t6

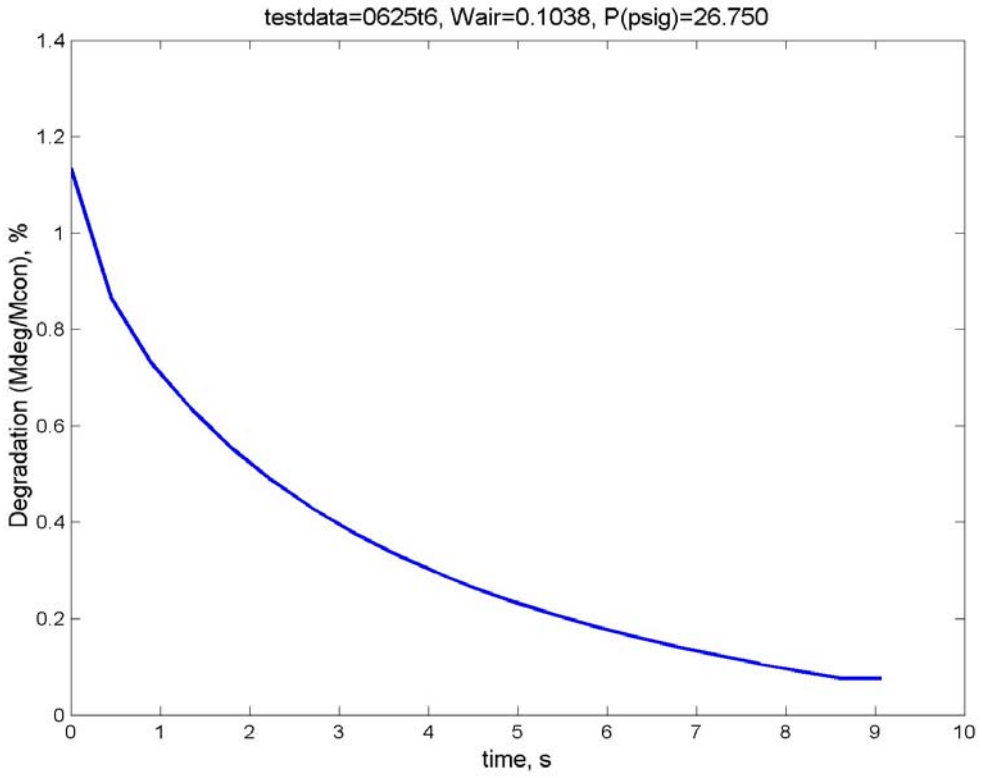

Figure B.4. Degradation Curves for testdata=0625t6

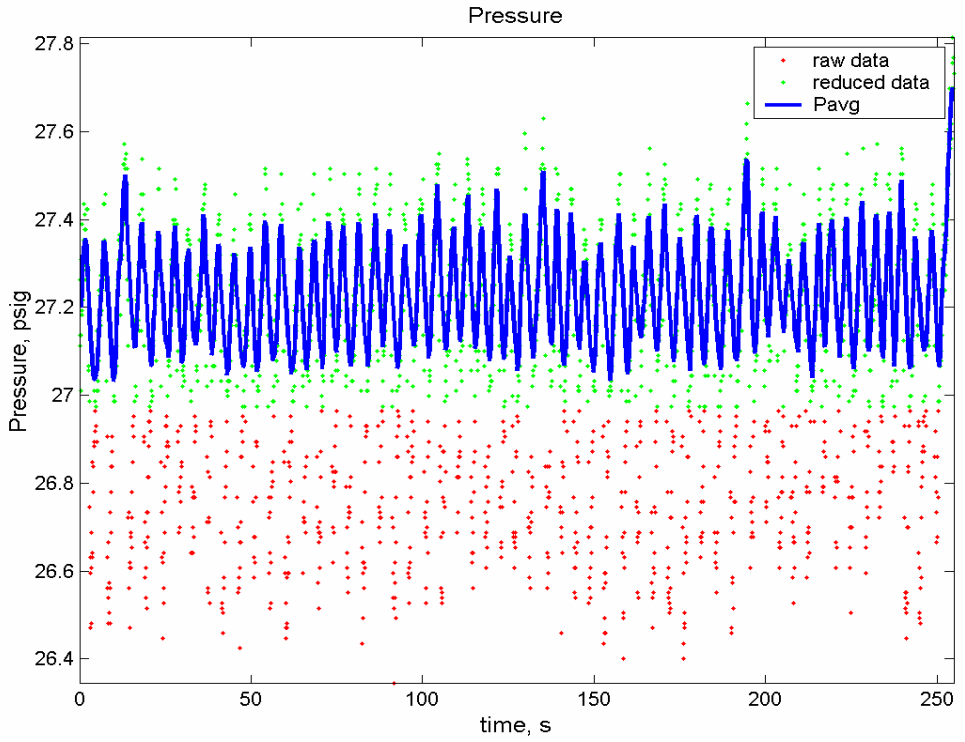

Figure B.5. Pressure: Raw Data, Reduced Data, and Averaged Data for testdata=0625t12

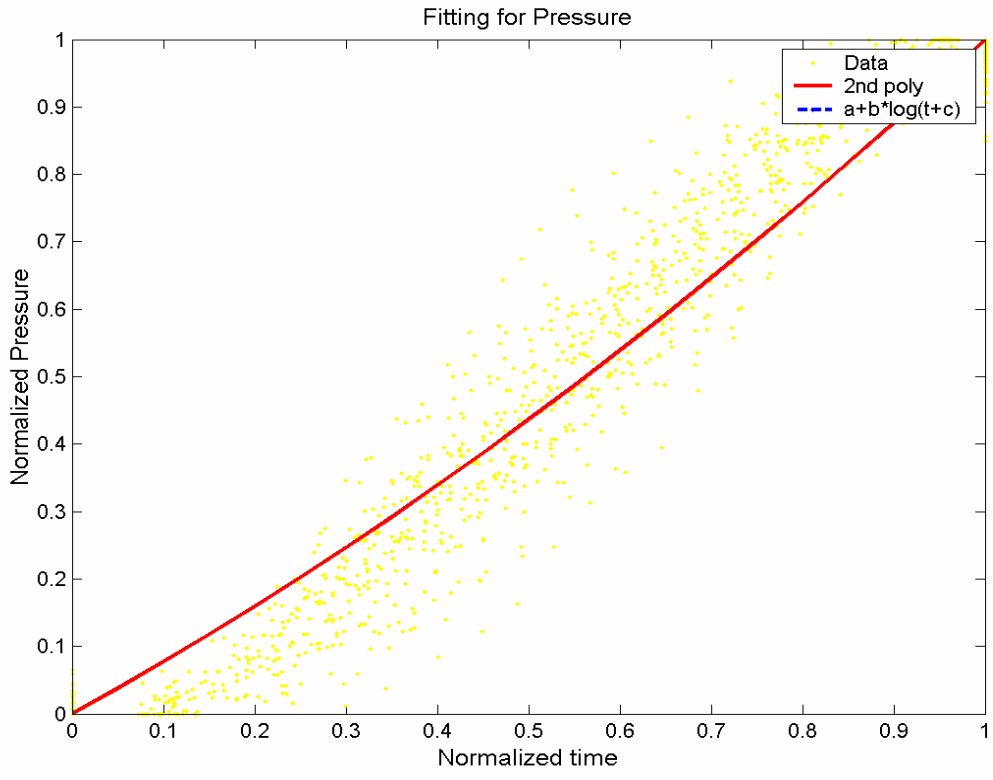

Figure B.6. Data Fitting for the Averaged Pressure for testdata=0625t12

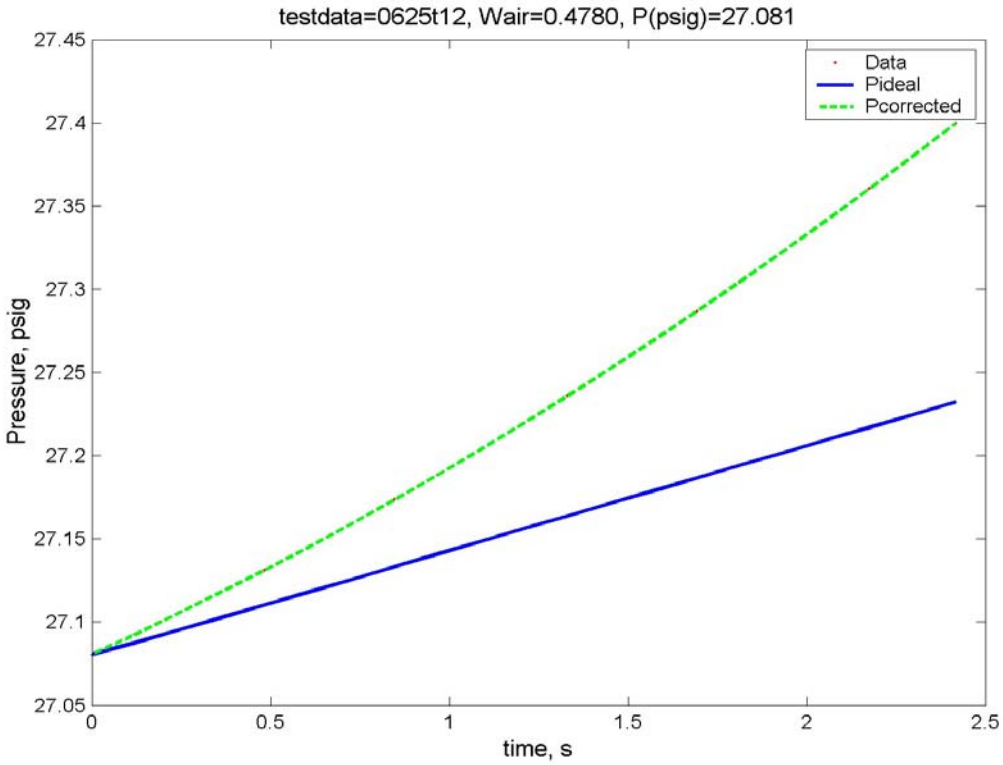

Figure B.7. Pressurization Curves for testdata=0625t12

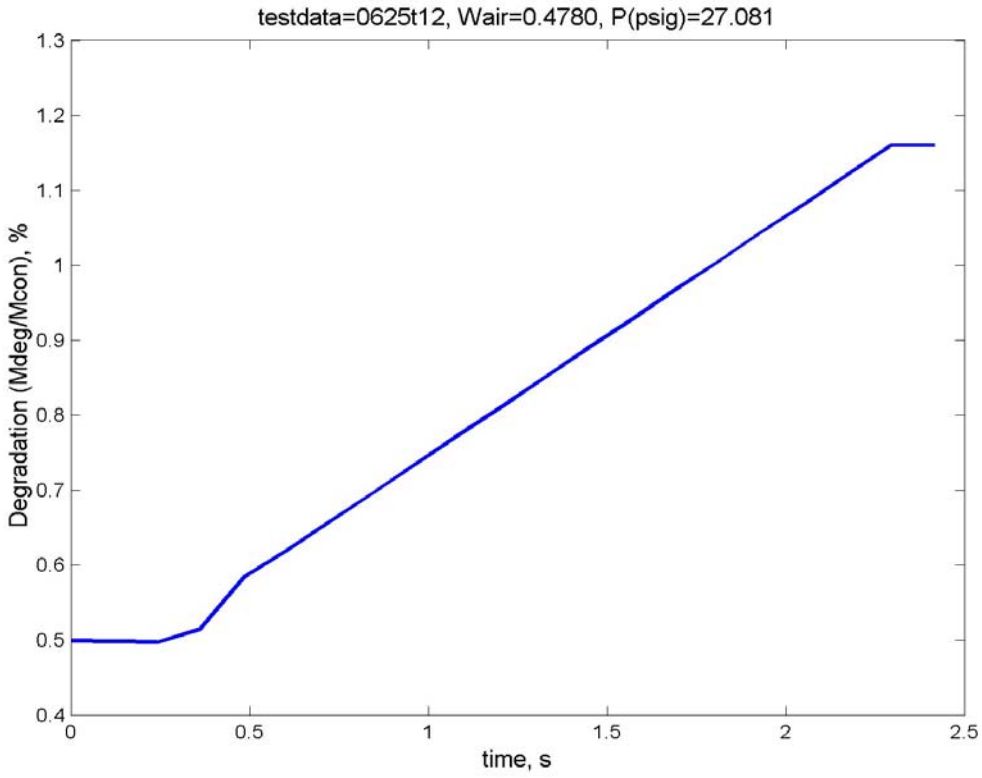

Figure B.8. Degradation Curves for testdata=0625t12

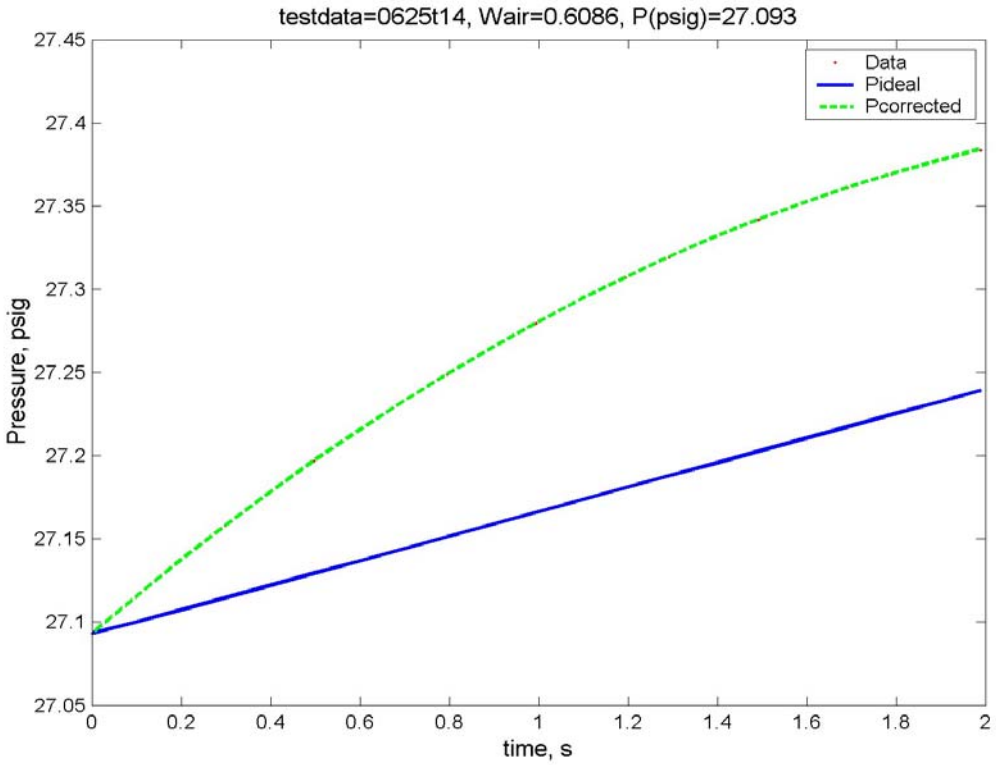

Figure B.9. Pressurization Curves for testdata=0625t14

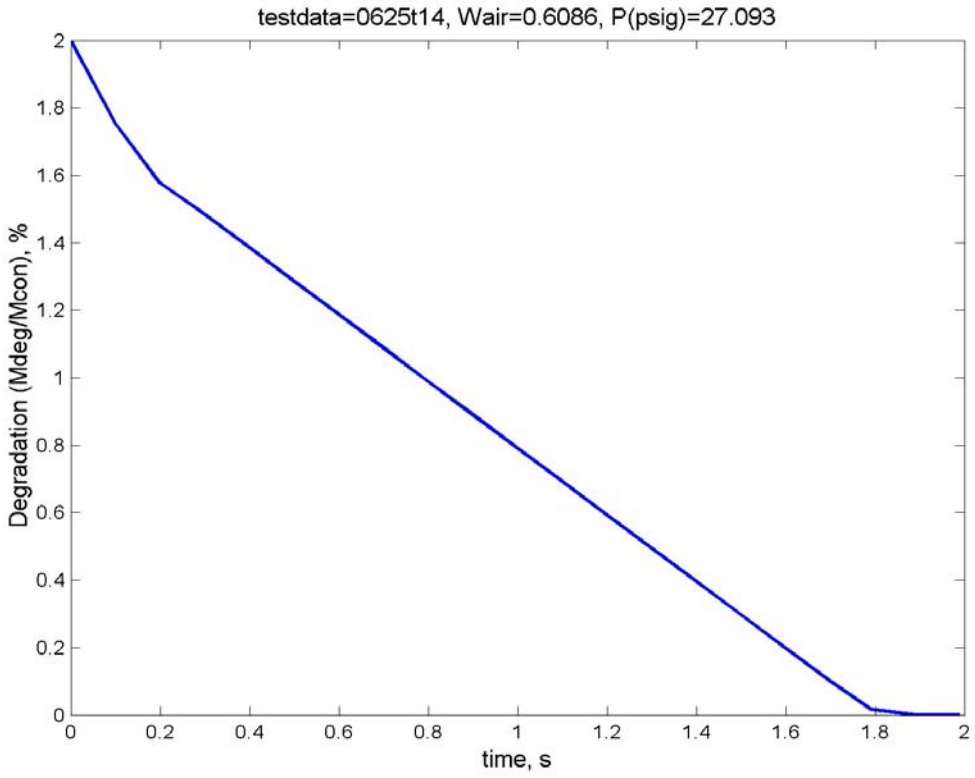

Figure B.10. Degradation Curves for testdata=0625t14

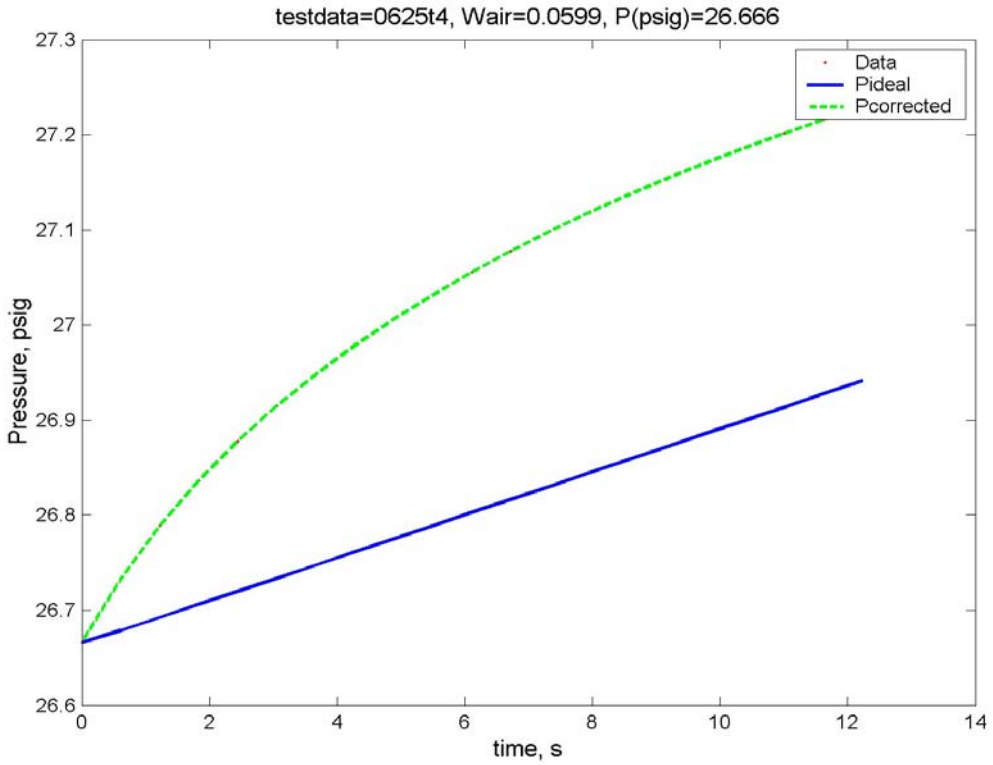

Figure B.11. Pressurization Curves for testdata=0625t4

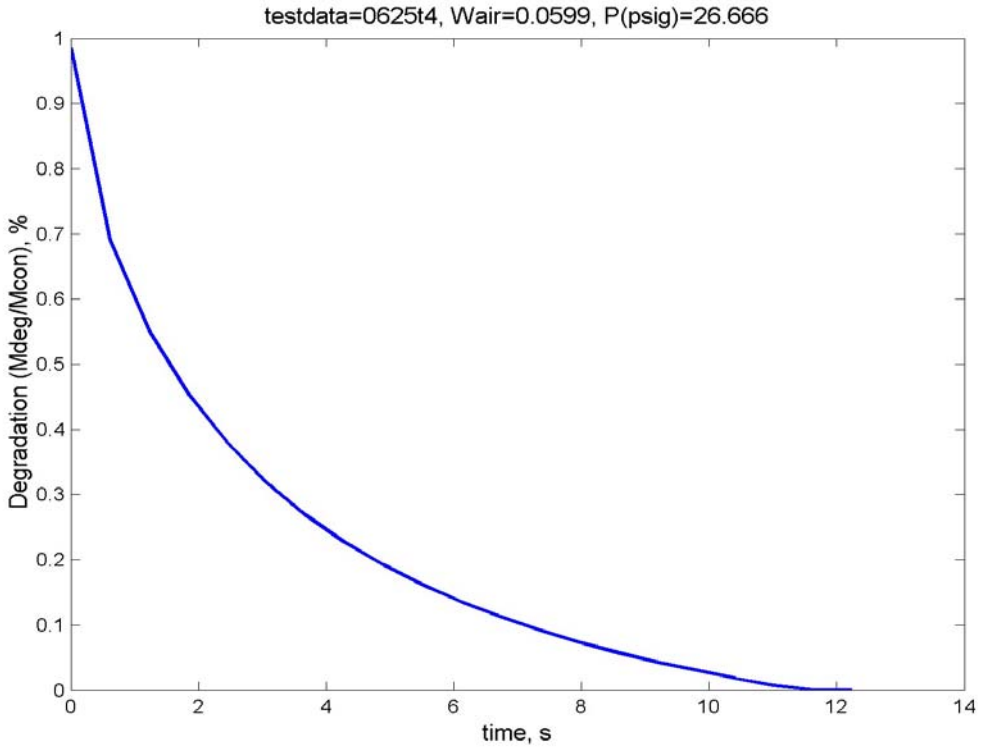

Figure B.12. Degradation Curves for testdata=0625t4

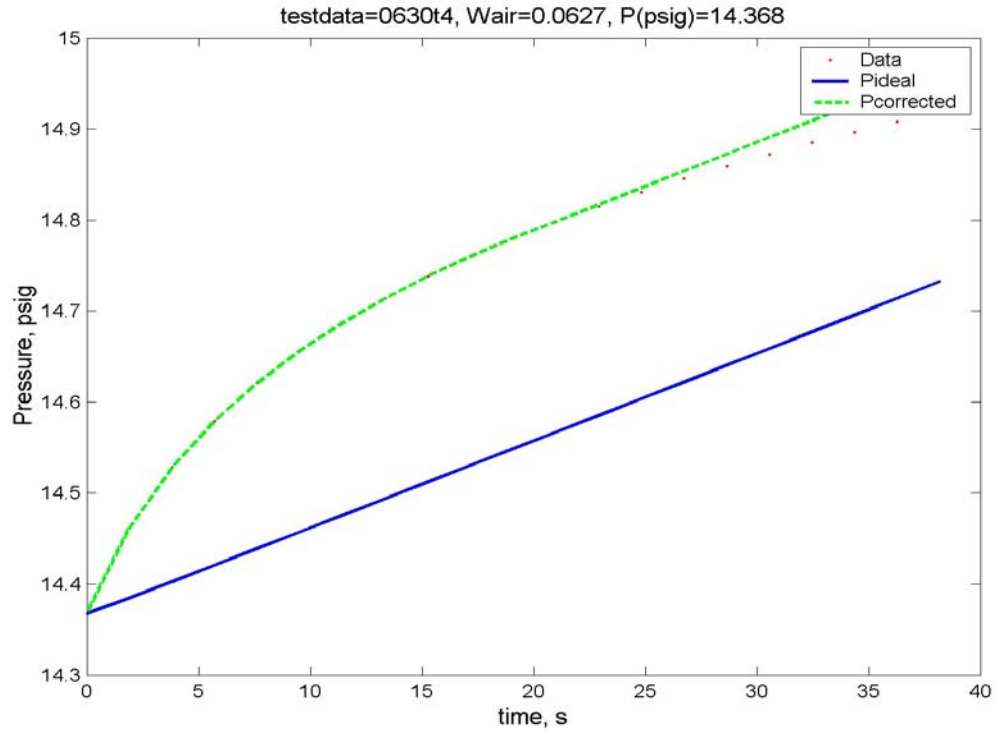

Figure B.13. Pressurization Curves for testdata=0630t4

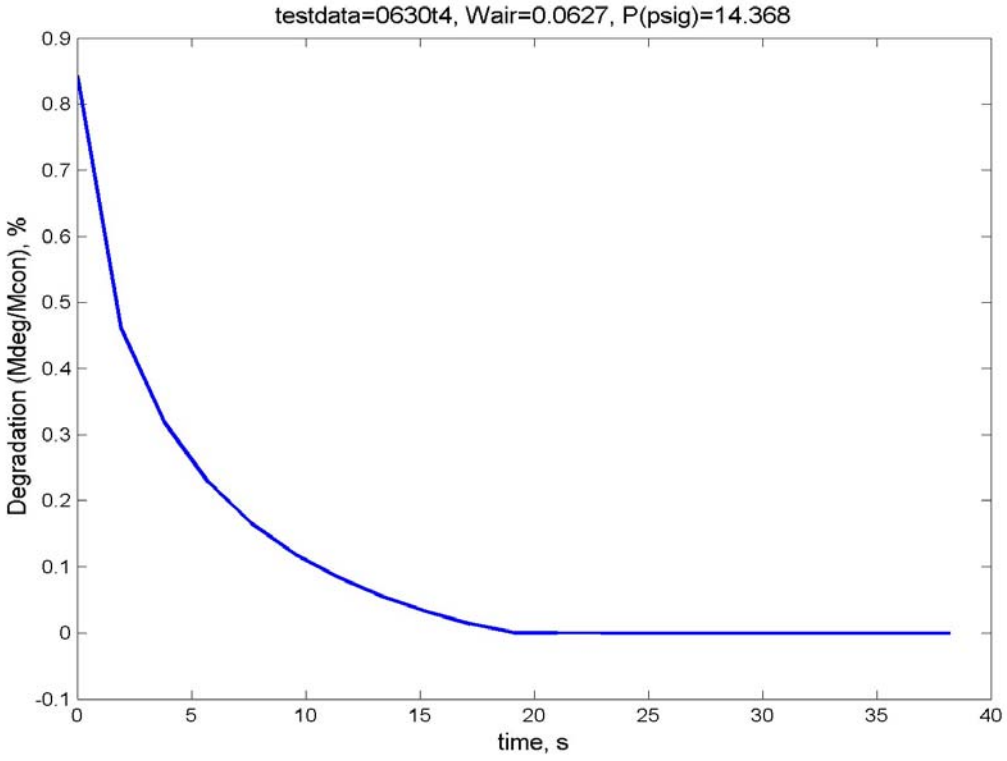

Figure B.14. Degradation Curves for testdata=0630t4

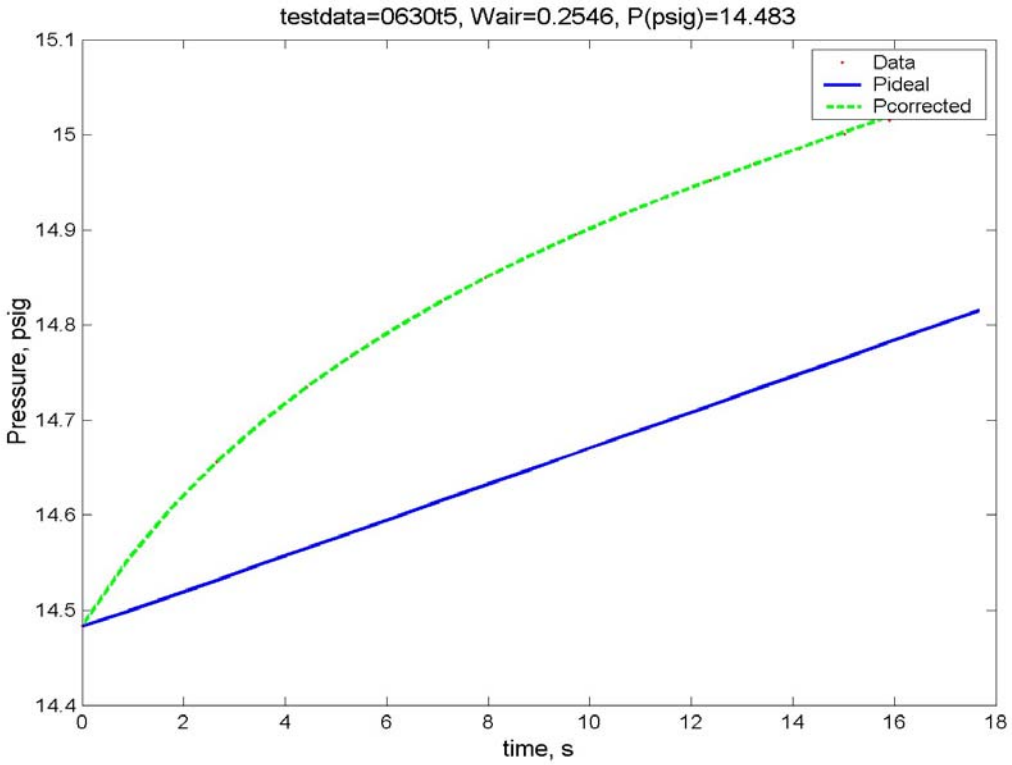

Figure B.15. Pressurization Curves for testdata=0630t5

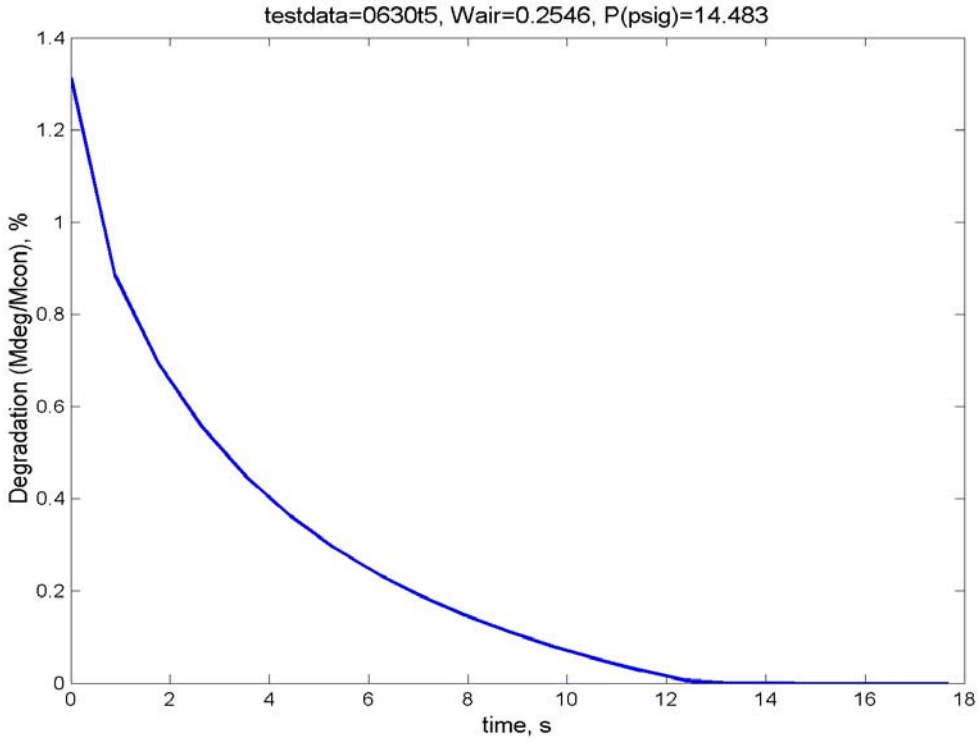

Figure B.16. Degradation Curves for testdata=0630t5

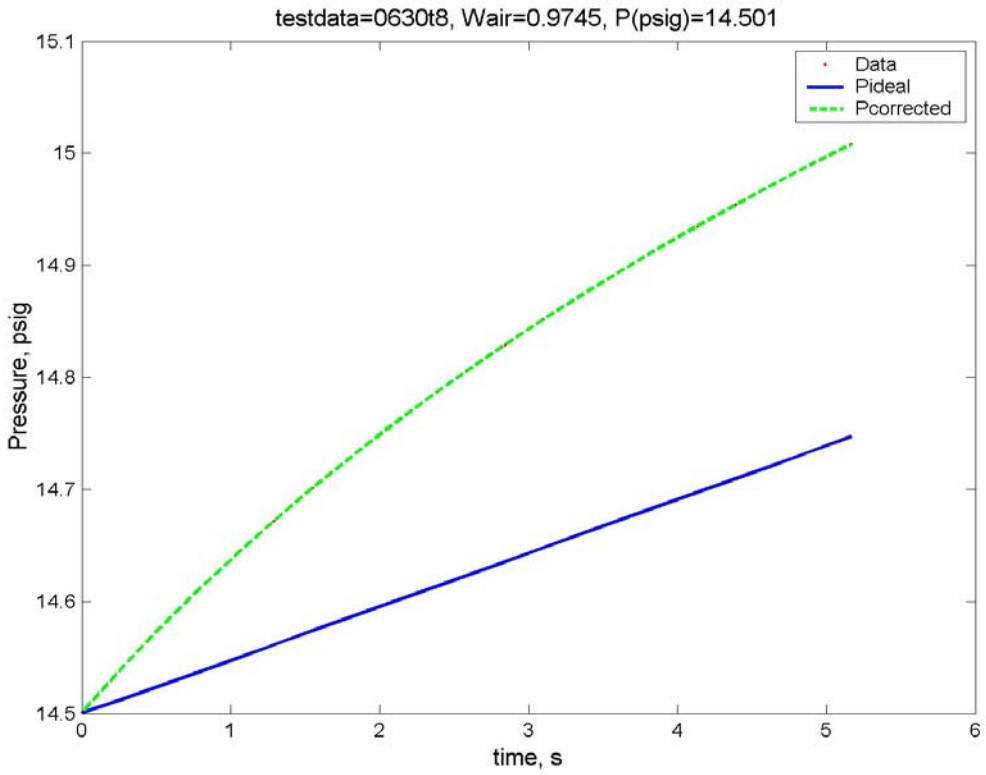

Figure B.17. Pressurization Curves for testdata=0630t8

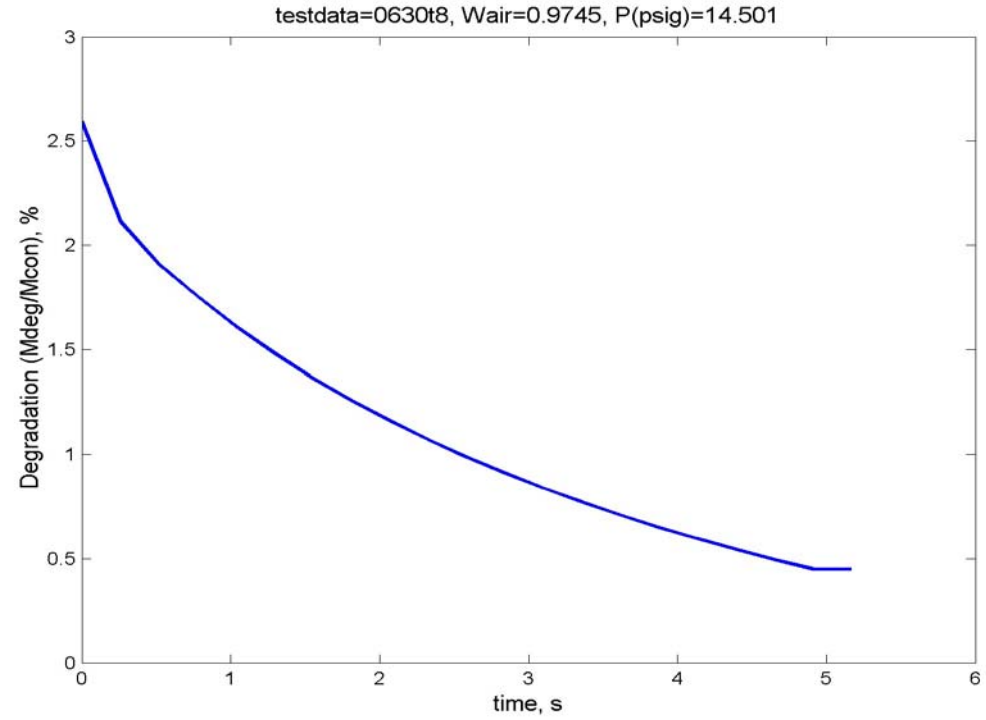

Figure B.18. Degradation Curves for testdata=0630t8

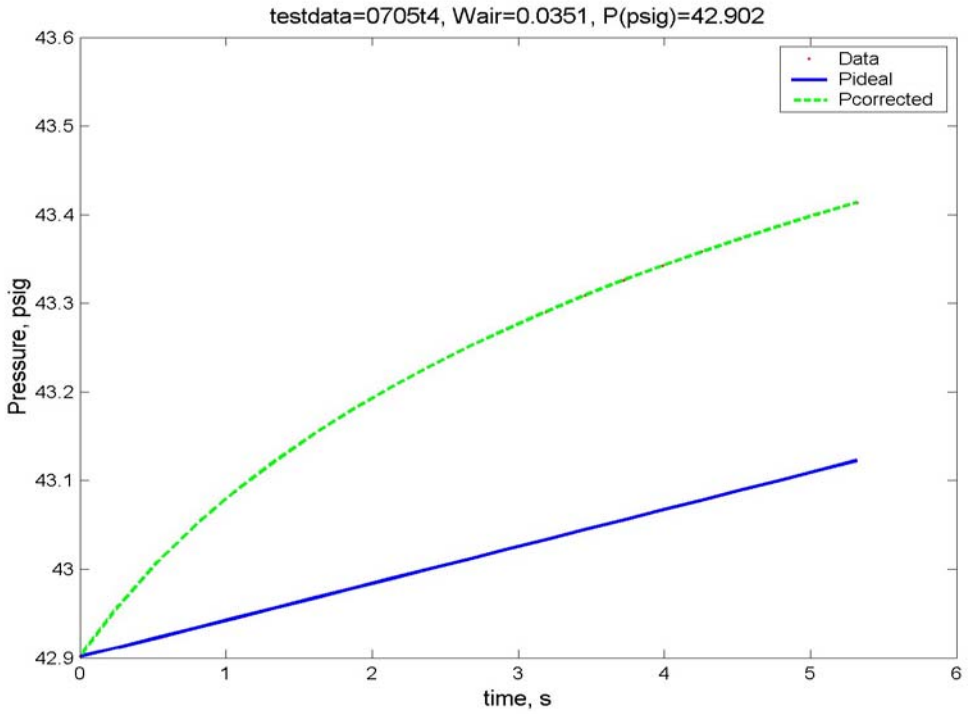

Figure B.19. Pressurization Curves for testdata=0705t4

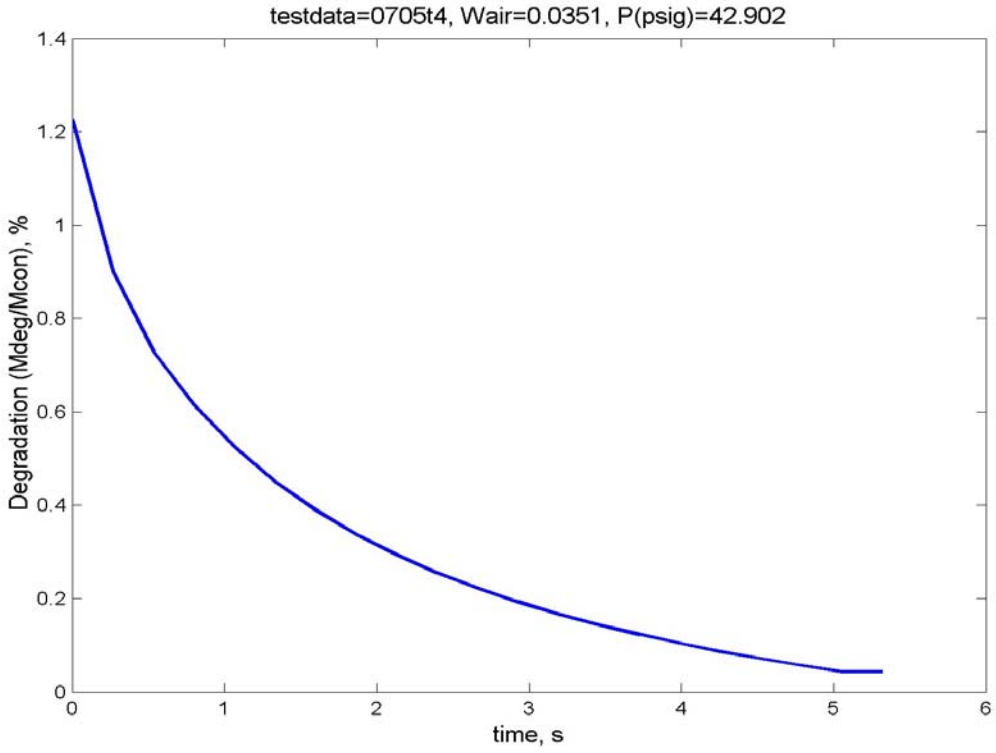

Figure B.20. Degradation Curves for testdata=0705t4

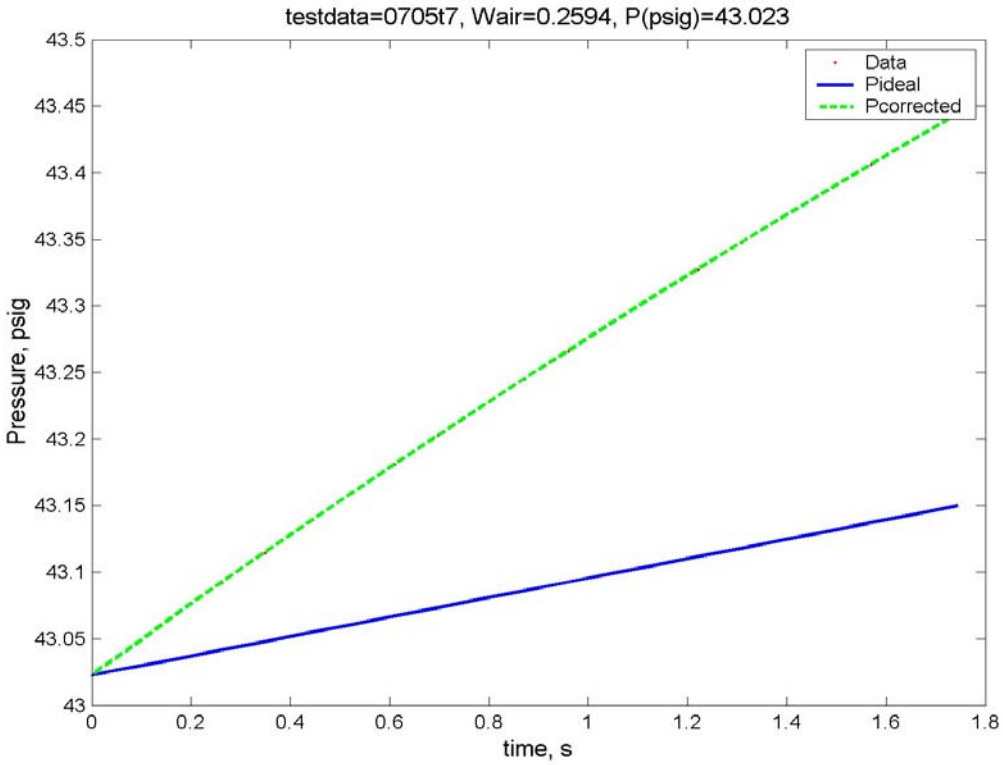

Figure B.21. Pressurization Curves for testdata=0705t7

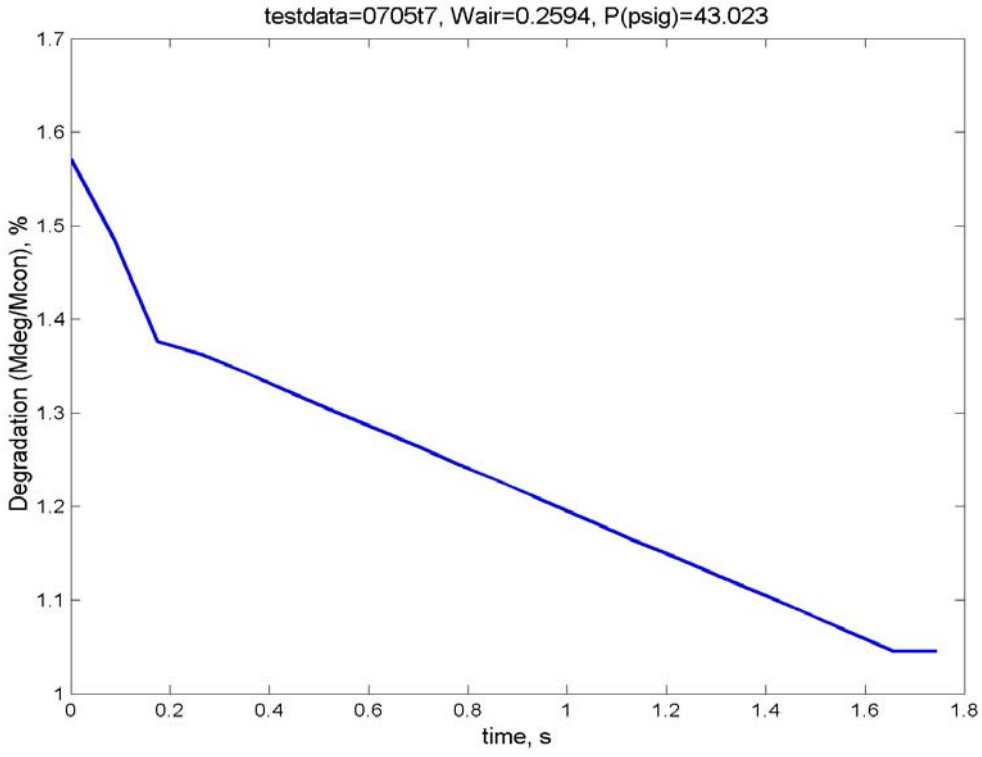

Figure B.22. Degradation Curves for testdata=0705t7